

NASA TECHNICAL
MEMORANDUM



UB
NASA TM X-1690

UB
NASA TM X-1690

NASA LIBRARY
AMES RESEARCH CENTER
MOFFETT FIELD, CALIF.
NOV. 21 1968

COPY
No. 2

HYPersonic AERODYNAMIC CHARACTERISTICS OF THE M2-F2 LIFTING ENTRY CONFIGURATION

by John A. Axelson and Jack A. Mellenthin

Ames Research Center

Moffett Field, Calif.

NATIONAL AERONAUTICS AND SPACE ADMINISTRATION • WASHINGTON, D. C. • NOVEMBER 1968

~~CONFIDENTIAL~~
UNCLASSIFIED

~~CONFIDENTIAL~~

NASA TM X-1690

HYPERSONIC AERODYNAMIC CHARACTERISTICS OF THE M2-F2 LIFTING ENTRY CONFIGURATION

By John A. Axelson and Jack A. Mellenthin

Ames Research Center
Moffett Field, Calif.

GROUP 4
Downgraded at 3 year intervals;
declassified after 12 years

CLASSIFIED DOCUMENT-TITLE UNCLASSIFIED

This material contains information affecting the national defense of the United States within the meaning of the espionage laws, Title 18, U.S.C., Secs. 793 and 794, the transmission or revelation of which in any manner to an unauthorized person is prohibited by law.

NOTICE

This document should not be returned after it has satisfied your requirements. It may be disposed of in accordance with your local security regulations or the appropriate provisions of the Industrial Security Manual for Safe-Guarding Classified Information.

NATIONAL AERONAUTICS AND SPACE ADMINISTRATION

~~CONFIDENTIAL~~

~~CONFIDENTIAL~~

HYPERSONIC AERODYNAMIC CHARACTERISTICS OF THE
M2-F2 LIFTING ENTRY CONFIGURATION*

By John A. Axelson and Jack A. Mellenthin

Ames Research Center

SUMMARY

The hypersonic aerodynamic characteristics of the M2-F2 lifting entry configuration have been measured in the Ames 3.5-Foot Hypersonic Wind Tunnel at Mach numbers of 5.2, 7.4, and 10.4 with test Reynolds numbers varying between 0.7 and 1.6 million. Aerodynamic force and static-stability characteristics are presented for a range of angles of attack from -15° to $+45^{\circ}$, extending from negative lift coefficients to maximum lift coefficient.

The trimmed maximum lift-drag ratio was 1.30 at the three test Mach numbers and occurred at a lift coefficient of 0.20 near an angle of attack of 12° . The maximum trimmed lift coefficient was 0.45 and occurred at an angle of attack of 37° with a corresponding lift-drag ratio of 0.8. The lower pitch flap provided an effective longitudinal trim capability from maximum lift to zero lift. The static margin was 6 percent of the reference length at maximum lift-drag ratio and increased at the higher and at the lower angles of attack. Differential rudder deflection provided favorable lateral-directional control characteristics, and rudder flare was very effective for augmenting the otherwise marginal directional stability and for increasing the ratio of directional to lateral stability.

INTRODUCTION

Analytical studies, typified by references 1 and 2, indicated that significant reductions in peak heating and in peak deceleration could be achieved during atmosphere entry through the use of a lifting body. Favorable reductions in stagnation-point aerodynamic heating rate were indicated to accrue from flying at high lift coefficients, which shifts the peak heating to higher altitudes. Trajectory studies indicated an attractive lateral-range capability of 1000 nautical miles (the approximate spacing between consecutive orbits at the latitudes of the United States) with a hypersonic lift-drag ratio of 1.3, and also indicated the need for a capability of reducing the lift during part of the entry trajectory to avoid "skipping out" of the atmosphere.

The development of the lifting body initially designated the M2 was reported in references 3 and 4 and was in accord with the foregoing hypersonic

*Title, Unclassified

~~CONFIDENTIAL~~

~~CONFIDENTIAL~~

requirements, that is, stable, controllable flight over the wide range of angles of attack from zero lift to maximum lift and a maximum lift-drag ratio of 1.3. In addition, the stability and controllability were to be maintained throughout the flight envelope down through a conventional landing capability.

Studies in support of the lifting-body flight-test program at the NASA Flight Research Center led to three modifications of the M2, namely, the aft extension of the boattail, aft displacement of the rudders, and replacement of the former pair of lower flaps by a single larger flap mounted farther aft. Intervening studies of this modified version which is designated the M2-F2 are reported in references 5, 6, and 7. The purpose of the present report is to document the updated hypersonic aerodynamic characteristics for the M2-F2.

NOTATION

b	model span
C_D	drag coefficient, $\frac{\text{drag}}{qS}$
C_L	lift coefficient, $\frac{\text{lift}}{qS}$
C_l	rolling-moment coefficient, $\frac{\text{rolling moment}}{qSb}$
C_{l_β}	lateral-stability parameter, $\frac{\partial C_l}{\partial \beta}$
C_m	pitching-moment coefficient, $\frac{\text{pitching moment}}{qSl}$
C_N	normal-force coefficient, $\frac{\text{normal force}}{qS}$
C_n	yawing-moment coefficient, $\frac{\text{yawing moment}}{qSb}$
C_{n_β}	directional-stability parameter, $\frac{\partial C_n}{\partial \beta}$
C_Y	side-force coefficient, $\frac{\text{side force}}{qS}$
$\frac{L}{D}$	lift-to-drag ratio
l	model reference length
M_∞	free-stream Mach number
q	dynamic pressure
S	planform area
α	angle of attack
β	sideslip angle
δ	control deflection

Subscripts

f	lower pitch flap
r	rudder
s	moments referred to stability axes

EXPERIMENT

Facility and Test Conditions

The measurements were performed in the Ames 3.5-Foot Hypersonic Wind Tunnel, a blowdown type in which compressed air is heated during passage through a pebble-bed heater and is then accelerated through one of several interchangeable nozzles leading to the 3.5-foot-diameter test section. The total temperature of the air passing through the test section was nominally 1900° R (~1050° K) for the three test Mach numbers of 5.2, 7.4, and 10.4. The total pressures were approximately 7 atmospheres at $M = 5.2$, 36 atmospheres at $M = 7.4$, and either 36 or 68 atmospheres at $M = 10.4$. The test Reynolds numbers for the present model of 1-foot reference length were 0.9 million at $M = 5.2$, 1.5 million at $M = 7.4$, and 0.7 or 1.1 million at $M = 10.4$.

The model was sting mounted on a hydraulically actuated, servo-controlled support system which was operated through an angle-of-attack range from -5° to $+15^\circ$. In order to cover a broader range of angles extending from -15° to $+45^\circ$, the model was tested in both the inverted and upright attitudes for each of two model-sting attachments accommodating 0° or 30° model incidence. Sideslip tests were performed by rolling the model 90° on the sting support and testing at 0° and 30° model incidences through sideslip angles from -15° to $+5^\circ$. The aerodynamic forces and moments acting on the model were measured with a 1-inch-diameter, six-component, strain-gage balance maintained at room temperature by a circulating water jacket.

Model

The details of the model, dimensionless with respect to the reference 1-foot length, are shown in figure 1. The present model is the same 12-inch model reported in reference 3 but modified to the M2-F2 configuration by the addition of the boattail afterbody and the alteration of the rudders and lower pitch flap. Photographs in figures 2 and 3 show details of the model, including the boattail addition, the simulated flared rudders, the 0° and 30° incidence mounts, and two representative canopies which were also investigated. Further details of these canopies are shown in figure 4. Unless otherwise specified, the aerodynamic measurements presented in this report are for the model without the canopy.

Precision

The test Mach numbers are considered to be accurate within limits of ± 0.03 at $M = 5.2$ and within ± 0.05 at $M = 7.4$ and 10.4 . The dimensionless aerodynamic coefficients are considered accurate within ± 2 percent at $M = 5.2$ and within ± 3 percent at $M = 7.4$ and 10.4 . The angles of attack and sideslip are accurate within $\pm 0.2^\circ$, which uncertainty is included in the preceding quoted accuracies for the coefficients. The deflection angles of the controls are accurate within $\pm 0.3^\circ$.

PRESENTATION OF RESULTS

The order of presentation of the results is summarized here and in table I. The experimental results are first introduced in their entirety here and then are discussed in detail in the discussion section of the report. Finally, empirical equations for the longitudinal characteristics and numerical values for the lateral-directional parameters are presented in the appendix for use in future simulator studies.

Longitudinal Characteristics

The lift coefficients, pitching moment coefficients, and lift-drag ratios for the basic model (canopy removed) with 0° and 25° rudder flare are presented in figures 5, 6, and 7 for the three test Mach numbers of 5.2, 7.4, and 10.4, respectively. The corresponding drag polars are presented in figure 8. These data (figs. 5 through 8) are for the model with 0° flap and identify the maximum trimmed angles of attack and the untrimmed conditions throughout the lower angles of attack.

Figures 9 through 12 present the effects of pitch-flap deflection on the longitudinal characteristics and show the conditions for longitudinal trim. Included in figures 6, 8(b), and 12(b) are the test results for the model with fins removed, and with both the fins and the boattail addition removed. The effects of adding the large and the small canopies are shown in figure 13 for $M = 5.2$ and in figure 14 for $M = 10.4$. Figure 15 summarizes the longitudinal aerodynamic characteristics at trim and includes the drag due to lift for the model longitudinally trimmed and untrimmed.

Lateral-Directional Stability

The variations of yawing-moment and rolling-moment coefficients with sideslip angle for an angle of attack of 0° are shown in figures 16, 17, and 18 for the model with several different rudder flare angles, in figure 19 for the model with the large canopy, and in figure 20 for the model with the small canopy. Two sets of yawing-moment and rolling-moment coefficients are shown for the model at 30° angle of attack in figures 21 through 28, one set being referenced to the body axes and the other to the stability axes. Results for the model with several rudder flare angles comprise figures 21 through 26,

while figures 27 and 28 show the effects of adding the canopies at 10.4 Mach number. A summary of the effects of rudder flare on static directional and lateral stabilities is presented in figure 29, which includes theoretical estimates for comparison with experiment.

Differential-Rudder Characteristics

The yawing-moment and rolling-moment coefficients for the model with differentially deflected rudders are presented in figures 30 and 31 for sideslip tests at 0° angle of attack and in figures 32 and 33 for 30° angle of attack. The yawing-moment and rolling-moment coefficients at 0° sideslip throughout the test range of angles of attack are shown in figures 34 and 35 for Mach numbers of 7.4 and 10.4, respectively.

Side-Force Coefficients

The variations of side-force coefficient with sideslip angle for model angles of attack of 0° and 30° and for several different rudder flare angles are presented in figure 36. Side-force coefficients for the model with the large canopy and with the small canopy are shown in figure 37.

Body-Alone Lateral-Directional Characteristics

The yawing-moment, rolling-moment, and side-force coefficients for the model with and without the fins and rudders are shown in figures 38 and 39.

DISCUSSION

Lift

The lift curves for the model with the flap retracted were almost linear between angles of attack of 0° and 30° (figs. 5(a), 6(a), 7(a)). As the deflection angle of the pitch flap was increased, there was an increase in the slope of the lift curves corresponding to fixed flap settings (figs. 9, 10, 11). Interestingly enough, however, the trimmed lift curve (fig. 15(b)) had the same 0.011 per degree slope as the model with the flap retracted (figs. 5, 6, 7).

The highest lift coefficients measured near 45° angle of attack were 0.45 at $M=7.4$ (fig. 6(a)) and 0.48 at $M=5.2$ and 10.4 (figs. 5(a), 7(a)). The maximum trimmed lift coefficient varied from 0.44 at $M=10.4$ to 0.42 at $M=5.2$; these values reflect the corresponding reduction in maximum trim angle of attack from 37° to 33° . (Somewhat higher trimmed lift coefficients and greater angles of attack would result with a reference moment center closer to the neutral point, but this would, of course, entail a reduction in the static margin.)

The angle of attack for zero lift for the untrimmed model with the flap retracted was approximately -6° (figs. 5(a), 6(a), 7(a)). Deflecting the flap 60° produced trim very close to zero lift near $\alpha = -7^\circ$ at $M = 5.2$ (fig. 9). Trimmed zero lift was not quite reached with the 60° flap deflection at the two higher test Mach numbers (figs. 10(a), 11(a)).

Drag

The minimum drag coefficients for the M2-F2 model with various rudder and flap settings and with each of the two (large and small) canopies are as follows:

Mach number	Reynolds number, million	Canopy	Rudder flare, deg	Pitch flap, deg	$C_{D_{min}}$
5.2	0.9	Off	0	0	0.065
	0.9	Off	25	0	.074
	0.9	Off	25	45	.077
	0.9	Off	25	60	.081
	0.9	Large	25	60	.088
	0.9	Small	25	60	.086
7.4	1.6	Off	0	0	.061
	1.6	Off	25	0	.069
	1.4	Off	25	45	.073
	1.4	Off	25	60	.076
10.4	0.7	Off	0	0	.067
	0.7	Off	25	0	.072
	0.7	Off	25	45	.069
	0.7	Off	25	60	.075
	0.7	Large	25	60	.076
	0.6	Small	25	60	.076

The minimum drags generally occurred within $\pm 1^\circ$ of -4° angle of attack.

The variations of drag coefficient with lift coefficient (fig. 8) were very nearly parabolic for angles of attack up to 30° and lift coefficients to 0.4. This parabolic relationship, previously noted for the M2 shape in reference 3, is exemplified here for the M2-F2 by the almost linear plots of drag coefficient versus the square of the lift coefficient as shown in figure 15(a). It was pointed out earlier that the slopes of the trimmed and untrimmed ($\delta_f = 0^\circ$) lift curves were approximately equal. A similar relationship may be noted in figure 15(a) which indicates surprisingly close agreement between the drag due to lift for the trimmed model (symbols) and for the untrimmed model with the retracted flap (dashed lines).

~~CONFIDENTIAL~~

Lift-Drag Ratio

A lifting entry vehicle has the advantage of achieving favorable reductions in aerodynamic heating rate over the nose by flying at high lift coefficients during atmosphere entry (ref. 2), thus shifting the peak heating phase to increased altitudes. The attainment of high lift requires flight at higher angles of attack and subjects the vehicle's lower surface to greater windward exposure and increased local heating rates. The study in reference 8, however, indicates that the critical heating rate on the lower pitch flap decreases with increasing vehicle angle of attack because of the reduction in flap setting required for longitudinal trim.

The hypersonic lift characteristics of lifting bodies are similar to those exhibited by lifting surfaces of very low aspect ratio in that high angles of attack are required to develop maximum lift. As shown by the lift curves for both the untrimmed model (figs. 5(a), 6(a), 7(a)) and the trimmed model (figs. 9(a), 10(a), 11(a), 15(b)), achieving high lift coefficients requires angles of attack well beyond that for maximum lift-drag ratio. These angles of attack between $(L/D)_{\max}$ and $C_{L\max}$ define the so-called "backside" of the L/D curve, and here extend upward from approximately 10° .

As noted in reference 3 for the earlier M2, the present M2-F2 model also demonstrated an essentially linear reduction in lift-drag ratio with increasing angle of attack throughout the back side of the L/D curve. The maximum trimmed lift-drag ratio of 1.3 at 12° angle of attack decreased to 0.8 near 36° angle of attack (fig. 15(c)). The maximum value of 1.3 meets the original objective of providing a 1000 nautical-mile lateral-range capability, the approximate spacing between consecutive orbits at the latitudes of the United States.

Longitudinal Stability and Control

The highest trimmed angles of attack for the M2-F2 model with the flap retracted were 33° at $M=5.2$ and 37° at $M=7.4$ and 10.4 (fig. 15(d)). These angles were smaller than the 45° measured for the earlier M2 (ref. 3) which had the same reference moment center, but did not have the boattail addition.

The pitch flap provided an effective longitudinal trim capability over the angles of attack comprising the back side of the L/D curve and also down to zero lift (figs. 9, 10, 11). The 60° flap deflection was sufficient to achieve trimmed zero lift at $M=5.2$, but a slightly greater deflection would have been required at the other test Mach numbers. The flap deflection required for trim at $(L/D)_{\max}$ varied from 30° at $M=5.2$ to 38° at $M=10.4$.

The slopes at trim ($C_m = 0$) of the plots of normal-force coefficient versus pitching-moment coefficient for the several different pitch-flap settings (fig. 12) indicate that the longitudinal static margins (fig. 15(e)) were about 6 percent of the reference length near maximum lift-drag ratio and increased to values near 8 and 10 percent at the highest and lowest trim

~~CONFIDENTIAL~~

attitudes for all three Mach numbers. For any fixed flap setting, the untrimmed longitudinal stability increased with angle of attack because of the nonlinear pitching-moment characteristics (fig. 12).

Canopy

The most apparent effect of adding the large canopy to the model was the sizable reduction in negative trim angle of attack from -7° to -15° at $M=5.2$ with the flap deflected 60° (fig. 13(b)). The corresponding shift in trim angle of attack was only 2° at $M=10.4$ (fig. 14(b)). Adding the small canopy caused a minor trim change at $M=5.2$ but had a negligible effect at $M=10.4$. Neither canopy exerted any significant effect on the lift characteristics or on the maximum lift-drag ratios (figs. 13(a), (c), 14(a), (c)). As the angle of attack was increased, the canopies passed progressively into the leeward "shadow" of the nose and exerted a diminishing influence on the hypersonic aerodynamic characteristics in pitch and in sideslip. The addition of the large canopy at $\alpha = 0^\circ$ slightly decreased the directional stability from approximately 0.0040 (appendix A) to 0.0037 (fig. 19), but had no effect on $C_{n\beta}$ at $\alpha = 30^\circ$. The small canopy did not significantly reduce directional stability.

Lateral-Directional Reference Axes

Lateral-directional moment characteristics are usually presented for the body-axis system and generally suffice for studies of aircraft in the small angle-of-attack range ($\sim 10^\circ$) and when the principal axis is coincident with or very near the body longitudinal axis through the center of gravity. (The principal axis is that axis about which the minimum moment of inertia occurs and about which the aircraft tends to roll.) The principal axis of the M2-F2 configuration is inclined rearwardly downward with respect to the longitudinal body axis by an angle of about 7° for the present reference moment center (fig. 1). For higher locations of the center of gravity this angle is reduced. Because this inclination angle is reasonably small, the present experimental results for the body axes are considered representative of the characteristics about the principal axis. The more pertinent point in the present study is the very large range of angles of attack (approaching 40°). At the previously cited maximum trim angle of attack of 37° , the principal axis would be inclined 44° relative to the wind, considerably beyond the values characterizing conventional aircraft studies. To aid in interpreting the present experimental results, the rolling-moment and yawing-moment coefficients for the high angles of attack are shown for both the body axes and the stability axes. The body-axes results are considered more meaningful for assessing lateral control and response, while the stability-axes results should prove useful for studies relating to flight or to a simulator where orientation and response are sensed with respect to the horizon.

Lateral-Directional Stability

The most important point vividly demonstrated in the present plots of yawing-moment coefficient versus angle of sideslip (figs. 16 through 20 for $\alpha = 0^\circ$; figs. 21 through 28 for $\alpha = 30^\circ$) is the effectiveness of rudder flare in increasing hypersonic directional stability. Because of the difference in lever arms of the rolling and yawing moments produced by the rudders, rudder flare had relatively little effect on lateral stability as shown in the summary plot of figure 29. Another implication of these results is that rudder flare increased not only the directional stability, but also the ratio of directional to lateral stability, a parameter important in avoiding such dynamic problems as Dutch roll.

Theoretical estimates of the incremental effects of rudder flare on directional and lateral stability at an angle of attack of 0° are also shown in figure 29. Inviscid oblique-shock theory was used to estimate the loadings on the flared rudder surfaces, assuming the local Mach number at the rudder hinge line equal to the free-stream Mach number. There was good agreement at 5.2 Mach number (figs. 29(a), (b)) where the directional stability increased almost linearly with rudder flare. The inviscid theory underestimated the degree of nonlinearity and the peak stabilities measured for 35° rudder flare at the two higher Mach numbers (figs. 29(c) through (f)). This disagreement is attributed to the lack of the theory in accounting for the probable flow separation at the rudder hinge line and for the forward carry-over of flared-rudder loading on the upwind fin surface.

Principal-Axis Inclination and Lateral Control

It was previously pointed out that by flying at high lift coefficients, the lifting entry vehicle would encounter reduced aerodynamic heating rates during atmosphere entry (ref. 2). As the angle of attack and the principal-axis inclination are increased, however, an aerodynamically stable vehicle becomes incapable of performing pure roll maneuvers about its principal axis. To illustrate this point, consider the example of an abrupt 90° bank performed with a stable vehicle flying at a high angle of attack (e.g., the present M2-F2 at its maximum trim angle of attack of 37° , rolling about its 44° inclined principal axis). The important point is that the principal-axis inclination tends to convert to a large sideslip angle as the vehicle rolls toward the 90° bank angle. With the development of the large sideslip angle, there results a concurrent buildup of large, restoring, rolling, and yawing moments and an out-of-trim pitching moment. These counter-rolling and -yawing moments tend to be larger than the actuating rolling and yawing moments attainable with any reasonably sized aerodynamic roll control. Pure rolling motion is thus inhibited, and there results increased apparent lateral stability of the vehicle and excursions in both the angles of attack and of sideslip during attempted rolls. This apparent dilemma inhibiting rolling maneuvers, particularly at high angles of attack, may be circumvented by the use of differential rudder deflection which combines augmenting sideslip with dihedrally produced rolling moments acting in the desired roll direction, rather than oppositely as cited in the preceding "pure roll" maneuver. The rolling motion caused by

differential rudders (which has been demonstrated in flight and on a simulator) is not a one-degree-of-freedom roll but, rather, involves augmenting sideslip through the roll and a continual change in the orientation of the principal axis. This "coning" or constant angle-of-attack rolling motion of the principal axis is coupled to the sideslip response rate (which decreases as the coning angle and angle of attack are increased), and to the magnitude of the augmenting rolling moment prevailing at the trimmed sideslip angle.

Differential-Rudder Characteristics

The present experimental results for differential rudders indicate adequate rolling-moment coefficients at sideslip trim for 0° angle of attack (C_l between 0.003 and 0.007, figs. 30, 31) and larger values for 30° angle of attack (C_l between 0.010 and 0.017, fig. 32; C_{l_s} between 0.007 and 0.010, fig. 33).

The combined effects of differential rudder deflection on the sideslip angle for trim and on the degree of directional stability on each side of trim may be observed in figure 31. As the right-hand rudder having the 35° deflection became more windward, there was an increase in the directional stability. Conversely, as the 0° left rudder became more windward (at the large negative sideslip angles), there was a decrease in the directional stability. Thus the different slopes of the curves indicate different levels of stability on opposite sides of the trim points in sideslip (fig. 31) similar to the previously cited differences in longitudinal stability on opposite sides of the trim angle of attack (fig. 12).

The lateral-directional moment characteristics in sideslip (figs. 30 through 33) indicate adequate rudder effectiveness at angles of attack of 0° and 30° . The lateral-directional characteristics measured in pitch (figs. 34, 35) indicate rudder effectiveness at all angles of attack tested, but with reduced effectiveness around $\alpha = 5^\circ$ where the rudders were partially immersed in the body boundary layer. There was a small adverse rolling moment about the body axis in these measurements at $\beta = 0^\circ$, but this moment would be replaced by an augmenting rolling moment as the vehicle sought its trimmed sideslip angle (where $C_n = 0$).

Side-Force Coefficients

The only noteworthy features of the side-force coefficients were the increased values accompanying increased rudder flare angle (fig. 36) and increased angle of attack (appendix A).

Characteristics of Body Alone

The aerodynamic characteristics measured for the M2-F2 body (including the boattail addition) indicate that removing the fins and rudders had little effect on the longitudinal force characteristics (fig. 6) and on the lateral-moment and side-force characteristics (figs. 38, 39). The principal effects

~~CONFIDENTIAL~~

of removing the fins and rudders were to alter the longitudinal characteristics at negative angles of attack (fig. 6) and to render neutral directional stability about the body axes (fig. 38(a)). Removal of the fins and rudders did not significantly change the rolling-moment characteristics (figs. 38(b), 39(b)), because the lateral stability is derived primarily from the body pressure forces acting normal to the conical surface and converging to the body half-cone centerline, which is above the reference moment center (fig. 1).

CONCLUSIONS

The following hypersonic aerodynamic characteristics were indicated for the M2-F2 lifting entry configuration at the three test Mach numbers of 5.2, 7.4, and 10.4:

1. A trimmed, maximum lift-drag ratio of 1.3 near 12° angle of attack at a lift coefficient near 0.20,
2. A trimmed maximum lift coefficient near 0.45 with a corresponding lift-drag ratio of 0.8,
3. A longitudinal trim capability from zero lift to maximum lift using the lower pitch flap,
4. A longitudinal static margin near 6 percent of the reference length in the vicinity of $(L/D)_{\max}$; greater margins at lower and higher angles of attack,
5. Adequate lateral and directional stability including effective control of the level of directional stability and of the ratio of directional to lateral stability by the use of rudder flare,
6. Adequate lateral-directional control through the use of differential rudder deflection.

Ames Research Center

National Aeronautics and Space Administration

Moffett Field, Calif., 94035, June 3, 1968

124-07-02-22-00-21

~~CONFIDENTIAL~~

APPENDIX A

EMPIRICAL LONGITUDINAL AND TABULATED DIRECTIONAL CHARACTERISTICS

Empirical equations for the longitudinal aerodynamic parameters of the M2 were presented in reference 3 to assist computer and simulator studies. The following equations update these relations to fit the current M2-F2 results within ± 3 percent.

$$C_L = 0.060 + 0.011\alpha \quad (\text{fixed flap setting; } 0^\circ \leq \alpha \leq 30^\circ)$$

$$\text{trim } C_L = 0.075 + 0.011\alpha \quad (\text{varying flap setting; } 0^\circ \leq \alpha \leq 30^\circ)$$

$$C_D = 0.065 + 2.30 C_L^2 \quad (0^\circ \leq \alpha \leq 30^\circ)$$

$$L/D = 0.80 + 0.021 (36 - \alpha) \quad (10^\circ \leq \alpha \leq 45^\circ)$$

Values for the aerodynamic parameters in sideslip for the model without canopy and with 25° rudder flare are:

	α	M = 5.2	M = 7.4	M = 10.4
$C_{n\beta}$	0°	0.0040	0.0039	0.0041
$C_{l\beta}$	\downarrow	-.0022	-.0020	-.0018
$C_{Y\beta}$	\downarrow	-.0128	-.0125	-.0124
$C_{n\beta}$	30°	.0035	.0031	.0030
$C_{l\beta}$	\downarrow	-.0030	-.0030	-.0030
$C_{Y\beta}$	\downarrow	-.0180	-.0184	-.0195
$C_{n_{s\beta}}$	\downarrow	.0045	.0042	.0043
$C_{l_{s\beta}}$	\downarrow	-.0009	-.0011	-.0013

~~CONFIDENTIAL~~

REFERENCES

1. Eggers, Alfred J., Jr.: The Possibility of a Safe Landing. In: Space Technology, Howard S. Seifert, ed., John Wiley and Sons, Inc., 1959, pp. 13-01 to 13-53.
2. Chapman, Dean R.: An Approximate Analytical Method for Studying Entry Into Planetary Atmospheres. NASA TR R-11, 1959.
3. Axelson, John A.: Hypersonic Aerodynamic Characteristics of the Ames M-2 Lifting Entry Configuration. NASA TM X-1301, 1966.
4. Axelson, John A.: Pressure Distributions for the M-2 Lifting Entry Vehicle at Mach Numbers of 0.23, 5.2, 7.4, and 10.4. NASA TM X-997, 1964.
5. McKinney, Linwood W.; Boyden, Richmond P.; and Taylor, Robert T.: Investigation of the Aerial Launch Characteristics of the M2-F2 Launched From a Preliminary Location on the B-52 Airplane. NASA TM X-1225, 1966.
6. Mort, Kenneth W.; and Gamse, Berl: Low-Speed Wind Tunnel Tests of a Full-Scale M2-F2 Lifting Body Model. NASA TM X-1347, 1967.
7. Mort, Kenneth W.; and Gamse, Berl: Full-Scale Wind Tunnel Investigation of the Aerodynamic Characteristics of the M2-F2 Lifting Body Vehicle. NASA TM X-1588, 1968.
8. Seegmiller, H. Lee: Convective Heat Transfer to the Ames M2 and M2-F2 Lifting Entry Configurations. NASA TM X-1691, 1968.

~~CONFIDENTIAL~~

TABLE I.- DATA SUMMARY

Figure	Parameter	M	Flap setting, deg	Rudder flare, deg	Canopy	Additional
(a) Longitudinal aerodynamic characteristics (α variable, $\beta = 0^\circ$)						
5(a) (b) (c)	C_L vs. α C_m vs. α L/D vs. α	5.2	0	0,25	Off	Body included
6(a) (b) (c)	C_L vs. α C_m vs. α L/D vs. α	7.4	0	0,25	Off	
7(a) (b) (c)	C_L vs. α C_m vs. α L/D vs. α	10.4	0	0,25	Off	
8(a) (b) (c)	C_L vs. C_D	5.2 7.4 10.4	0	0,25	Off	Body included
9(a) (b) (c)	C_L vs. α C_m vs. α L/D vs. α	5.2	0,15,25, 35,45,60	25	Off	
10(a) (b) (c)	C_L vs. α C_m vs. α L/D vs. α	7.4	0,15,25, 35,45,60	25	Off	
11(a) (b) (c)	C_L vs. α C_m vs. α L/D vs. α	10.4	0,15,25, 35,45,60	25	Off	Body included
12(a) (b) (c)	C_m vs. C_N	5.2 7.4 10.4	0,15,25, 35,45,60	25	Off	
13(a) (b) (c)	C_L vs. α C_m vs. α L/D vs. α	5.2	60	25	Large & small	
14(a) (b) (c)	C_L vs. α C_m vs. α L/D vs. α	10.4	60	25	Large & small	Trimmed
15(a) (b) (c) (d) (e)	C_D vs. C_L^2 C_L vs. α L/D vs. α δ_F vs. α dC_m/dC_N vs. α	5.2,7.4, 10.4	0,15,25, 35,45,60	0,25 25	Off	

TABLE I.- DATA SUMMARY - Continued

Figure	Parameter	M	α	Flap setting, deg	Rudder flare, deg	Canopy
(b) Lateral-directional aerodynamic characteristics						
16(a) (b)	C_n vs. β C_l vs. β	5.2	0	60	0,25,35	Off
17(a) (b)	C_n vs. β C_l vs. β	7.4	0	60	0,15, 25,35	Off
18(a) (b)	C_n vs. β C_l vs. β	10.4	0	60	0,15, 25,35	Off
19(a) (b)	C_n vs. β C_l vs. β	5.2,7.4, 10.4	0	60	25	Large
20(a) (b)	C_n vs. β C_l vs. β	5.2,7.4, 10.4	0	60	25	Small
21(a) (b)	C_n vs. β C_l vs. β	5.2	30	15	0,25	Off
22(a) (b)	C_{n_s} vs. β C_{l_s} vs. β	5.2	30	15	0,25	Off
23(a) (b)	C_n vs. β C_l vs. β	7.4	30	15	0,15, 25,35	Off
24(a) (b)	C_{n_s} vs. β C_{l_s} vs. β	7.4	30	15	0,15, 25,35	Off
25(a) (b)	C_n vs. β C_l vs. β	10.4	30	0	0,15, 25,35	Off
26(a) (b)	C_{n_s} vs. β C_{l_s} vs. β	10.4	30	0	0,15, 25,35	Off
27(a) (b)	C_n vs. β C_l vs. β	10.4	30	35	25	Large & small
28(a) (b)	C_{n_s} vs. β C_{l_s} vs. β	10.4	30	35	25	Large & small

TABLE I.- DATA SUMMARY - Continued

Figure	Parameter	M	α	Flap setting, deg	Rudder flare, deg	Canopy
(b) Lateral-directional aerodynamic characteristics						
29(a)	Dir. Stab.	5.2	0,30	60,15	0,15,	Off
(b)	Lat. Stab.				25,35	
(c)	Dir. Stab.	7.4	0,30	60,15	0,15,	Off
(d)	Lat. Stab.				25,35	
(e)	Dir. Stab.	10.4	0,30	60,0	0,15,	Off
(f)	Lat. Stab.				25,35	
30(a)	C_n vs. β	5.2,7.4,	0	60	Left 15,	Off
(b)	C_l vs. β	10.4			right 35	
31(a)	C_n vs. β	5.2,7.4,	0	60	Left 0,	Off
(b)	C_l vs. β	10.4			right 35	
32(a)	C_n vs. β	5.2,7.4,	30	15,0	Left 15,	Off
(b)	C_l vs. β	10.4			right 35	
33(a)	C_{n_s} vs. β	5.2,7.4,	30	15,0	Left 15,	Off
(b)	C_{l_s} vs. β	10.4			right 35	
34(a)	C_n, C_{n_s} vs. α	7.4	Variable	45,25	Left 15,	Off
(b)	C_l, C_{l_s} vs. α				right 35	
35(a)	C_n, C_{n_s} vs. α	10.4	Variable	60,45,0	Left 15,	Off
(b)	C_l, C_{l_s} vs. α				right 35	
36(a)	C_Y vs. β	5.2	0	60	0,25,35	Off
(b)			30	15	0,25	
(c)		7.4	0	60	0,15,	
(d)			30	15	25,35	
(e)		10.4	0	60		
(f)			30	0		
37(a)	C_Y vs. β	5.2,7.4,	0	60	25	Large
(b)		10.4				
(c)		5.2,7.4,	0	60		Small
		10.4				
		10.4	30	35		Large & small

[REDACTED]

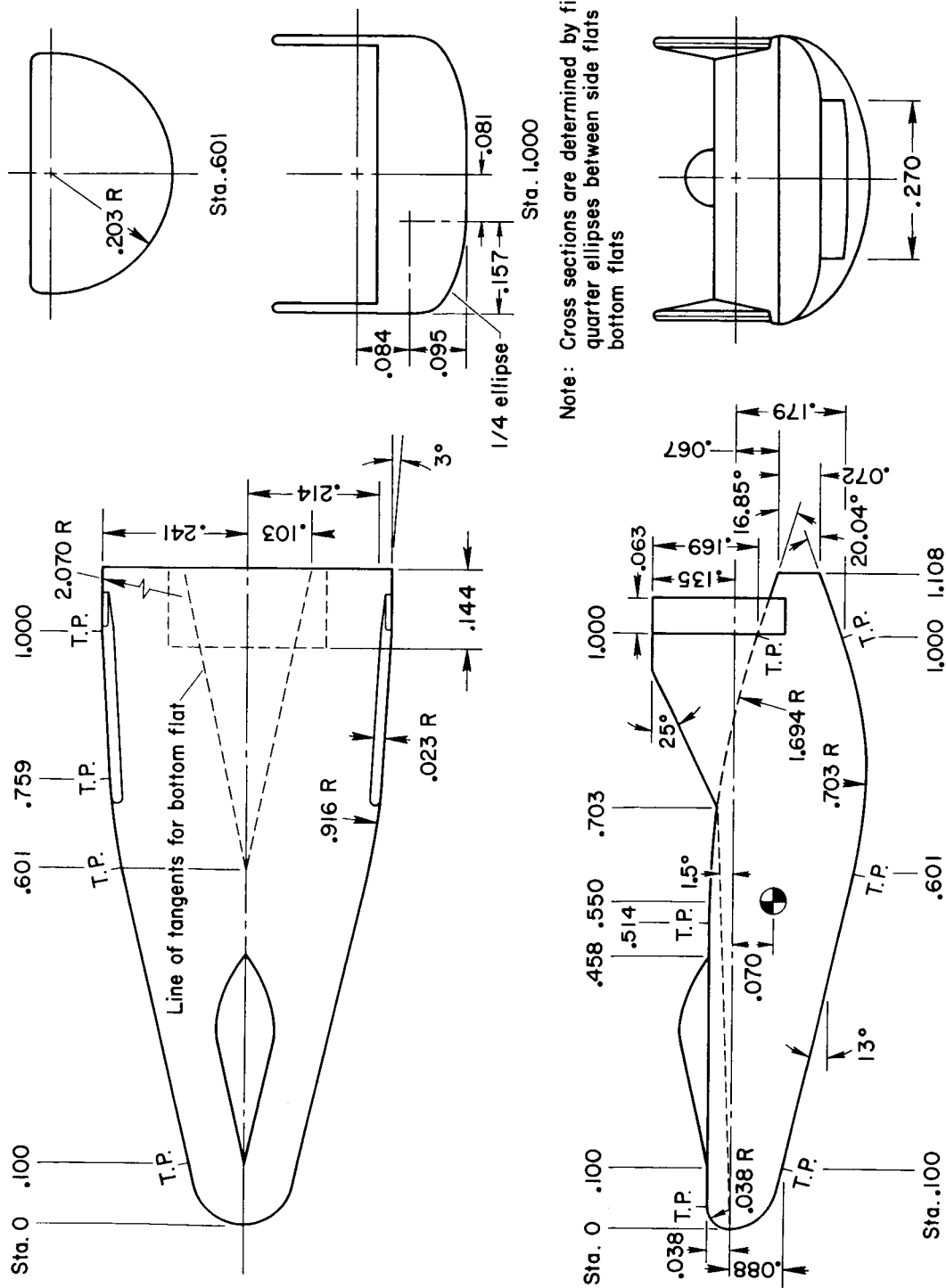
TABLE I. - DATA SUMMARY - Concluded

Figure	Parameter	M	α	Flap setting, deg	Rudder flare, deg	Canopy
(b) Lateral-directional aerodynamic characteristics						
38(a)	C_n vs. β	10.4	0	60,0	0 on & off	Off
(b)	C_l vs. β					
(c)	C_Y vs. β					
39(a)	C_n, C_{n_s} vs. β	10.4	30	0	0 on & off	Off
(b)	C_l, C_{l_s} vs. β					
	C_Y vs. β					

~~CONFIDENTIAL~~

~~CONFIDENTIAL~~

CONFIDENTIAL



Note: Cross sections are determined by fitting quarter ellipses between side flats and bottom flats

Note: All dimensions based on original model length λ

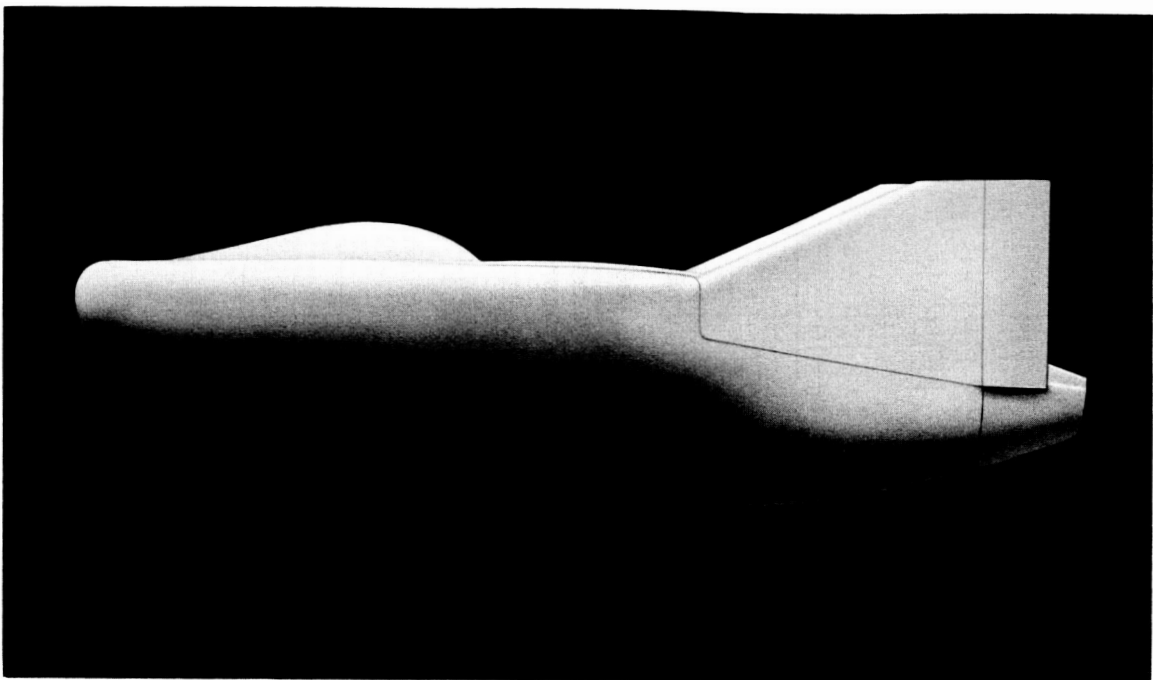
Present tests: $\lambda = 30.48 \text{ cm (12.00 in.)}$

Equation for nose shape:

$$\frac{z}{\lambda} = 386 \sqrt{\frac{x}{\lambda}} - .124 \frac{x}{\lambda} - 4.084 \left(\frac{x}{\lambda}\right)^2 + 18.702 \left(\frac{x}{\lambda}\right)^3$$

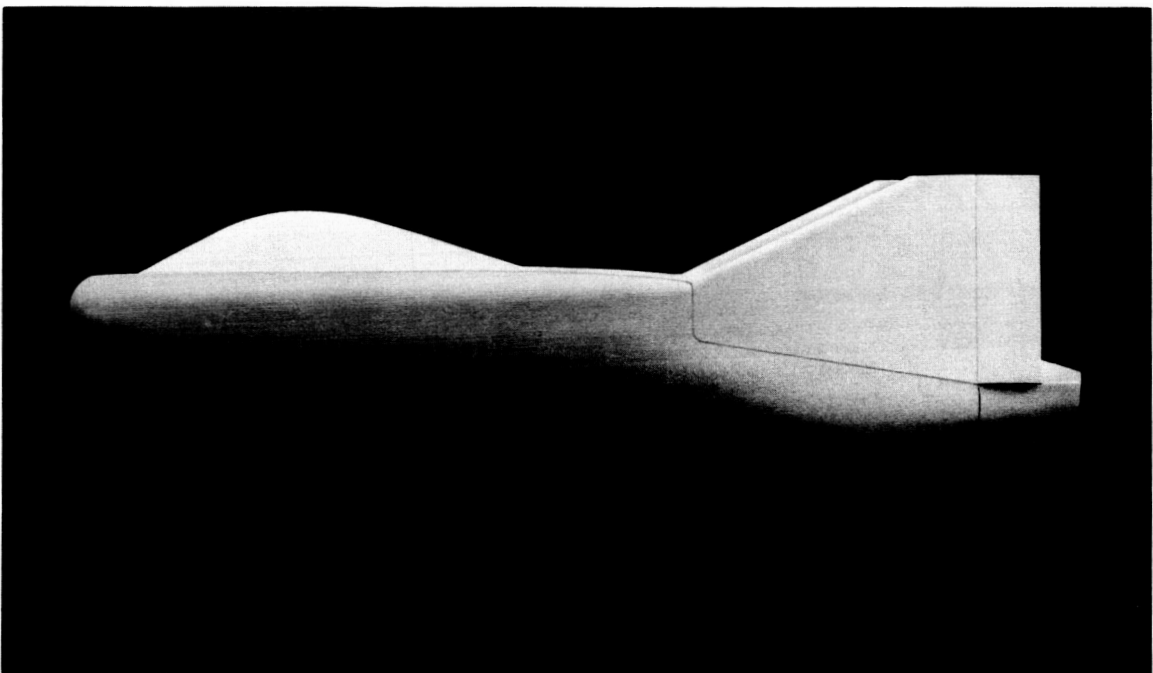
Figure 1.- Sketch of the M2-F2 model.

~~CONFIDENTIAL~~



(a) Small canopy.

A-36842

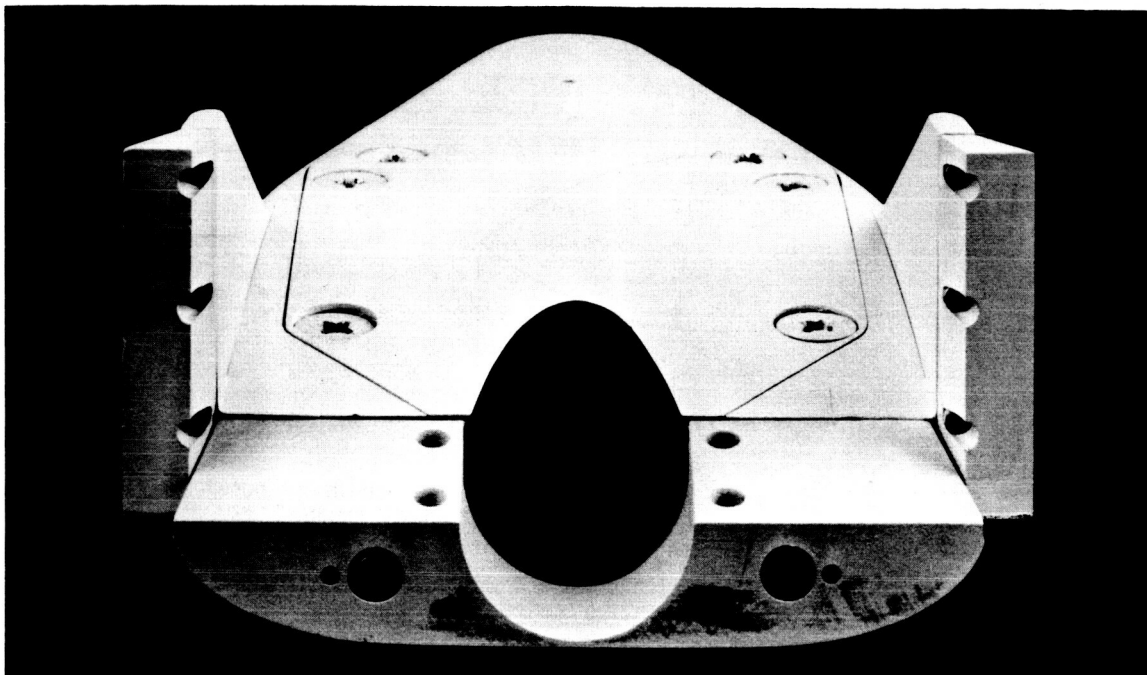


(b) Large canopy.

A-36843

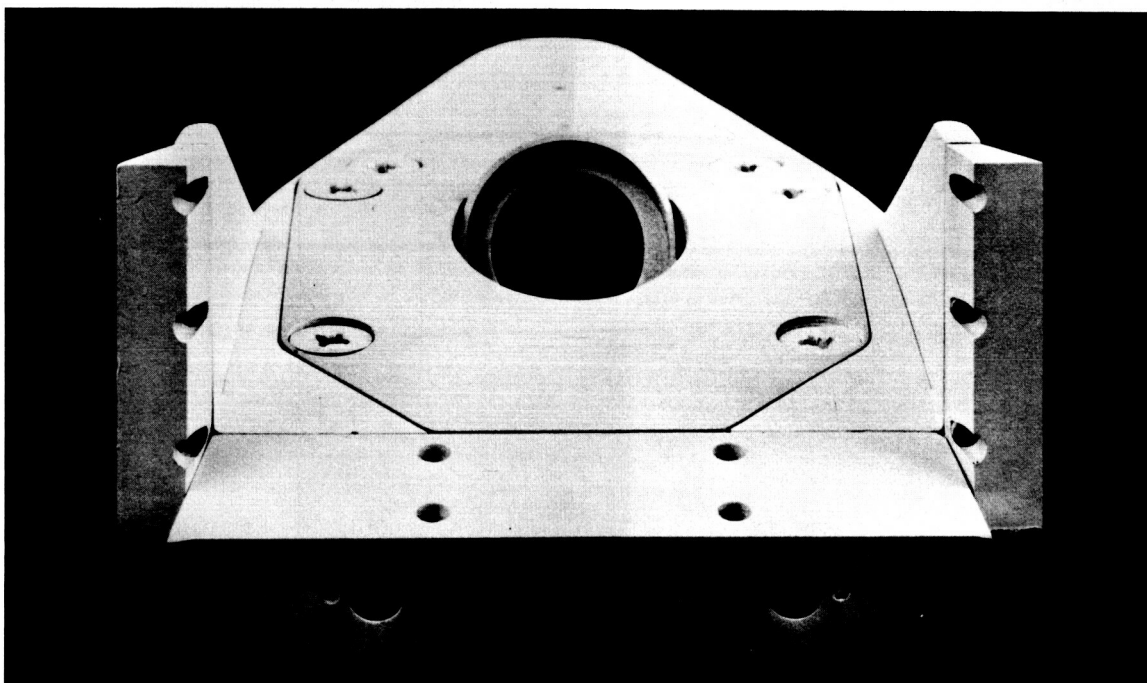
Figure 2.- Side views of the M2-F2 model with the large and small canopies.

~~CONFIDENTIAL~~



(a) 0° incidence mount.

A-36839



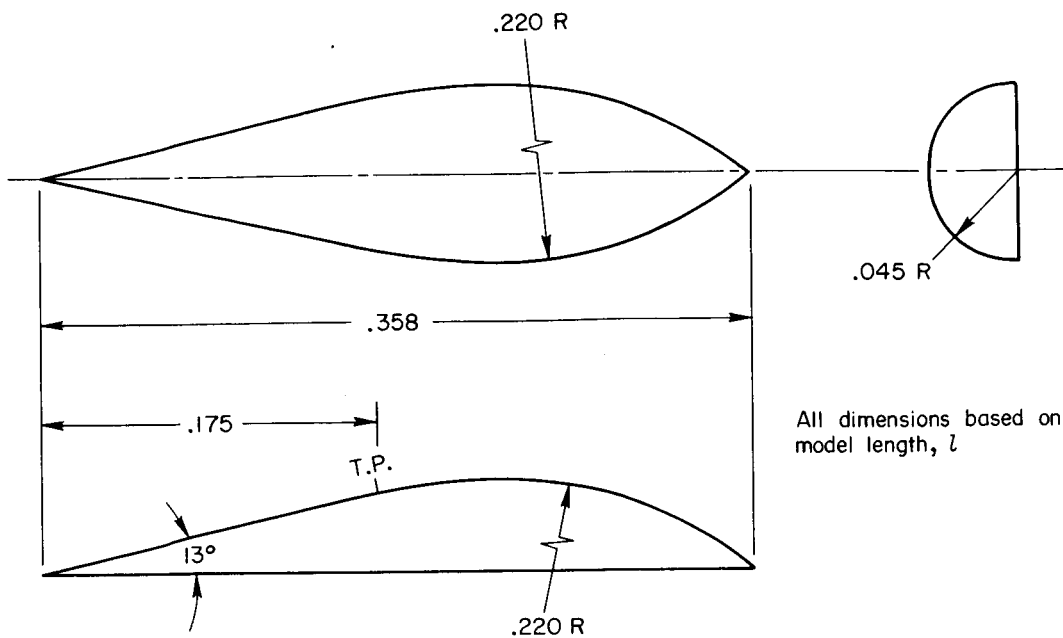
(b) 30° incidence mount.

A-36841

Figure 3.- Rear views of the M2-F2 model.

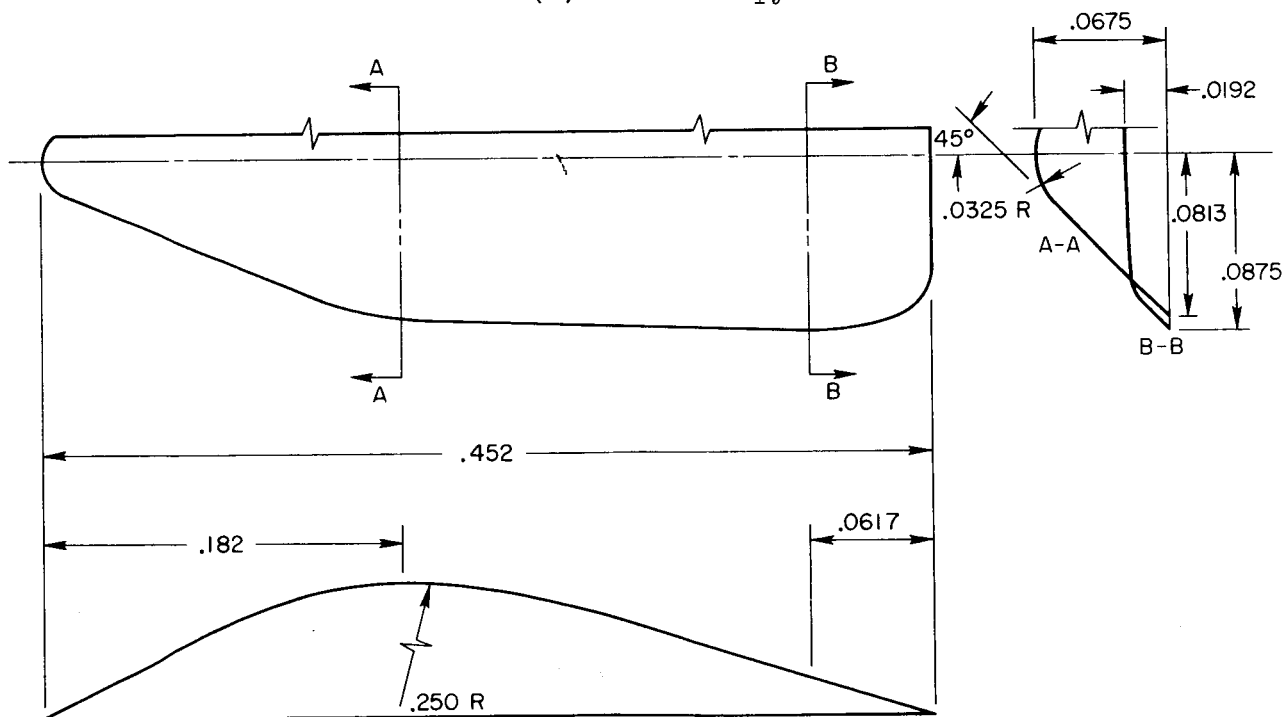
~~CONFIDENTIAL~~

CONFIDENTIAL



All dimensions based on model length, l

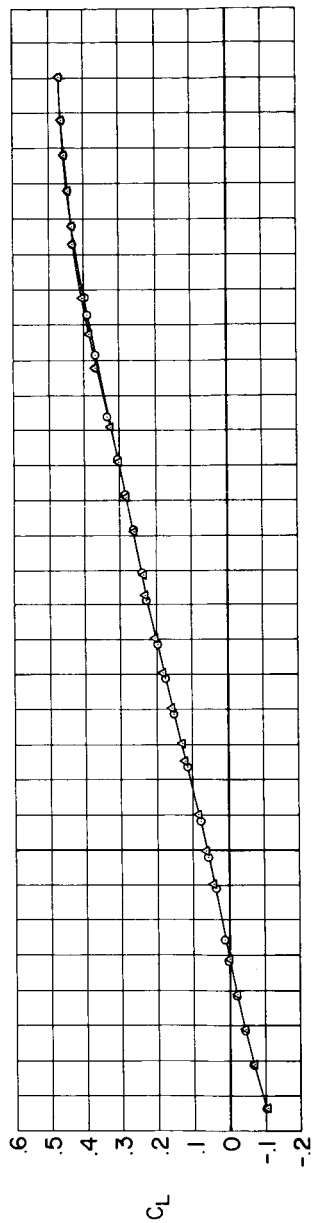
(a) Small canopy.



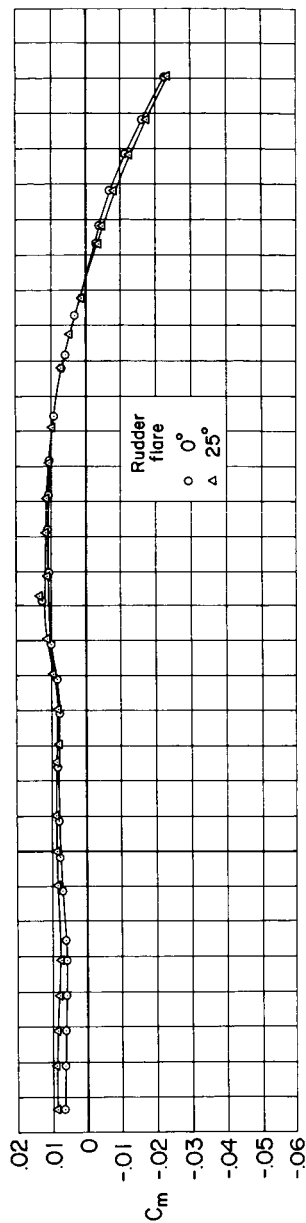
(b) Large canopy.

Figure 4.- Canopy details.

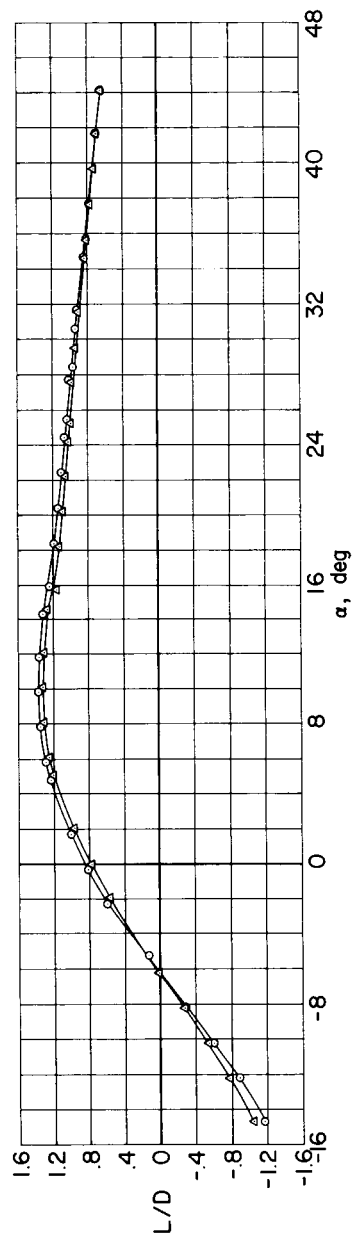
CONFIDENTIAL



(a) Lift coefficient.

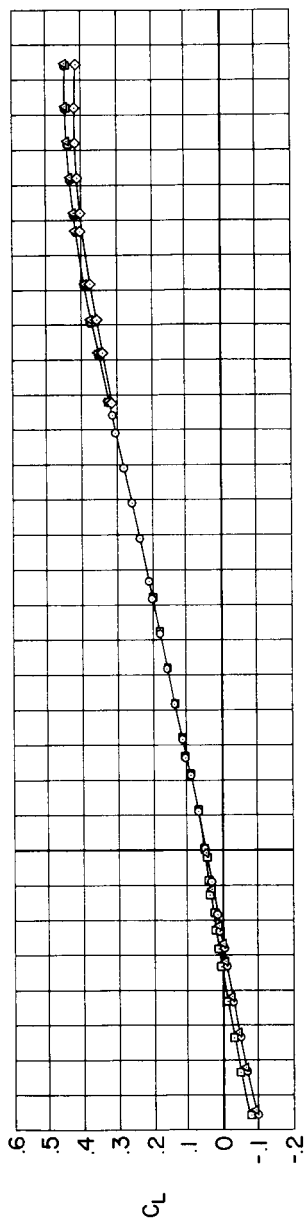


(b) Pitching-moment coefficient.

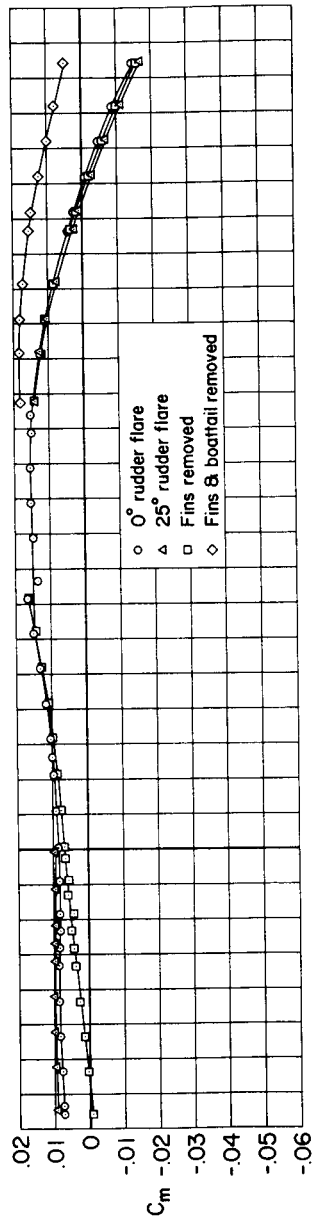


(c) Lift-drag ratio.

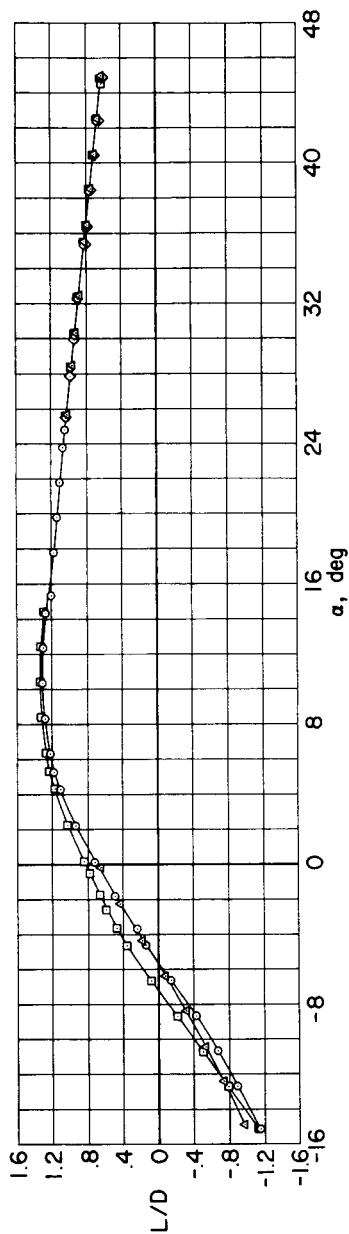
Figure 5.- Variations with angle of attack of the longitudinal aerodynamic characteristics for the M2-F2 model with rudder flares of 0° and 25° ; $M = 5.2$, $\delta_f = 0^\circ$.



(a) Lift coefficient.



(b) Pitching-moment coefficient.

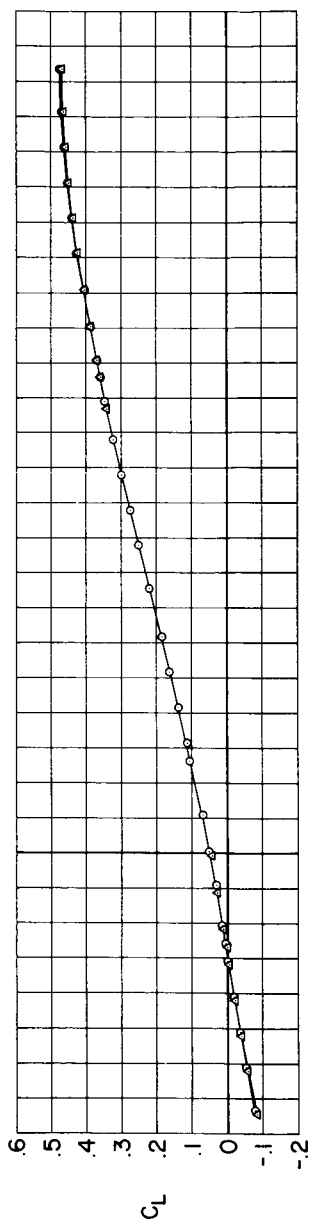


(c) Lift-drag ratio.

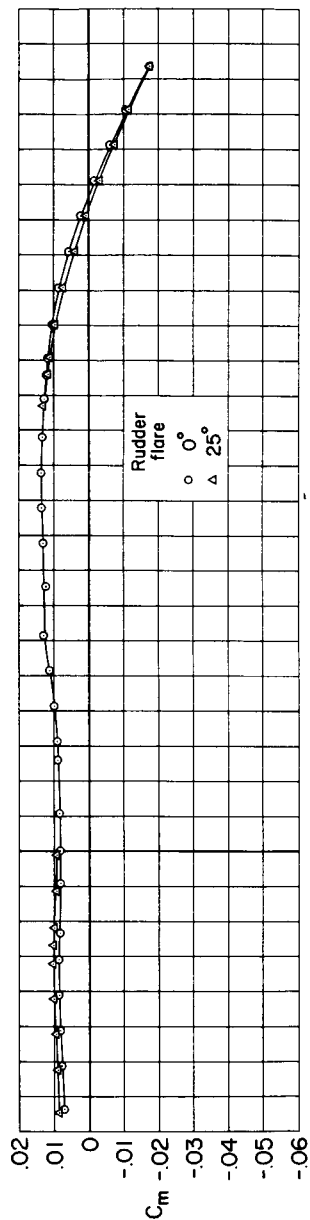
Figure 6.- Variations with angle of attack of the longitudinal aerodynamic characteristics of the M2-F2 model with rudder flares of 0° and 25° and of the body less fins with and without the boattail addition; $M = 7.4$, $\delta_f = 0^\circ$.

CONFIDENTIAL

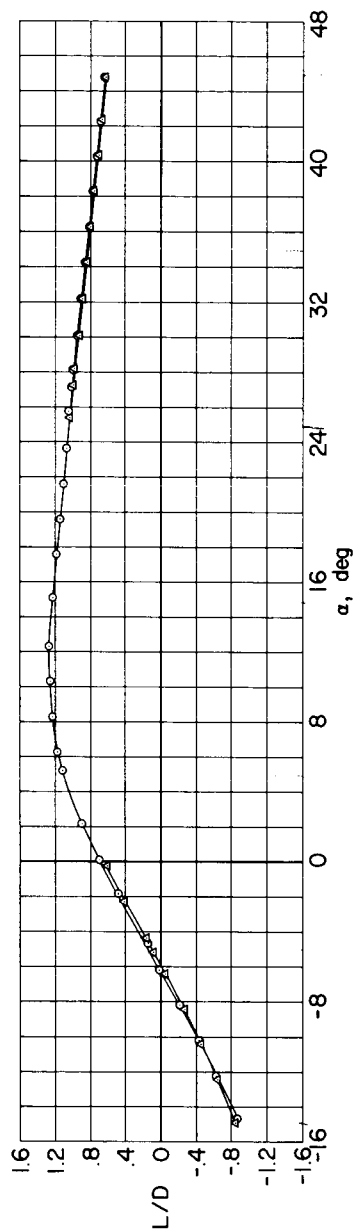
CONFIDENTIAL



(a) Lift coefficient.

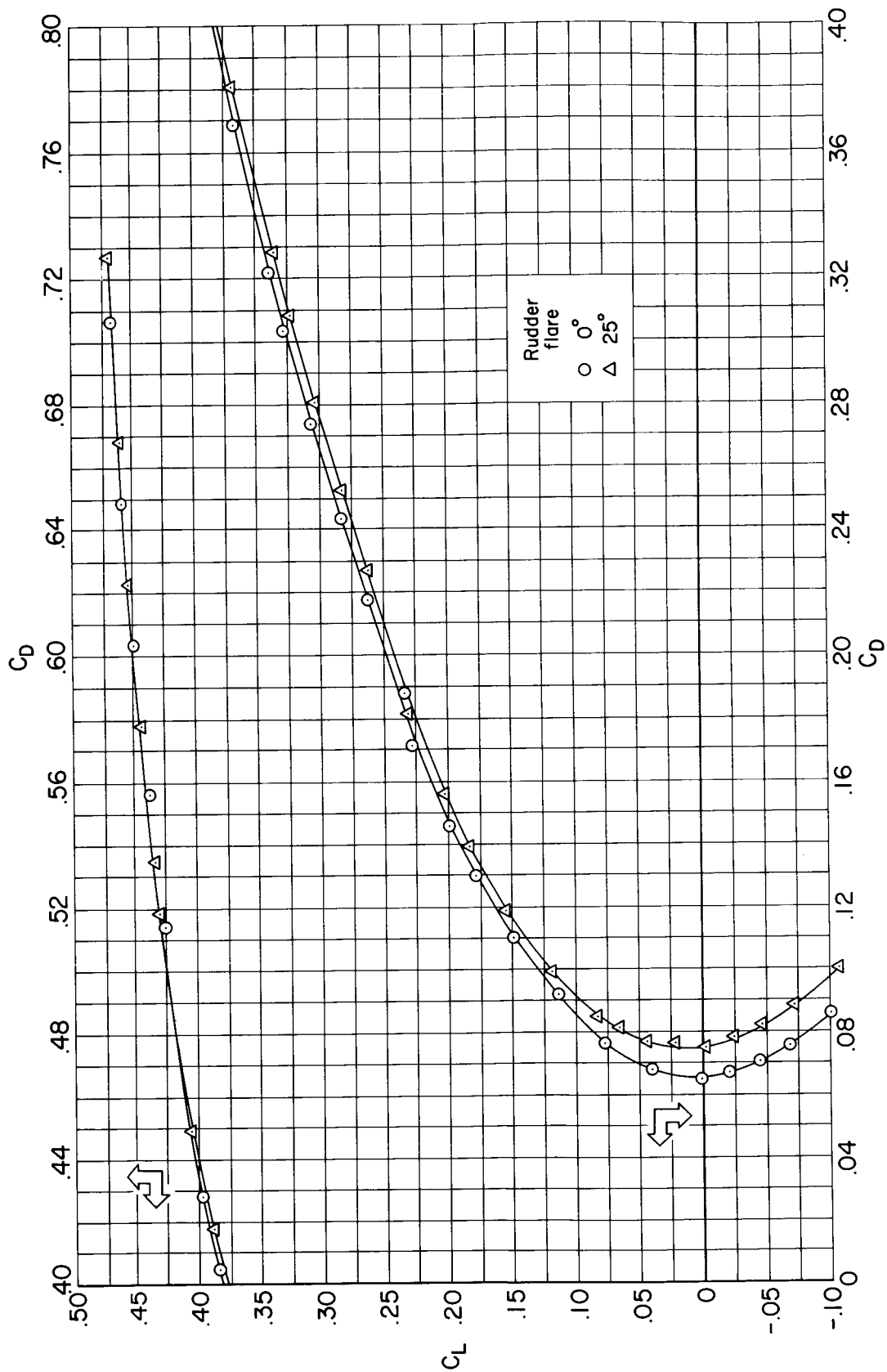


(b) Pitching-moment coefficient.



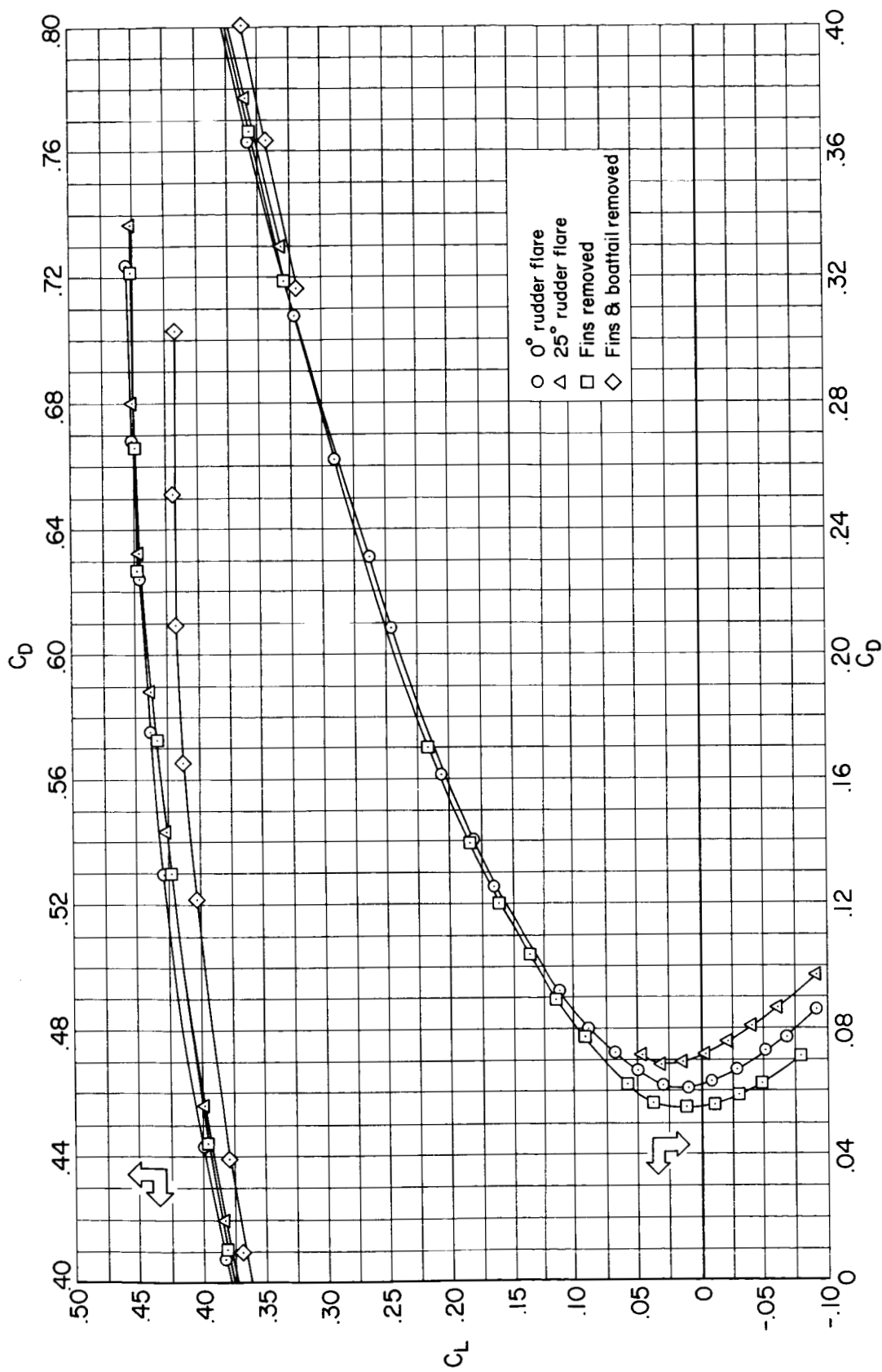
(c) Lift-drag ratio.

Figure 7.- Variations with angle of attack of the longitudinal aerodynamic characteristics for the M2-F2 model with rudder flares of 0° and 25°; $M = 10.4$, $\delta_f = 0^\circ$.



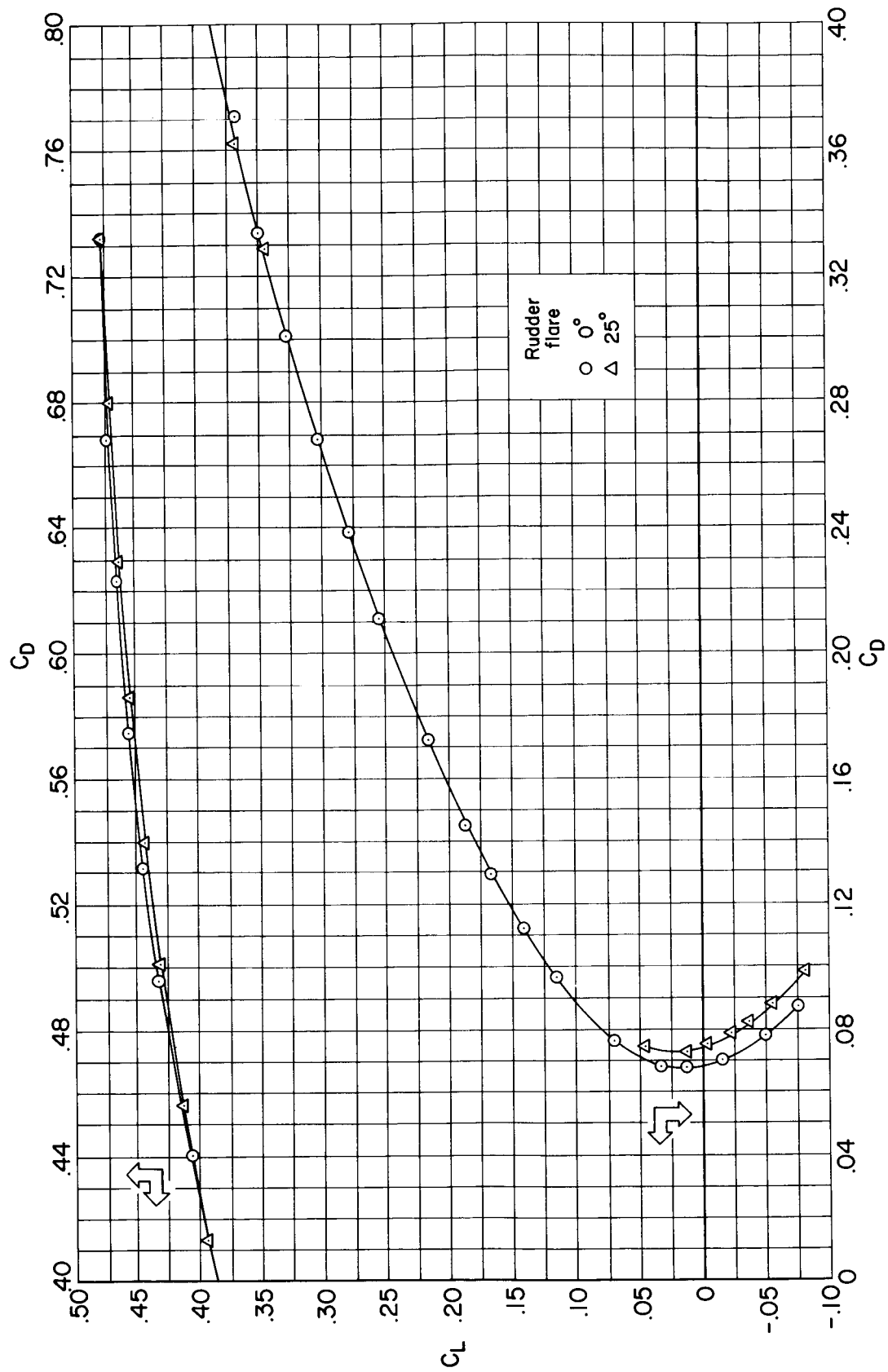
(a) $M = 5.2$

Figure 8.- Variations of drag coefficient with lift coefficient for the M2-F2 model with rudder flares of 0° and 25° ; $\delta f = 0^\circ$.



(b) $M = 7.4$

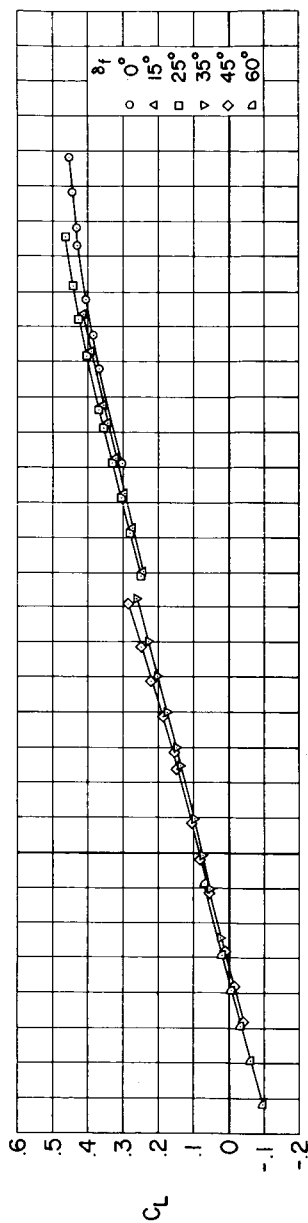
Figure 8.- Continued.



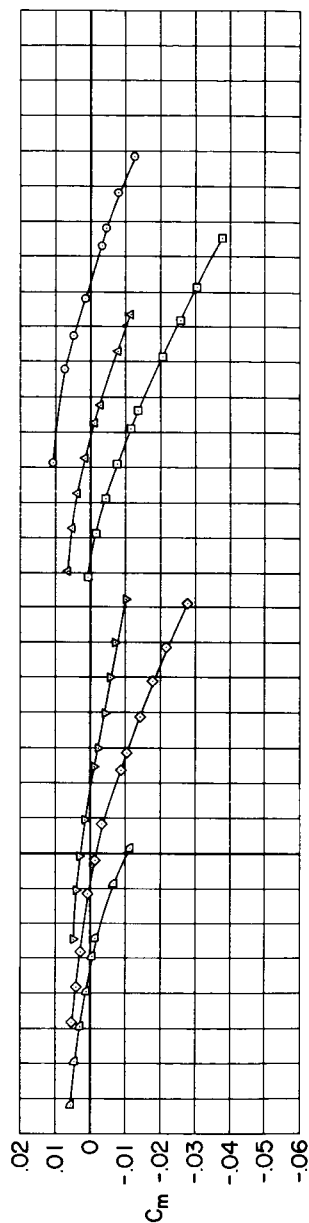
(c) $M = 10.4$

Figure 8.- Concluded.

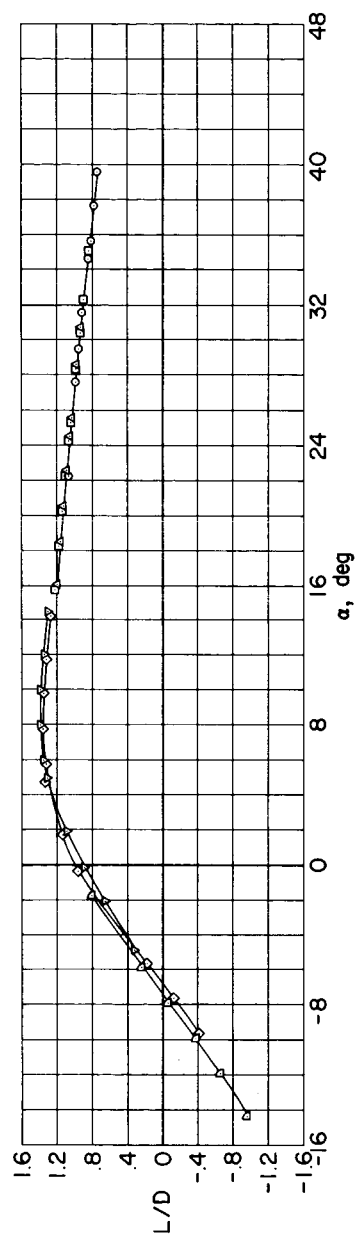
CONFIDENTIAL



(a) Lift coefficient.

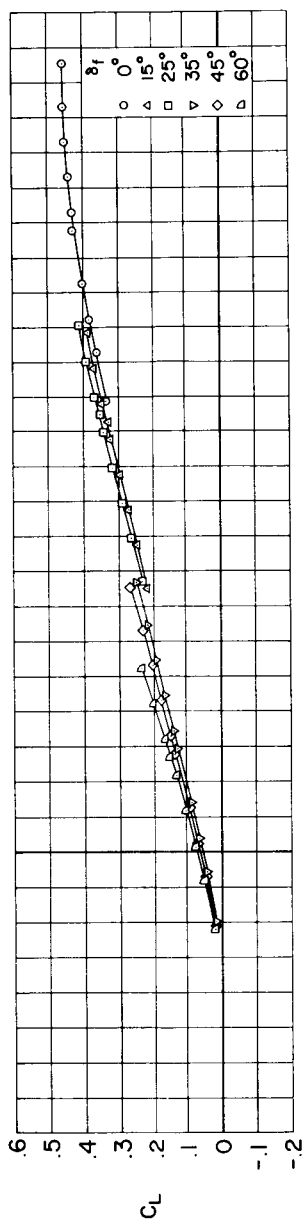


(b) Pitching-moment coefficient.

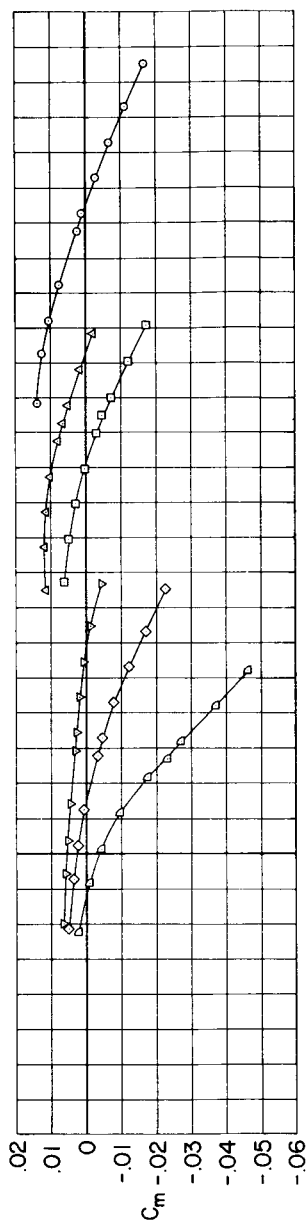


(c) Lift-drag ratio.

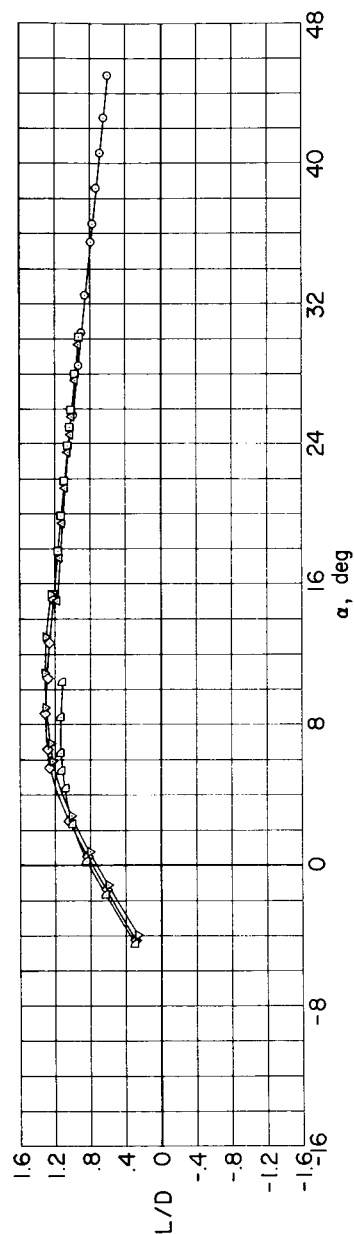
Figure 9.- Effects of pitch-flap deflection on the variations with angle of attack of the longitudinal aerodynamic characteristics of the M2-F2 model; 25° rudder flare, $M = 5.2$.



(a) Lift coefficient.

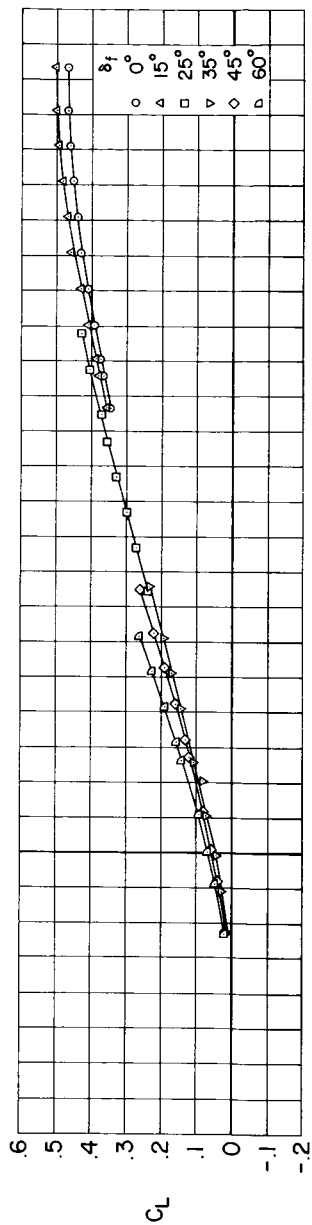


(b) Pitching-moment coefficient.

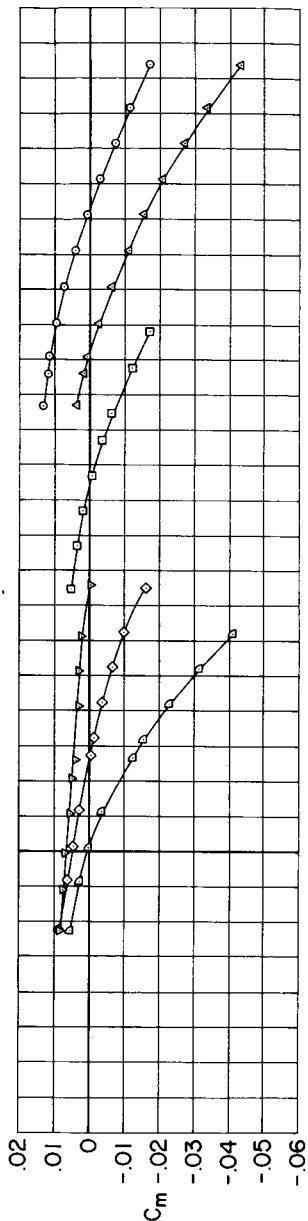


(c) Lift-drag ratio.

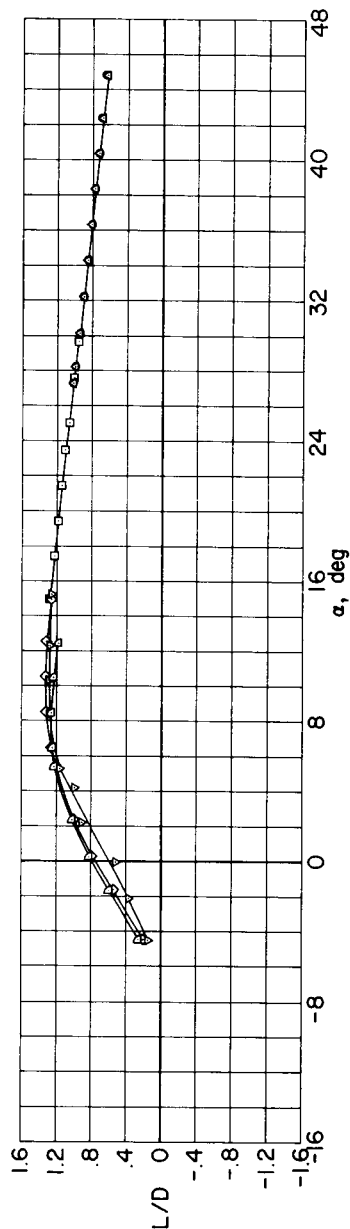
Figure 10.- Effects of pitch-flap deflection on the variations with angle of attack of the longitudinal aerodynamic characteristics of the M2-F2 model; 25° rudder flare, $M = 7.4$.



(a) Lift coefficient.

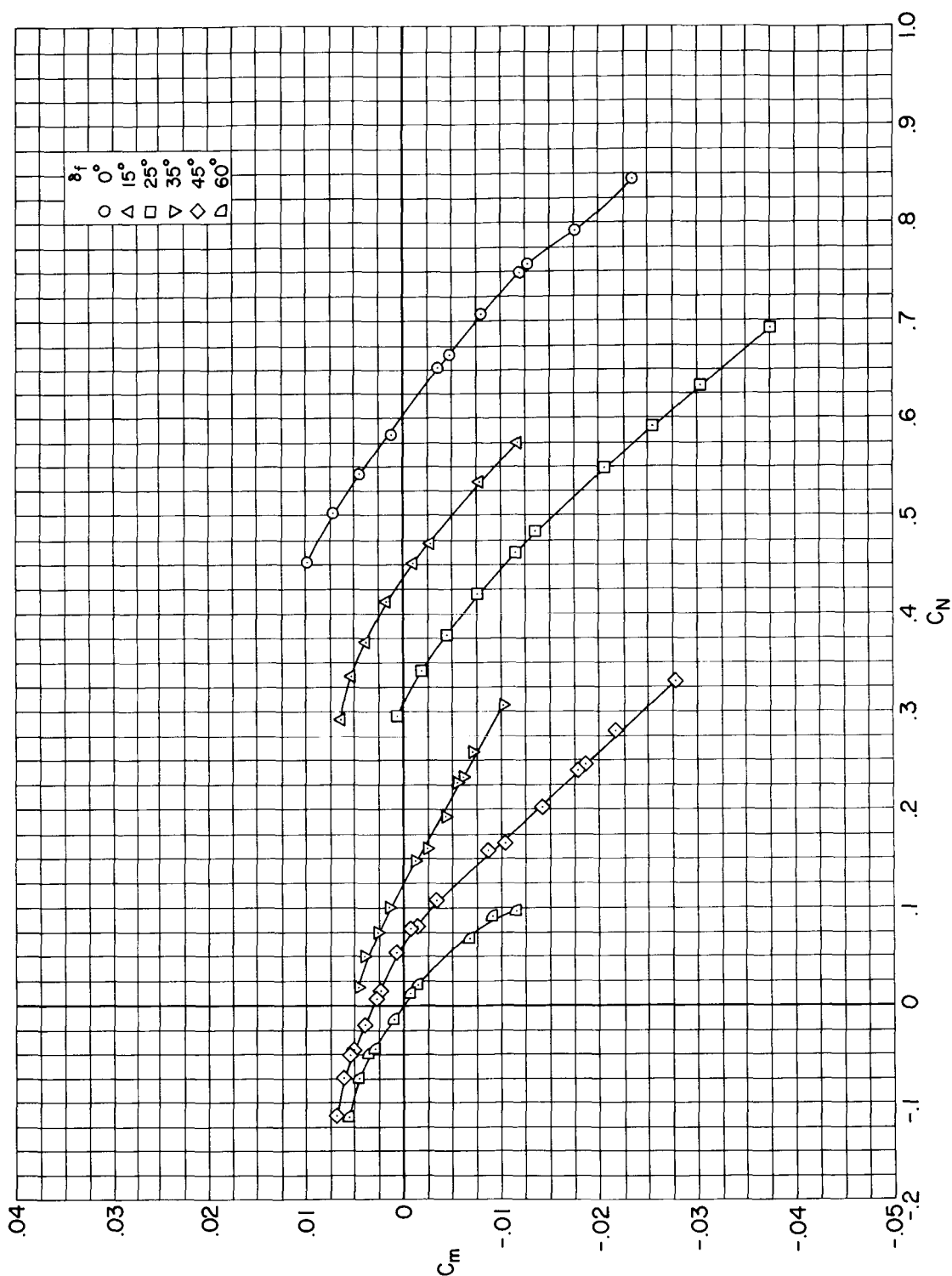


(b) Pitching-moment coefficient.



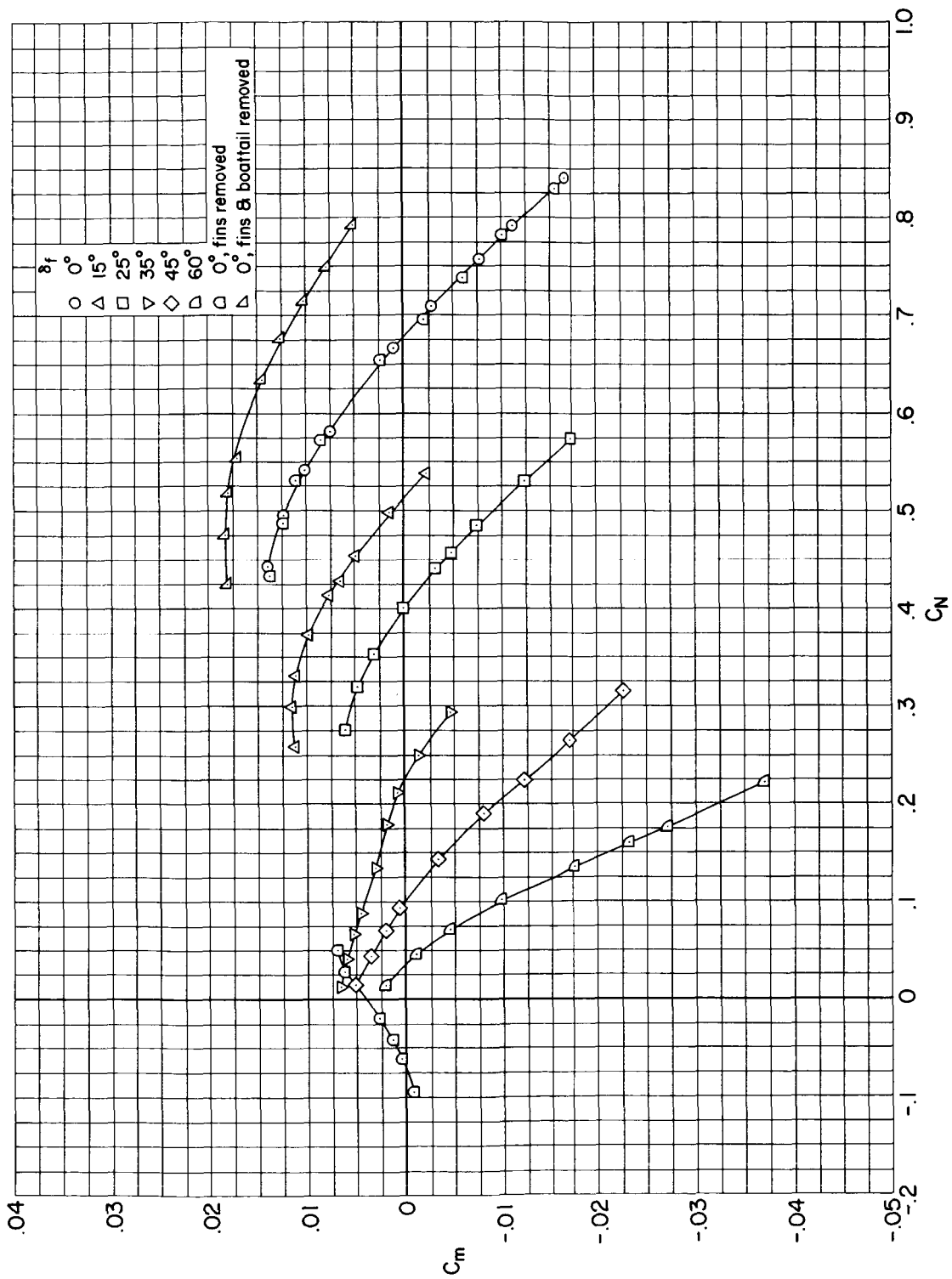
(c) Lift-drag ratio.

Figure 11.- Effects of pitch-flap deflection on the variations with angle of attack of the longitudinal aerodynamic characteristics of the M2-F2 model; 25° rudder flare, $M = 10.4$.



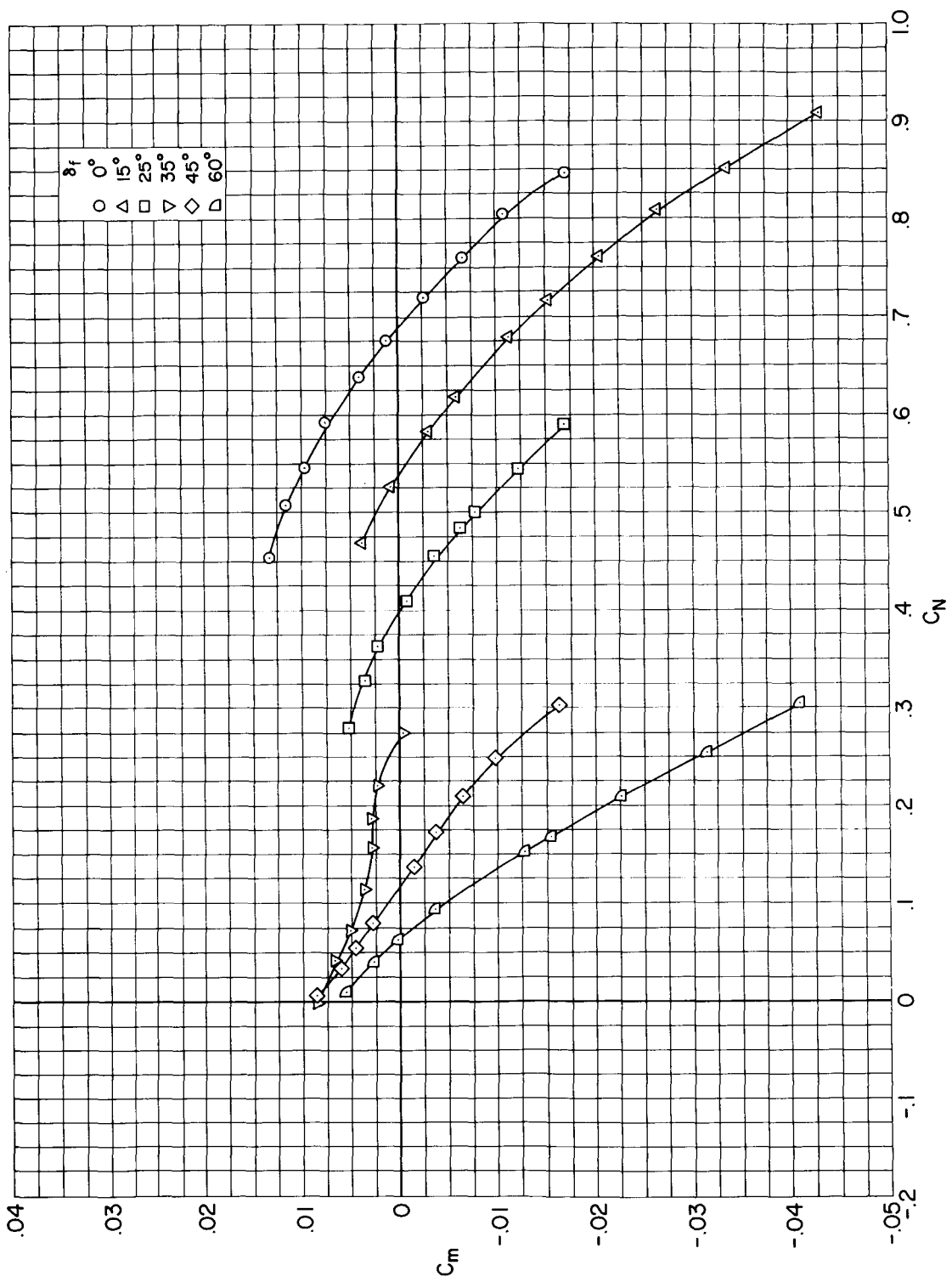
(a) $M = 5.2$

Figure 12.- Variation of pitching-moment coefficient with normal-force coefficient for the M2-F2 model with several pitch-flap settings; 25° rudder flare.



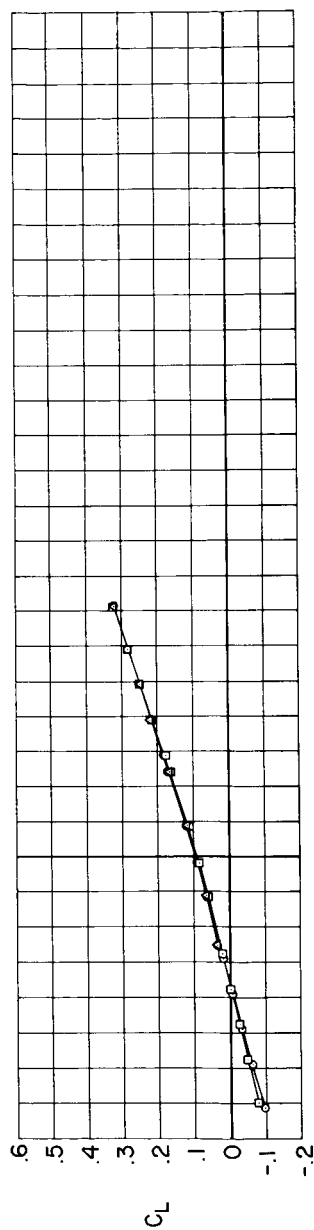
(b) $M = 7.4$

Figure 12.- Continued.

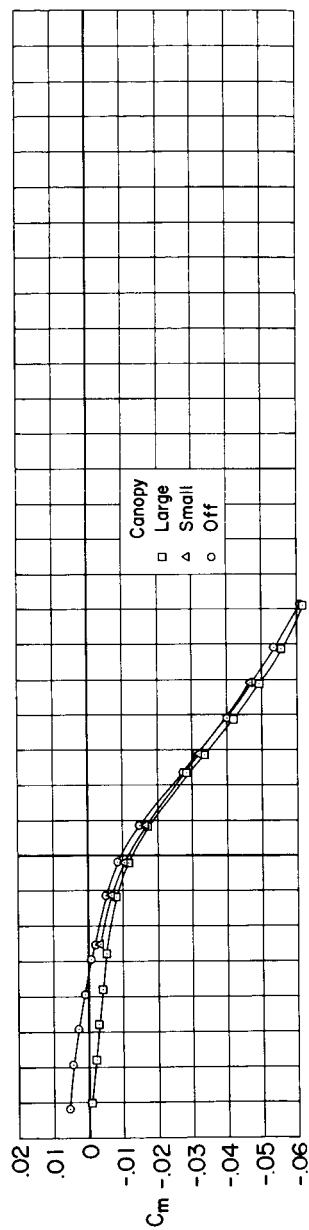


(c) $M = 10.4$

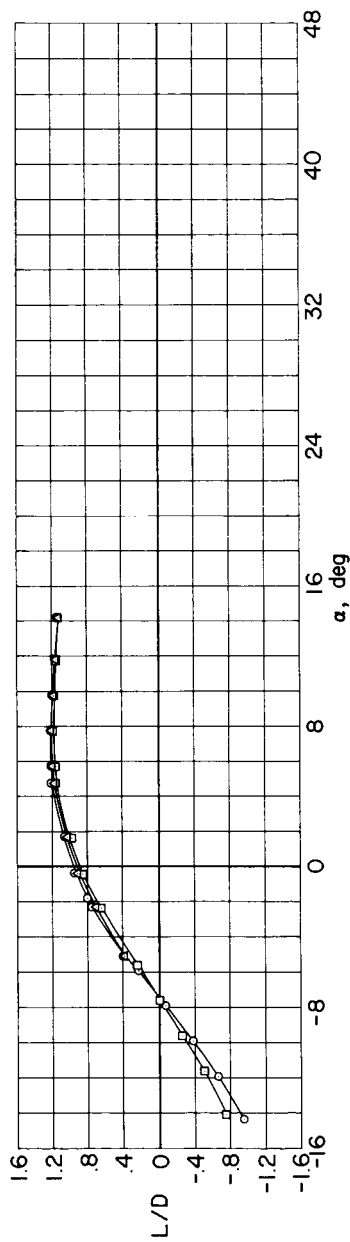
Figure 12.- Concluded.



(a) Lift coefficient.

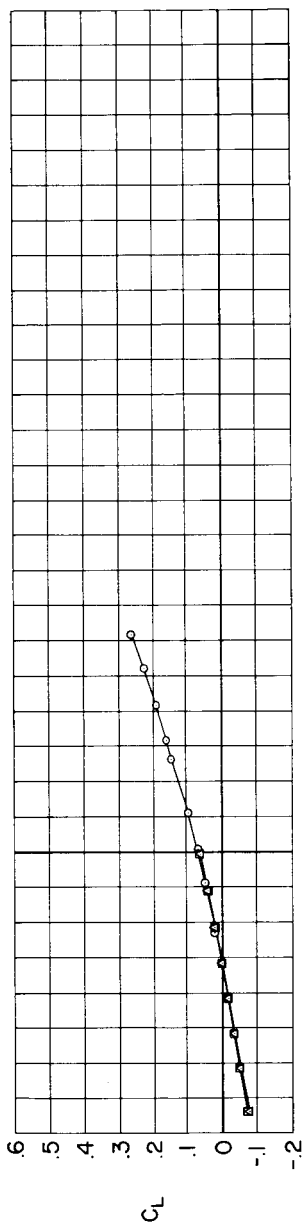


(b) Pitching-moment coefficient.

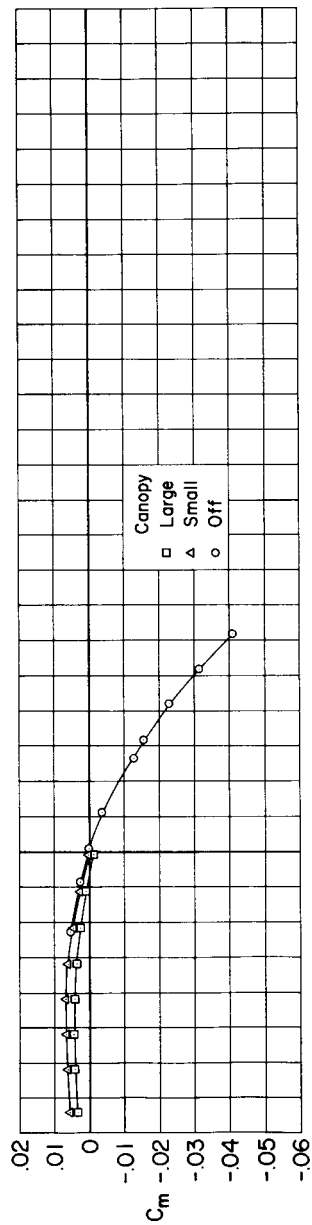


(c) Lift-drag ratio.

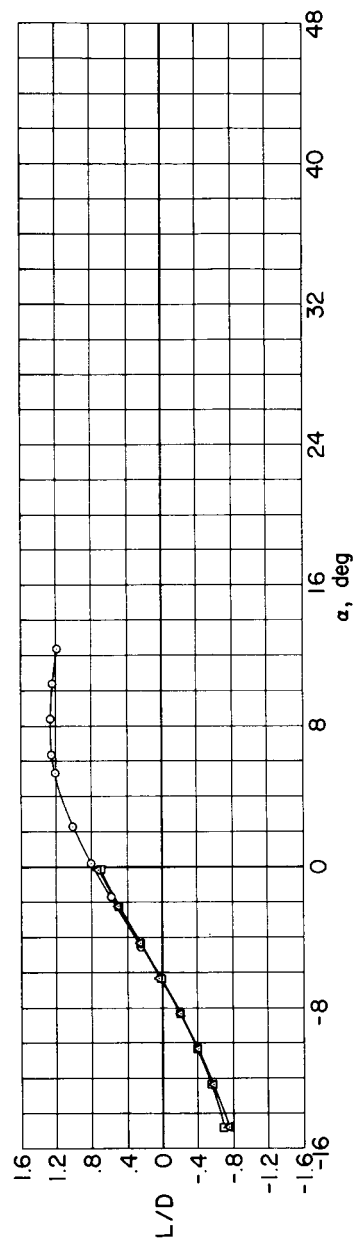
Figure 13.- Longitudinal aerodynamic characteristics of the M2-F2 model with the large and the small canopy; 25° rudder flare, $\delta_f = 60^\circ$, $M = 5.2$.



(a) Lift coefficient.

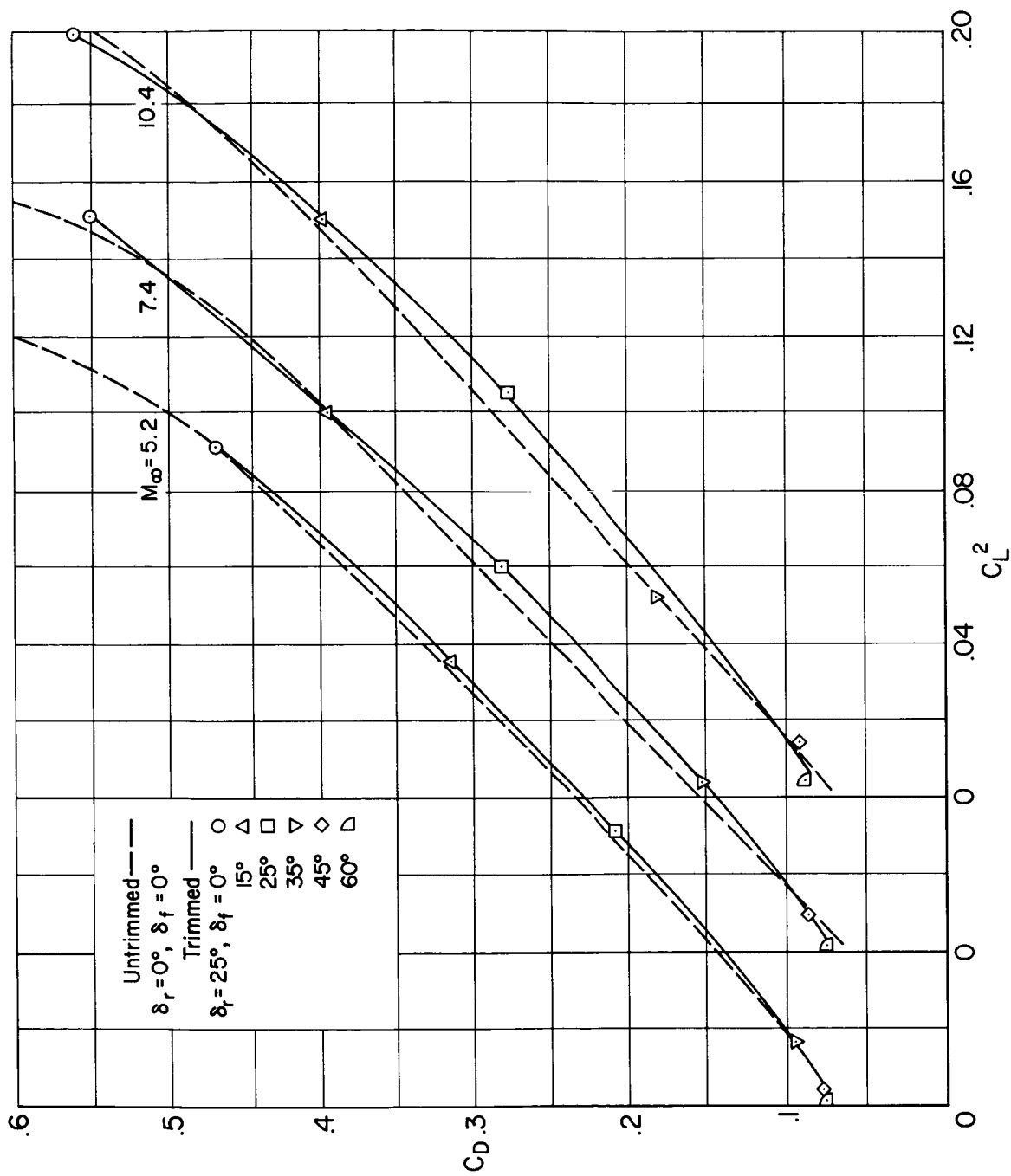


(b) Pitching-moment coefficient.



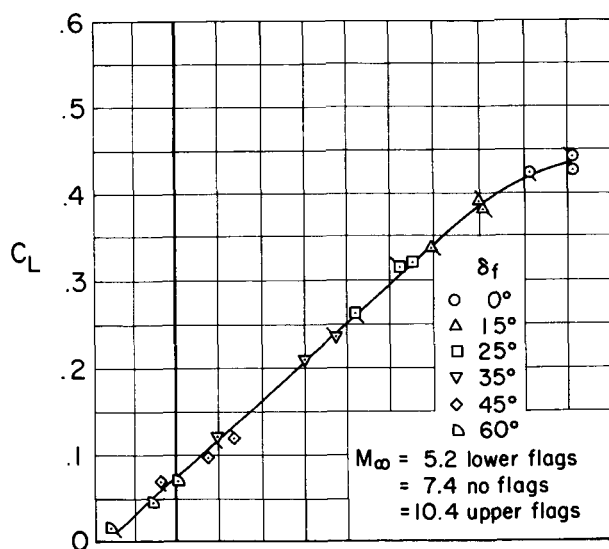
(c) Lift-drag ratio.

Figure 14.- Longitudinal aerodynamic characteristics of the M2-F2 model with the large and the small canopy; 25° rudder flare, $\delta_f = 60^\circ$, $M = 10.4$.

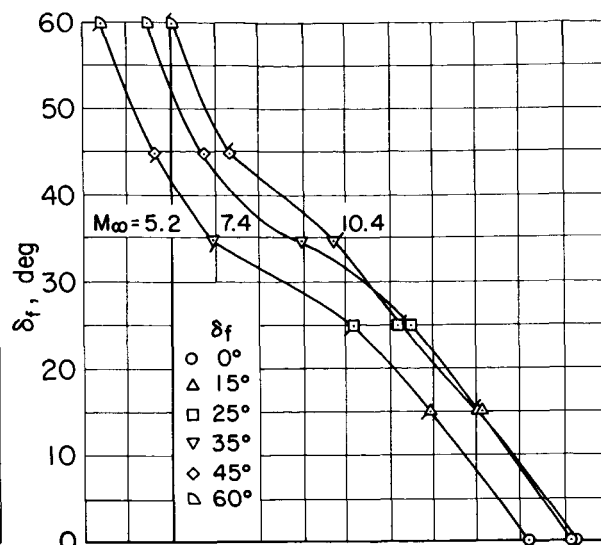


(a) Variation of drag coefficient with the square of the lift coefficient.

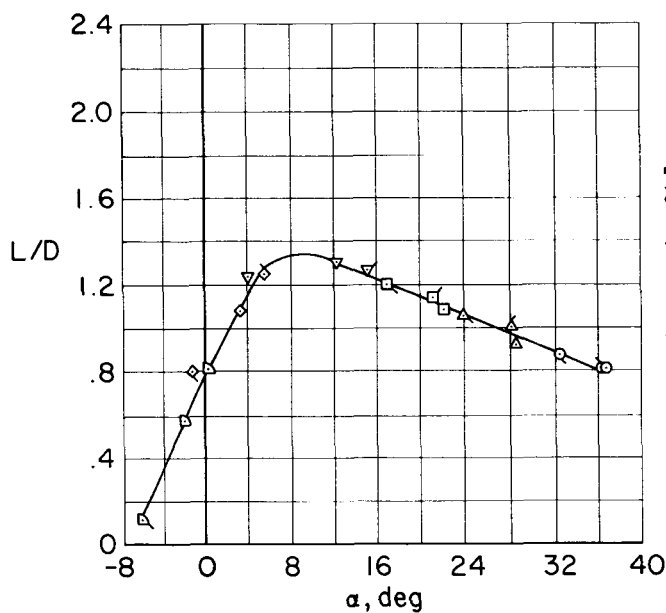
Figure 15.- Summary of longitudinal aerodynamic characteristics at trim; 25° rudder flare.



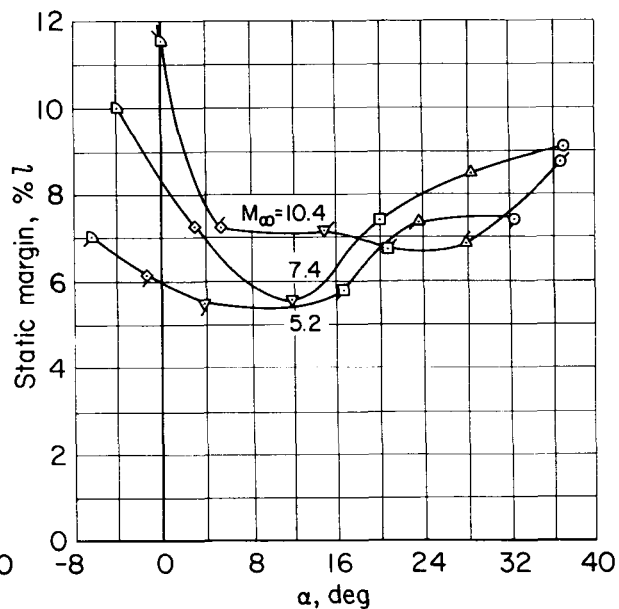
(b) Trimmed lift coefficient versus angle of attack.



(d) Pitch-flap deflection versus angle of attack.



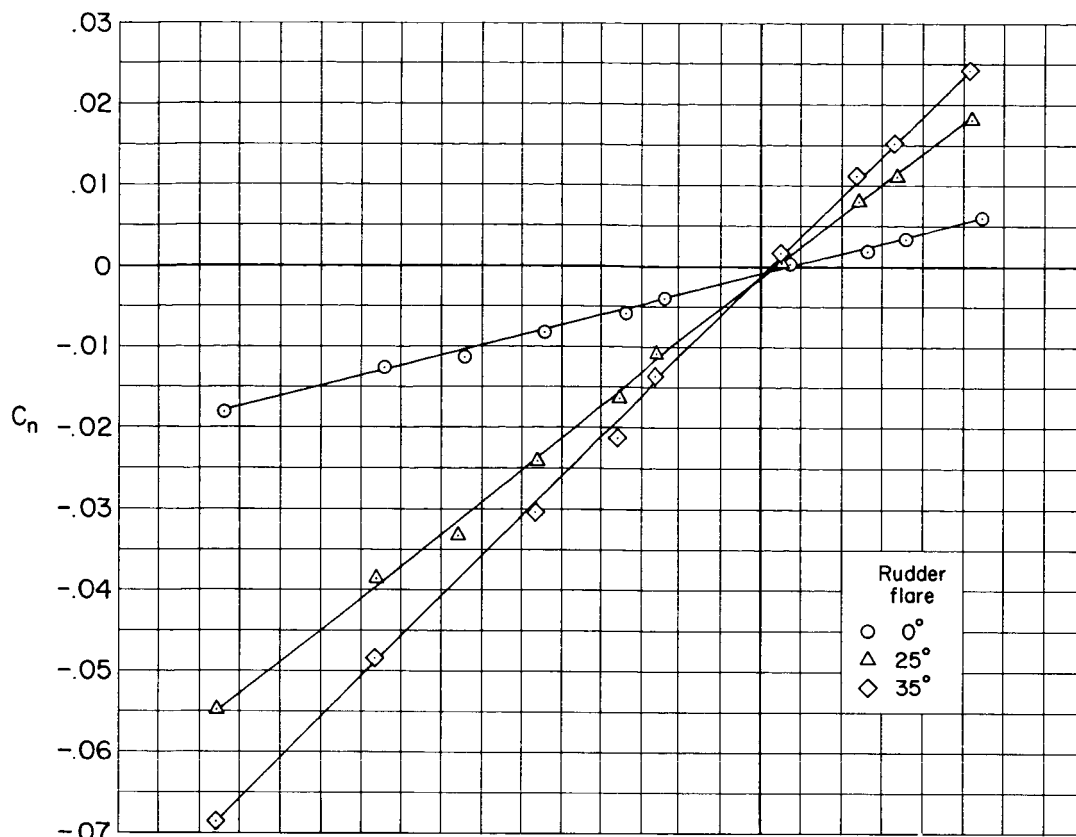
(c) Trimmed lift-drag ratio versus angle of attack.



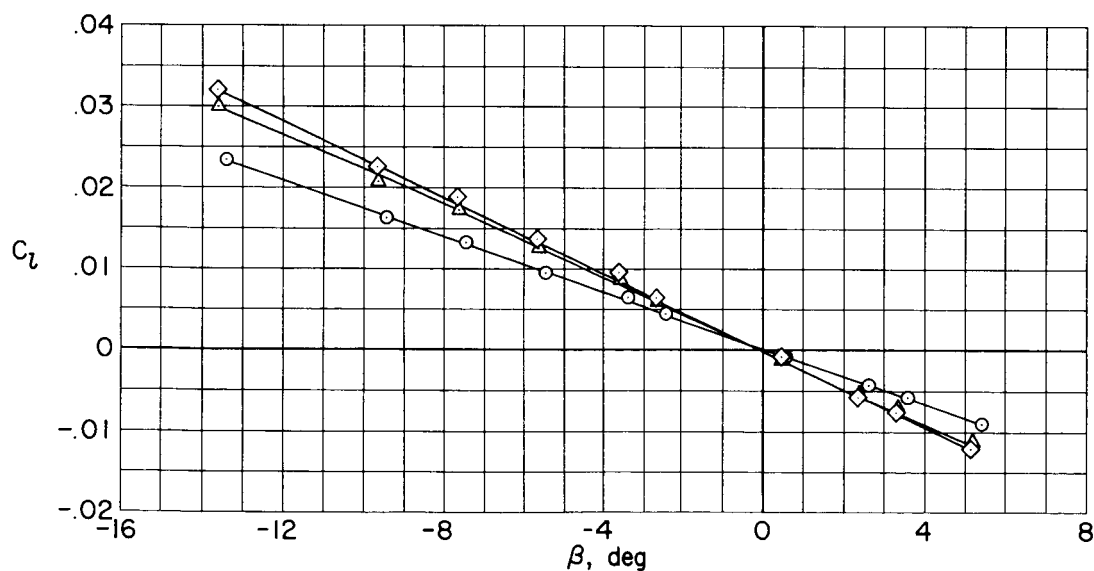
(e) Static margin versus angle of attack.

Figure 15.- Concluded.

CONFIDENTIAL



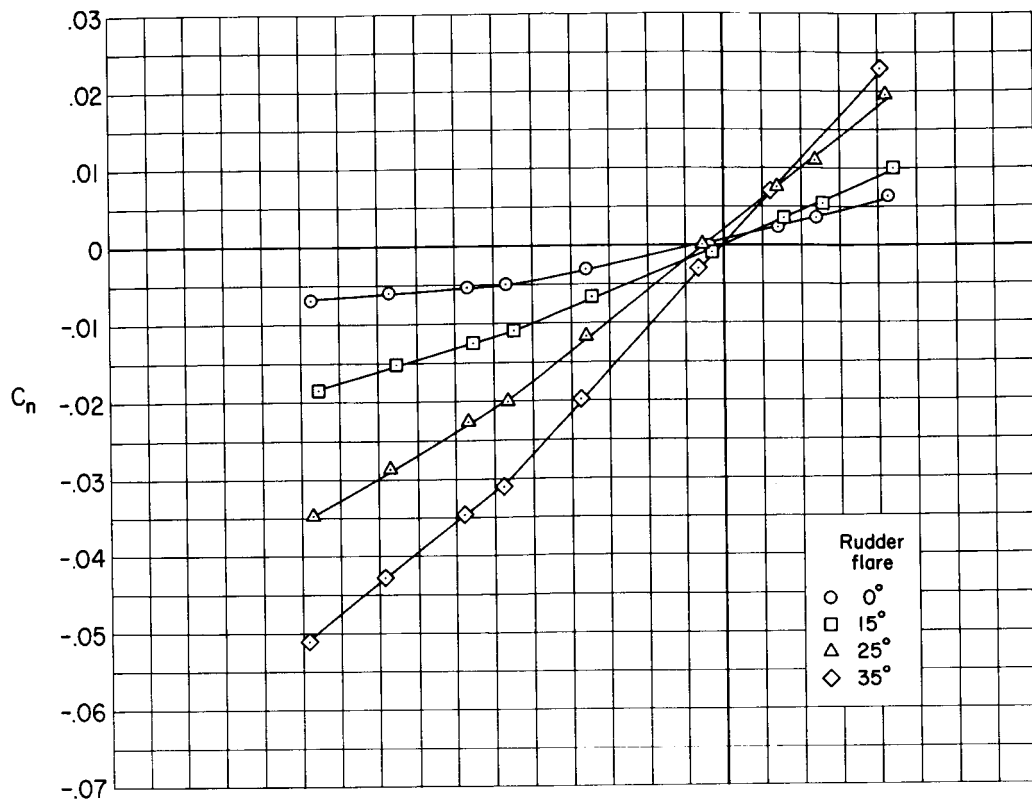
(a) Yawing-moment coefficient.



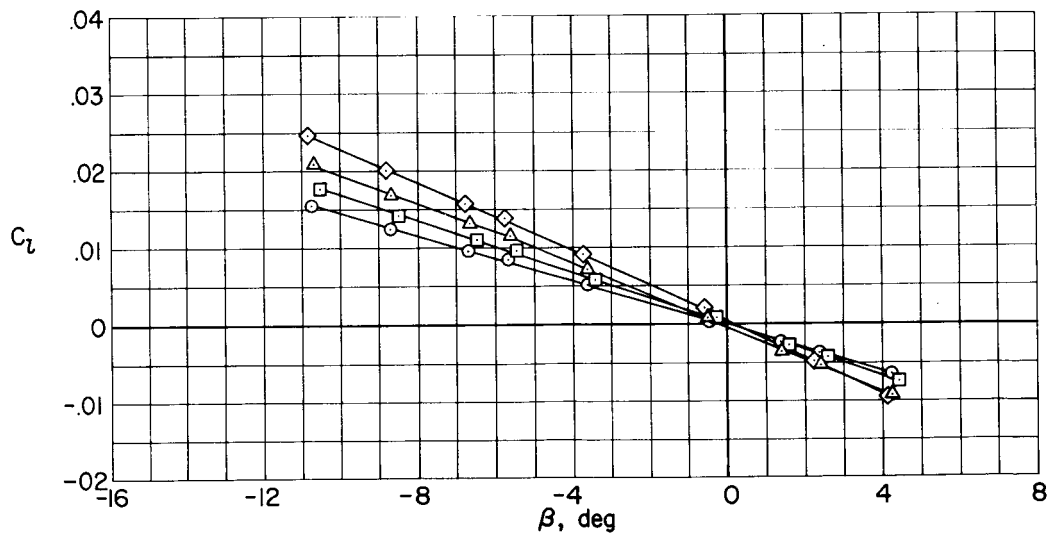
(b) Rolling-moment coefficient.

Figure 16.- Effects of rudder flare on the lateral-directional moment characteristics of the M2-F2 model in sideslip; $M = 5.2$, $\alpha = 0^\circ$, $\delta_f = 60^\circ$.

CONFIDENTIAL

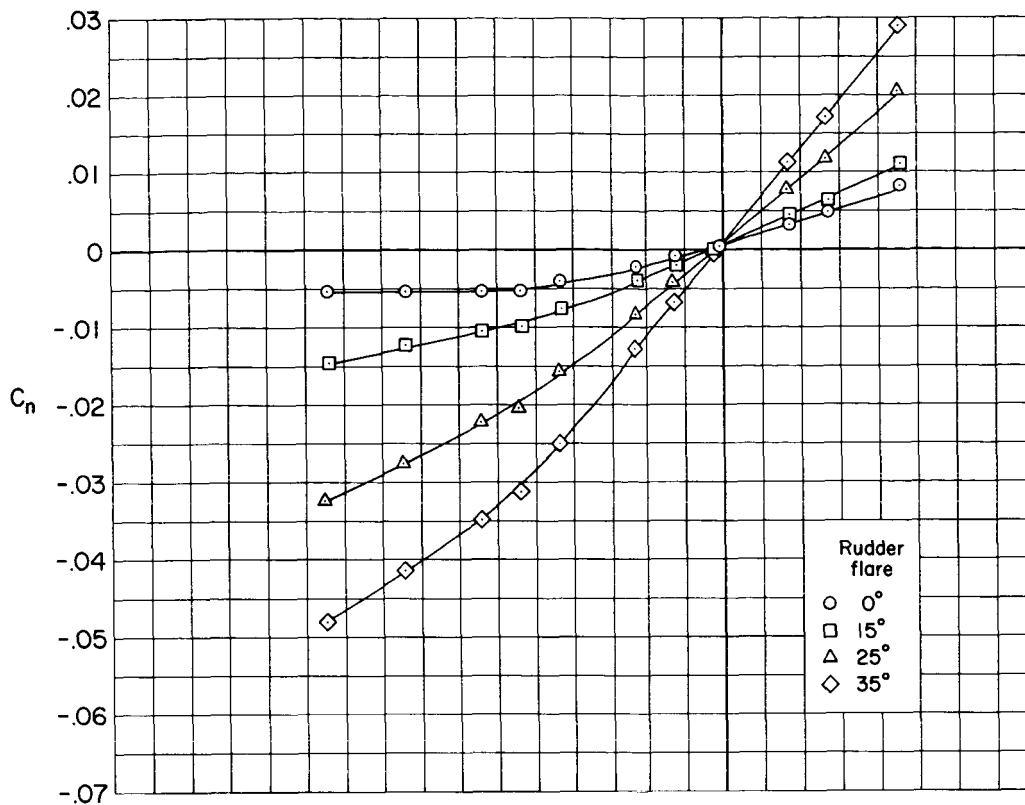


(a) Yawing-moment coefficient.

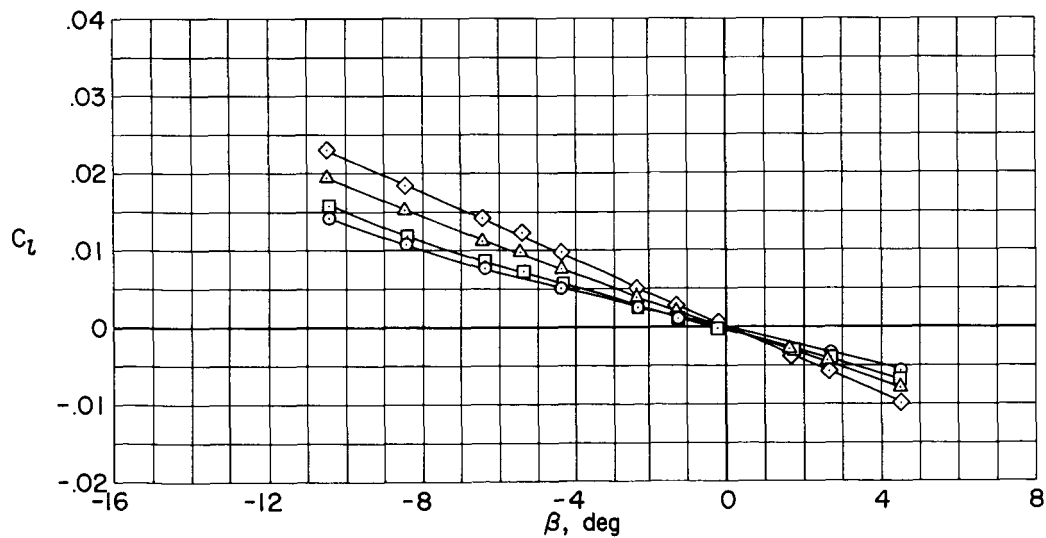


(b) Rolling-moment coefficient.

Figure 17.- Effects of rudder flare on the lateral-directional moment characteristics of the M2-F2 model in sideslip; $M = 7.4$, $\alpha = 0^\circ$, $\delta_f = 60^\circ$.



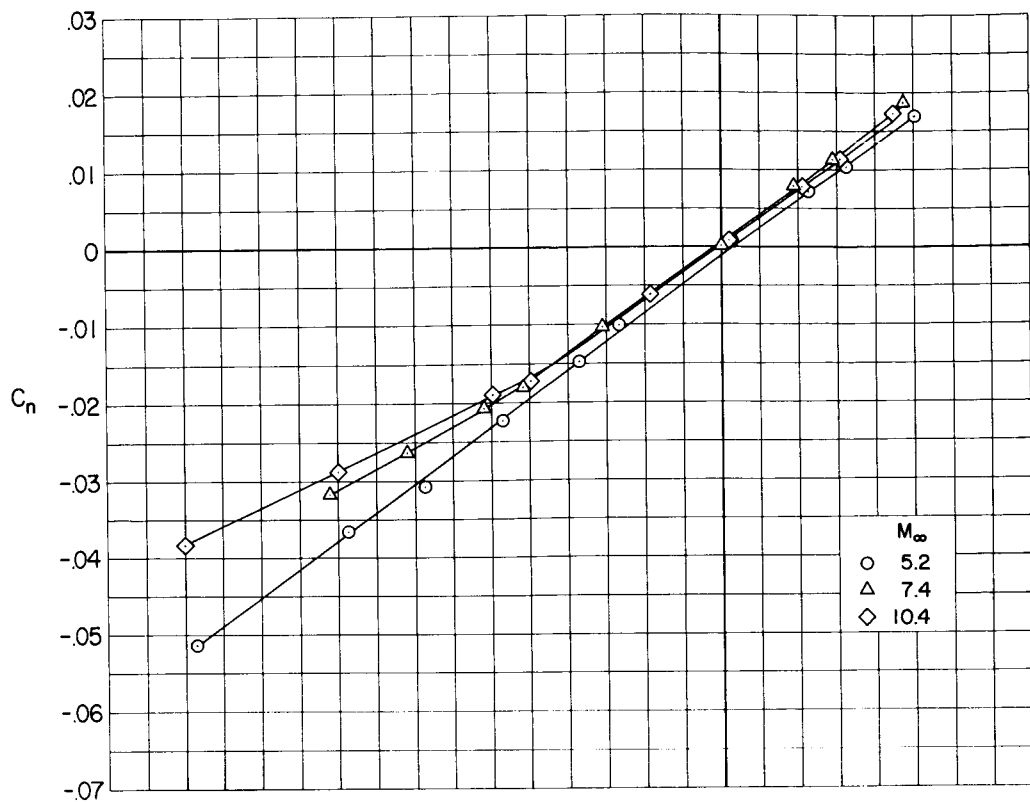
(a) Yawing-moment coefficient.



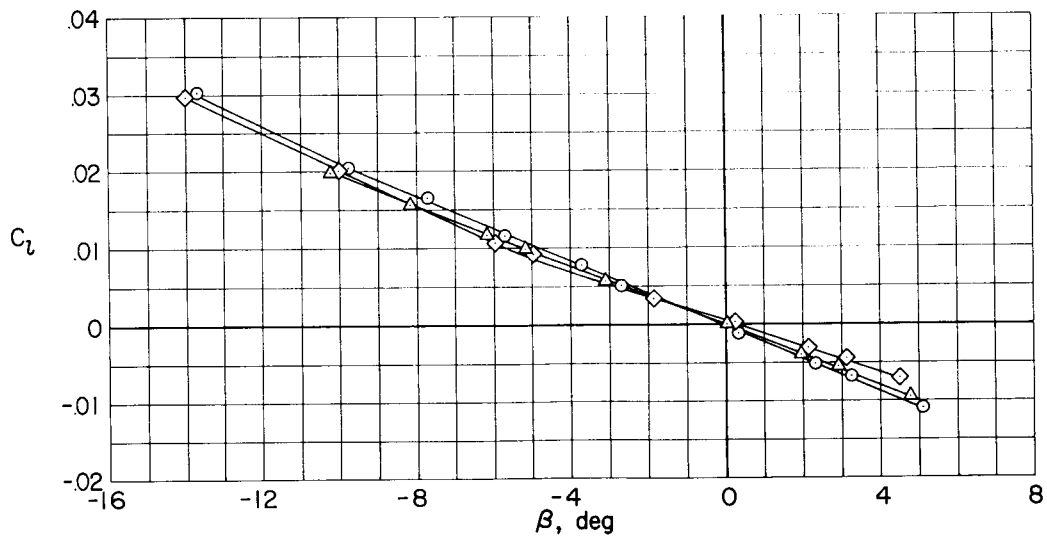
(b) Rolling-moment coefficient.

Figure 18.- Effects of rudder flare on the lateral-directional moment characteristics of the M2-F2 model in sideslip; $M = 10.4$, $\alpha = 0^\circ$, $\delta_f = 60^\circ$.

CONFIDENTIAL



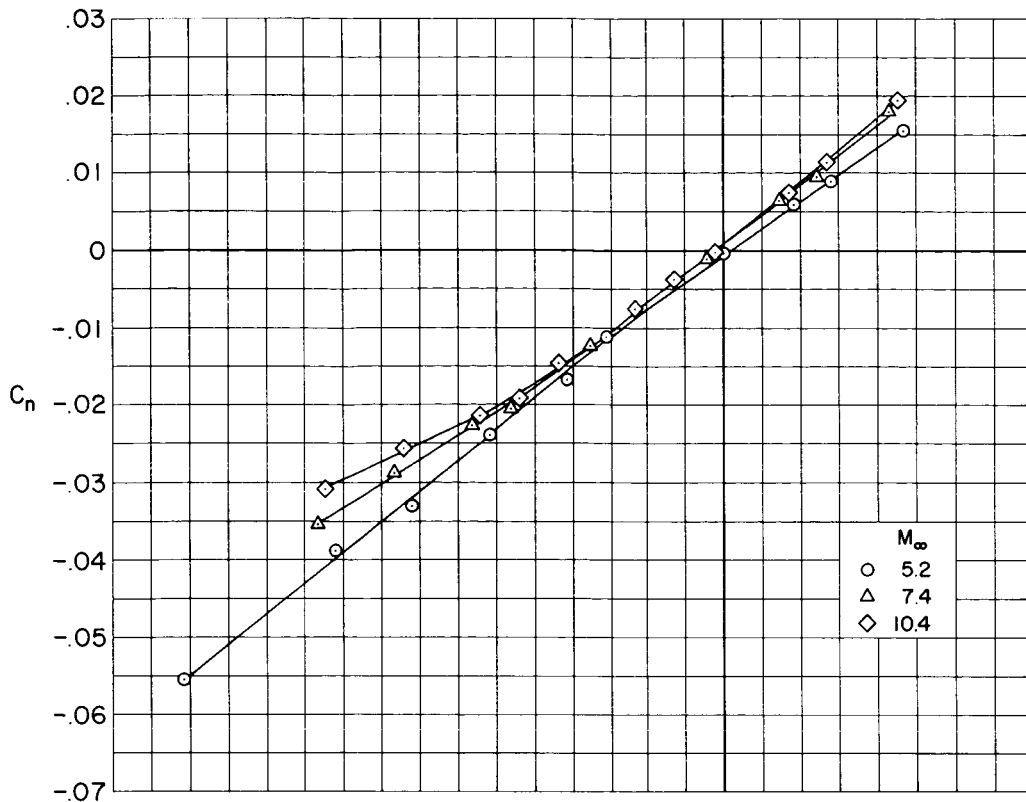
(a) Yawing-moment coefficient.



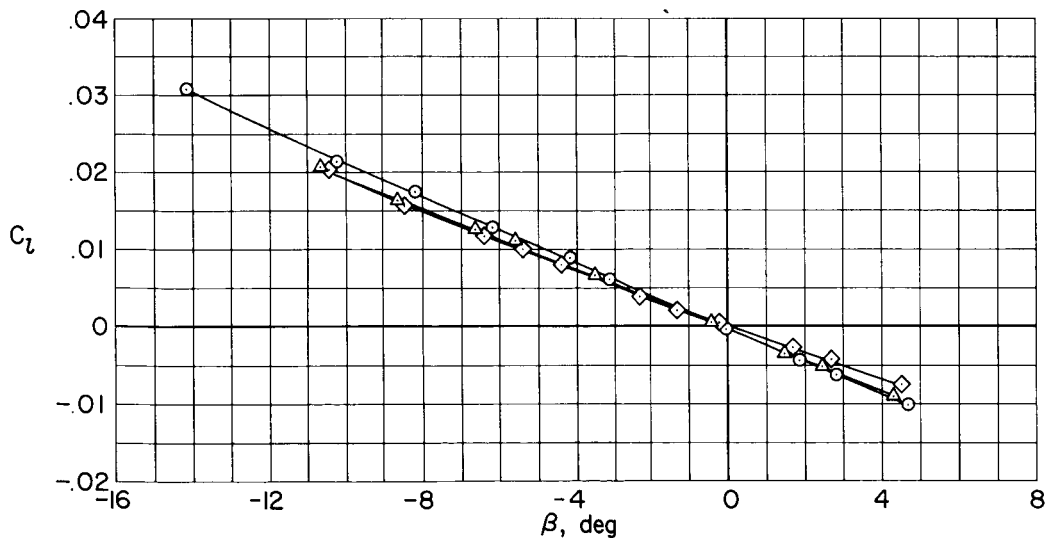
(b) Rolling-moment coefficient.

Figure 19.- Lateral-directional moment characteristics for the M2-F2 model with the large canopy; 25° rudder flare, $\alpha = 0^\circ$, $\delta_f = 60^\circ$.

CONFIDENTIAL

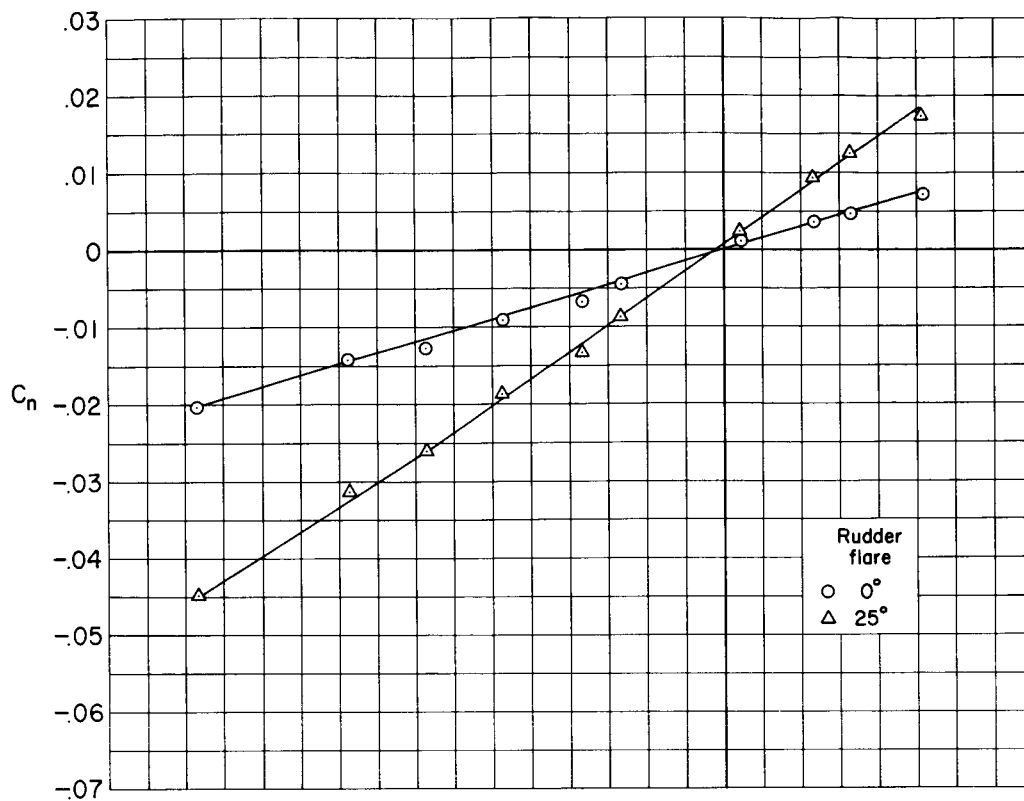


(a) Yawing-moment coefficient.

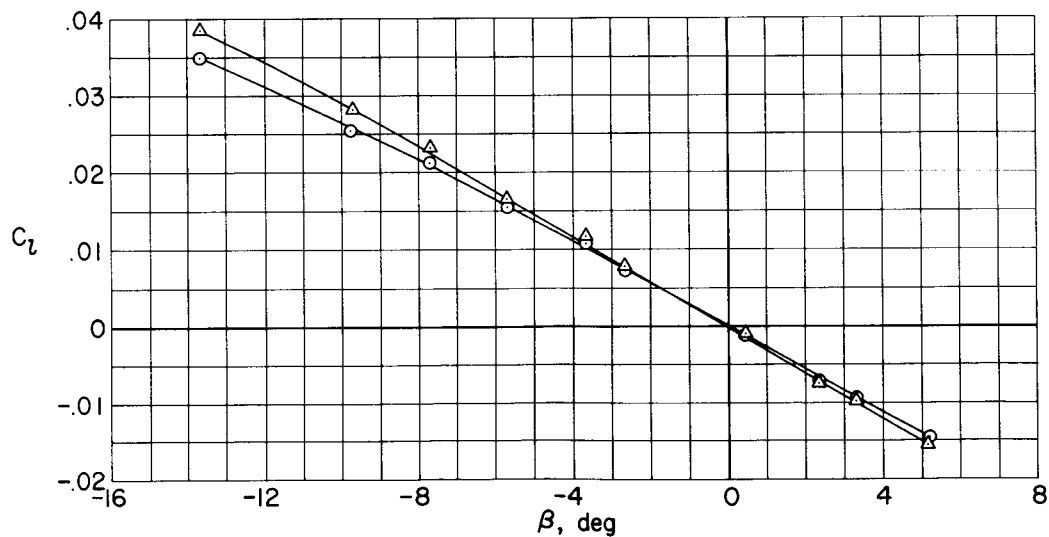


(b) Rolling-moment coefficient.

Figure 20.- Lateral-directional moment characteristics for the M2-F2 model with the small canopy; 25° rudder flare, $\alpha = 0^\circ$, $\delta_f = 60^\circ$.

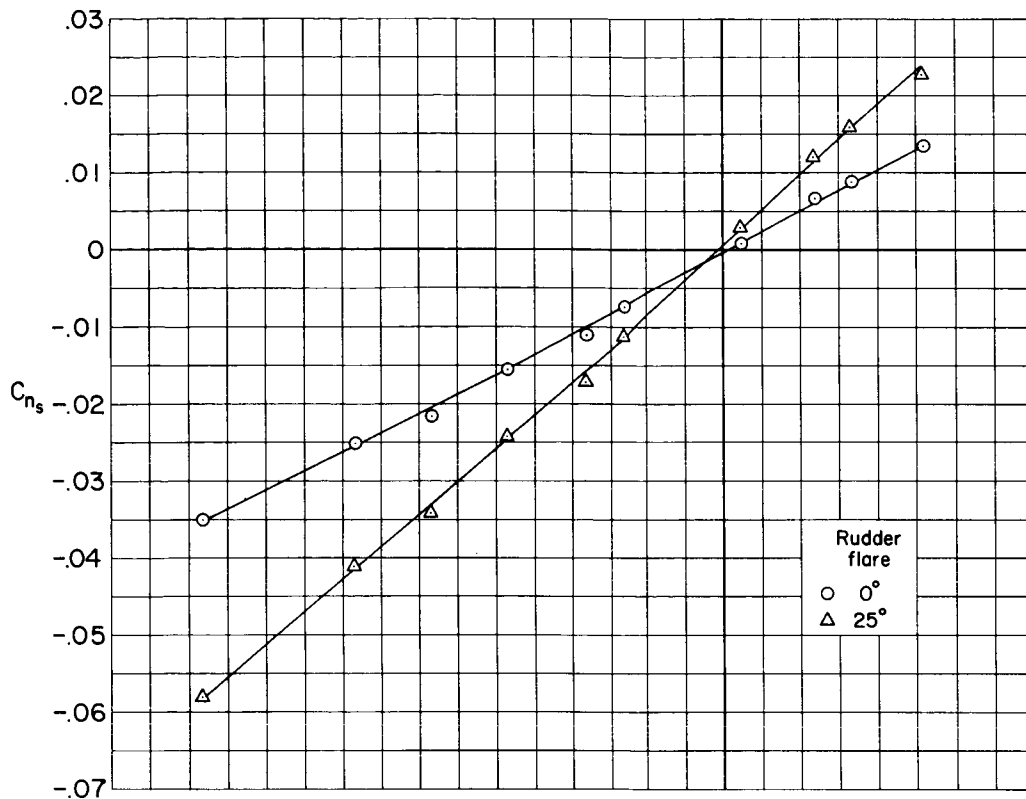


(a) Yawing-moment coefficient.

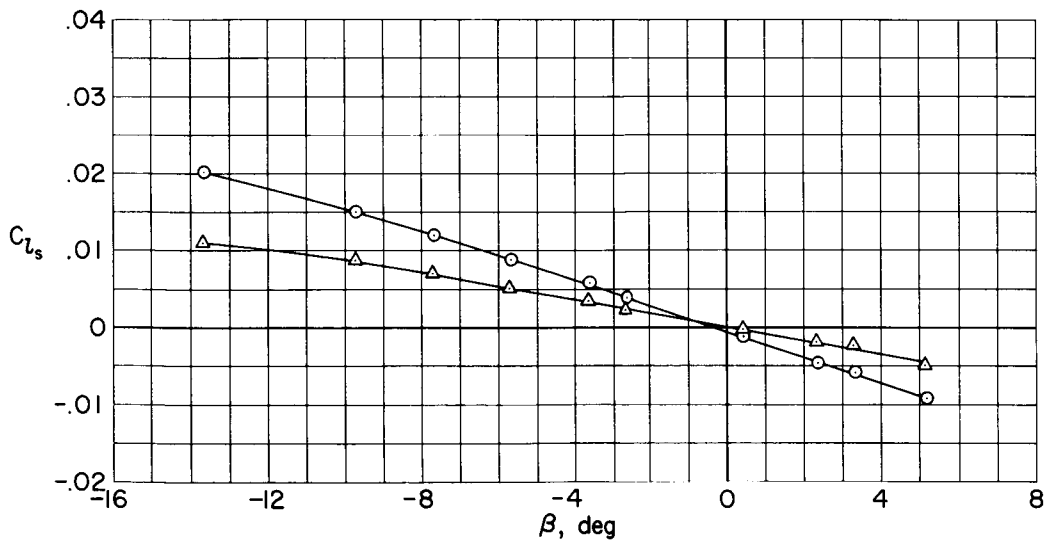


(b) Rolling-moment coefficient.

Figure 21.- Effects of rudder flare on the lateral-directional moment characteristics of the M2-F2 model in sideslip; $M = 5.2$, $\alpha = 30^\circ$, $\delta_f = 15^\circ$; body axes.

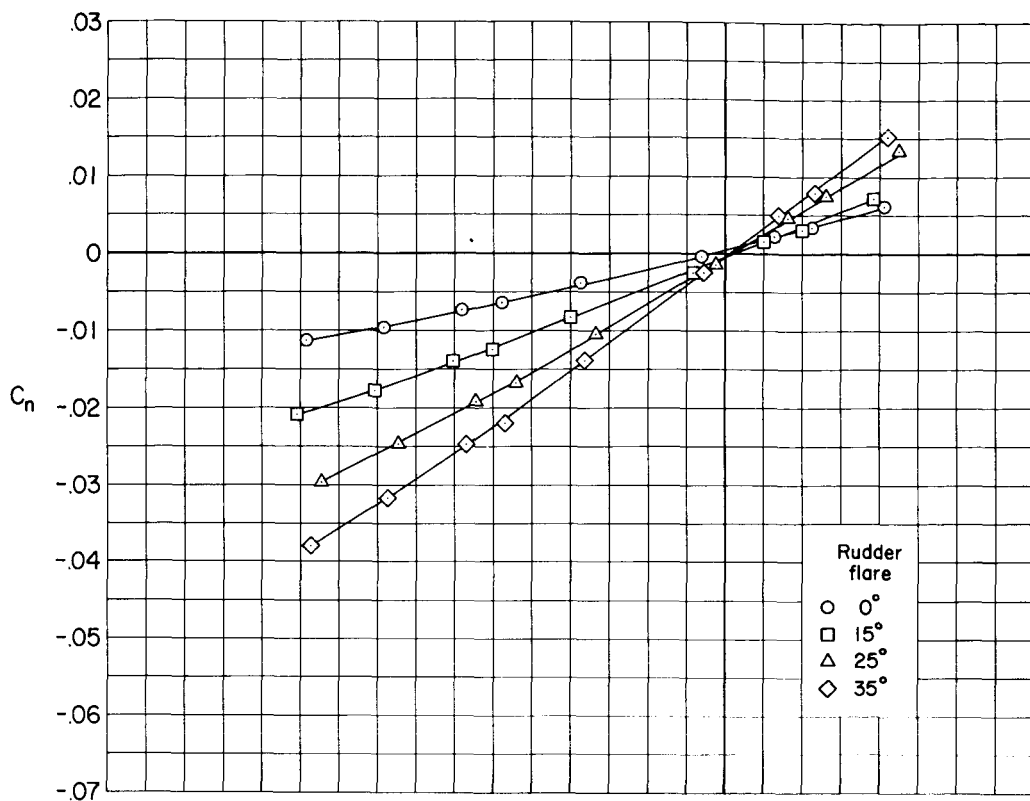


(a) Yawing-moment coefficient.

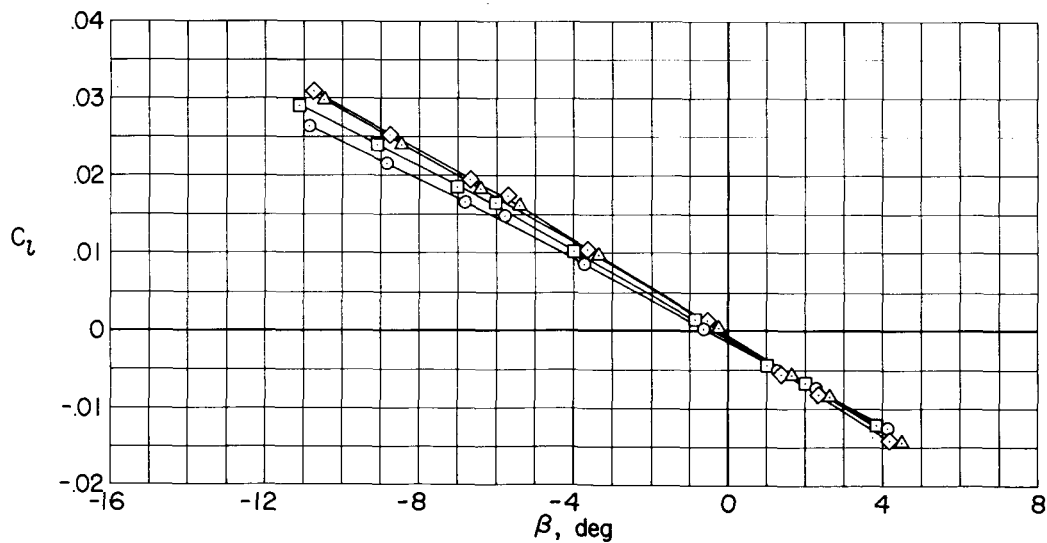


(b) Rolling-moment coefficient.

Figure 22.- Effects of rudder flare on the lateral-directional moment characteristics of the M2-F2 model in sideslip; $M = 5.2$, $\alpha = 30^\circ$, $\delta_F = 15^\circ$; stability axes.

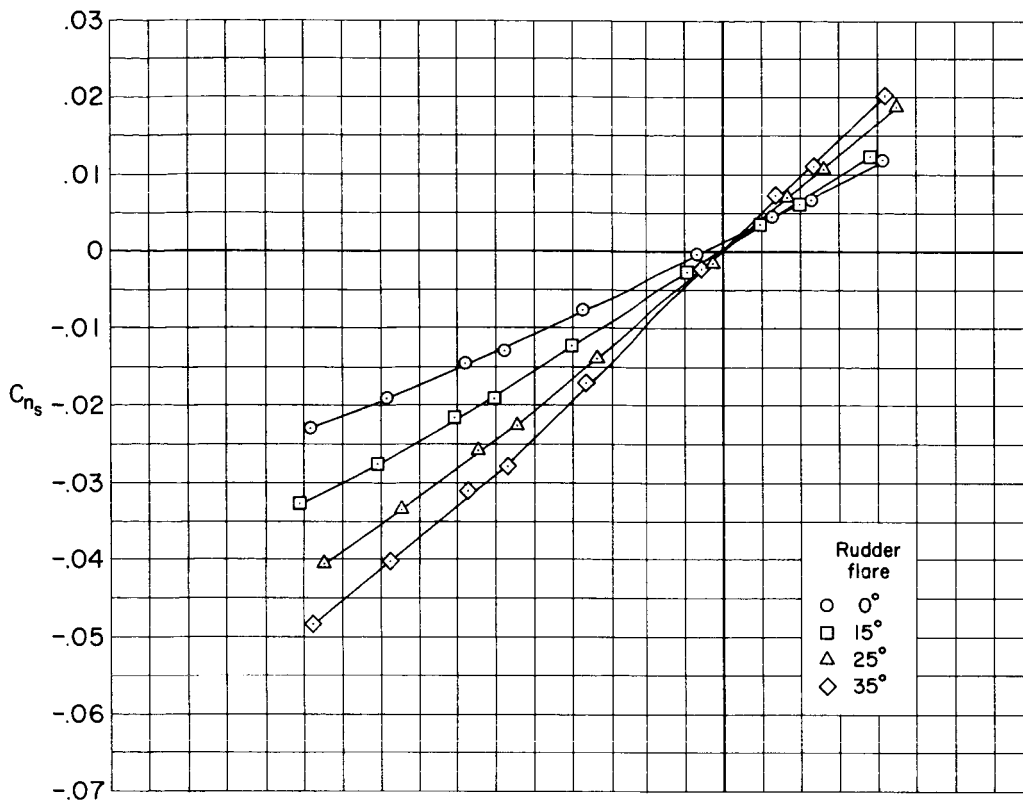


(a) Yawing-moment coefficient.

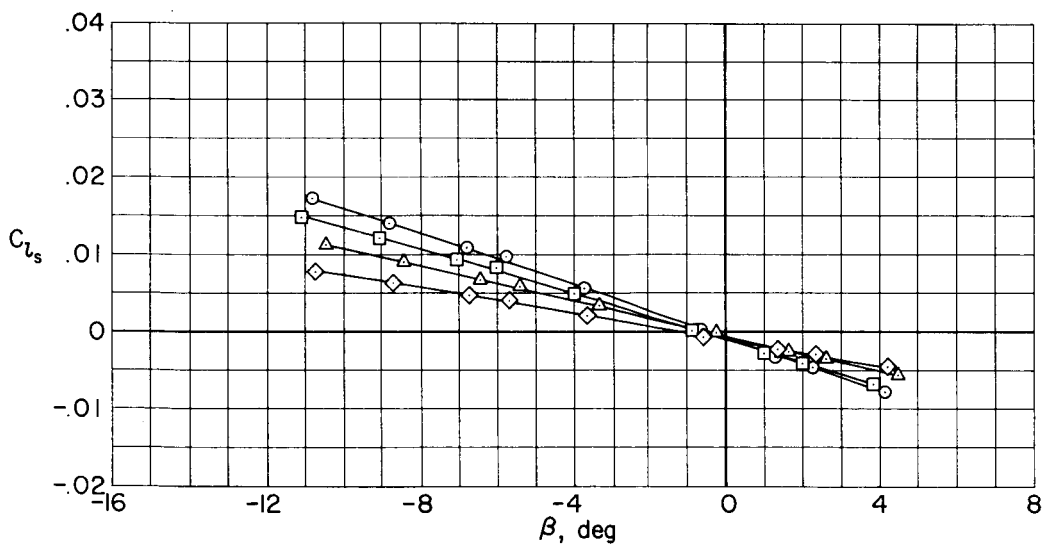


(b) Rolling-moment coefficient.

Figure 23.- Effects of rudder flare on the lateral-directional moment characteristics of the M2-F2 model in sideslip; $M = 7.4$, $\alpha = 30^\circ$, $\delta_f = 15^\circ$; body axes.

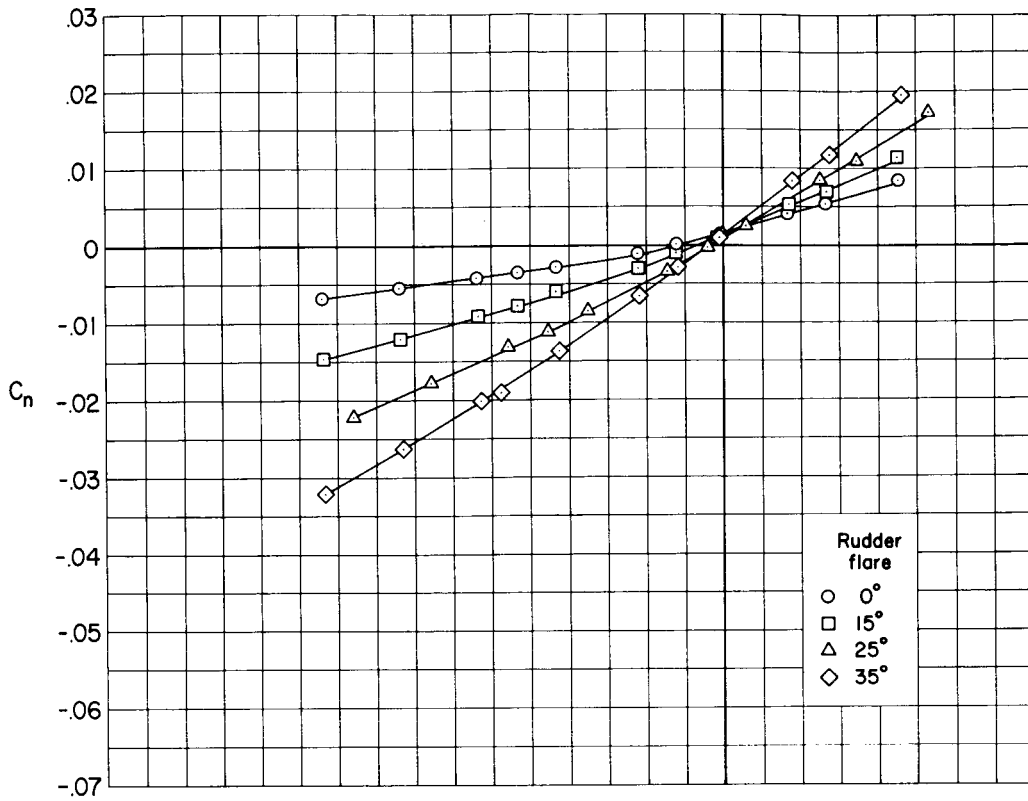


(a) Yawing-moment coefficient.

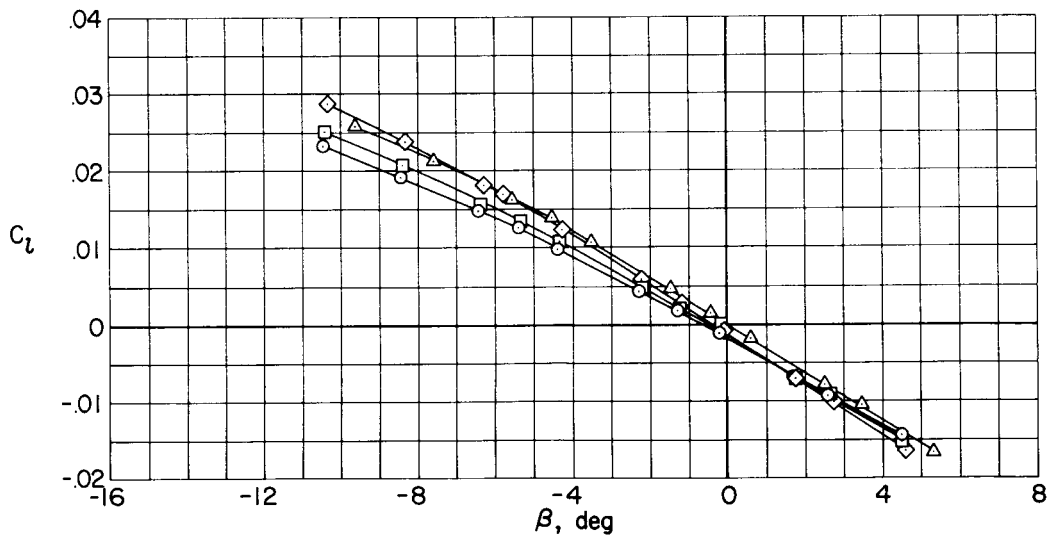


(b) Rolling-moment coefficient.

Figure 24.- Effects of rudder flare on the lateral-directional moment characteristics of the M2-F2 model in sideslip; $M = 7.4$, $\alpha = 30^\circ$, $\delta_f = 15^\circ$; stability axes.

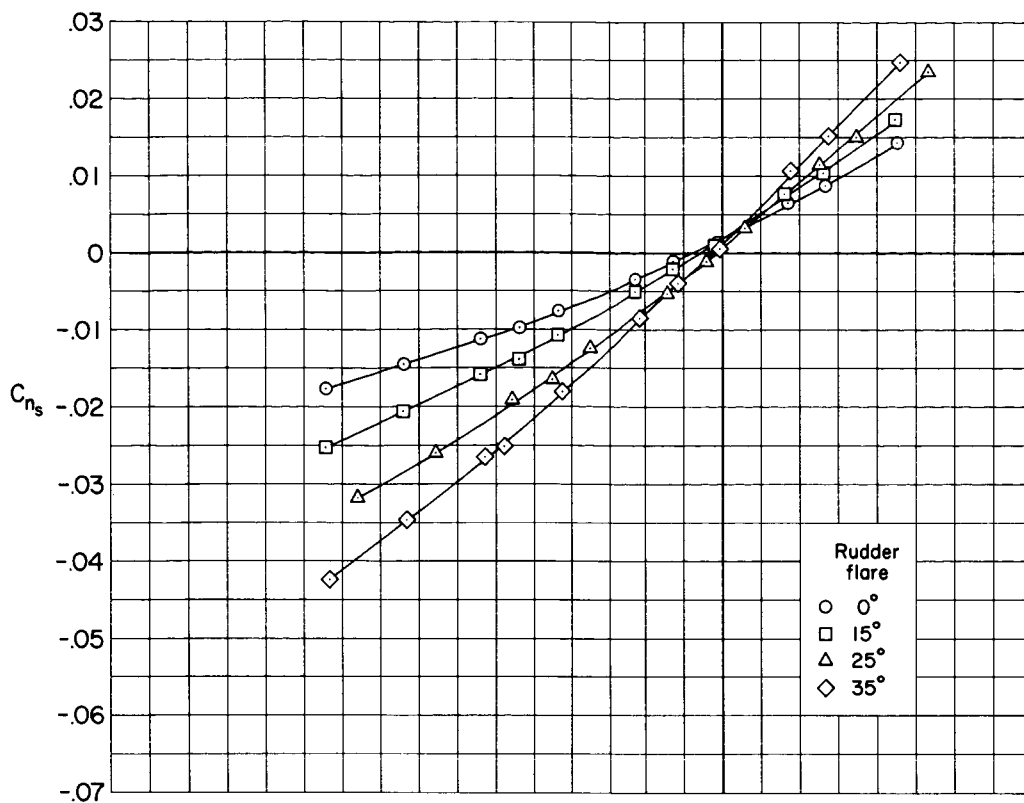


(a) Yawing-moment coefficient.

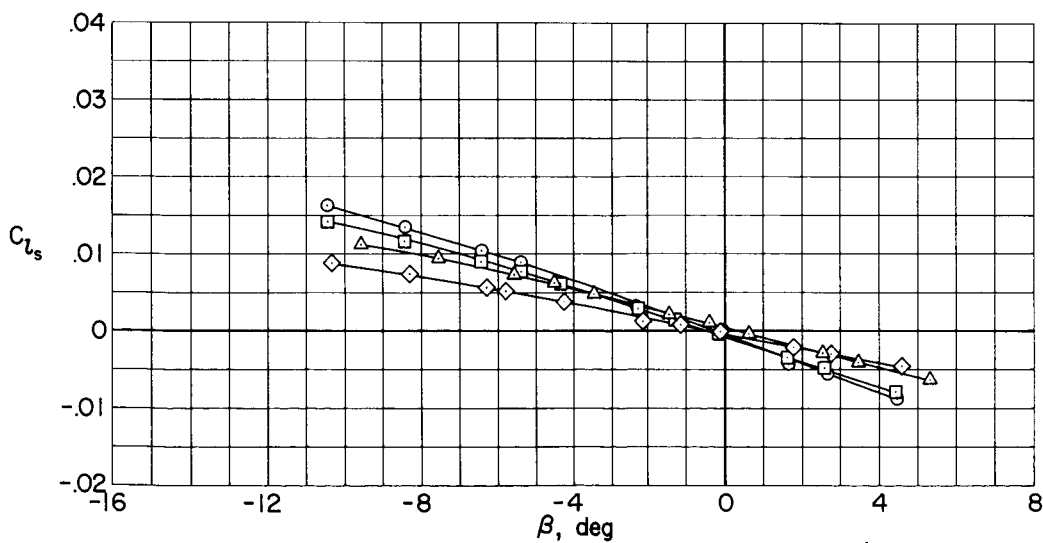


(b) Rolling-moment coefficient.

Figure 25.- Effects of rudder flare on the lateral-directional moment characteristics of the M2-F2 model in sideslip; $M = 10.4$, $\alpha = 30^\circ$, $\delta_F = 0^\circ$; body axes.

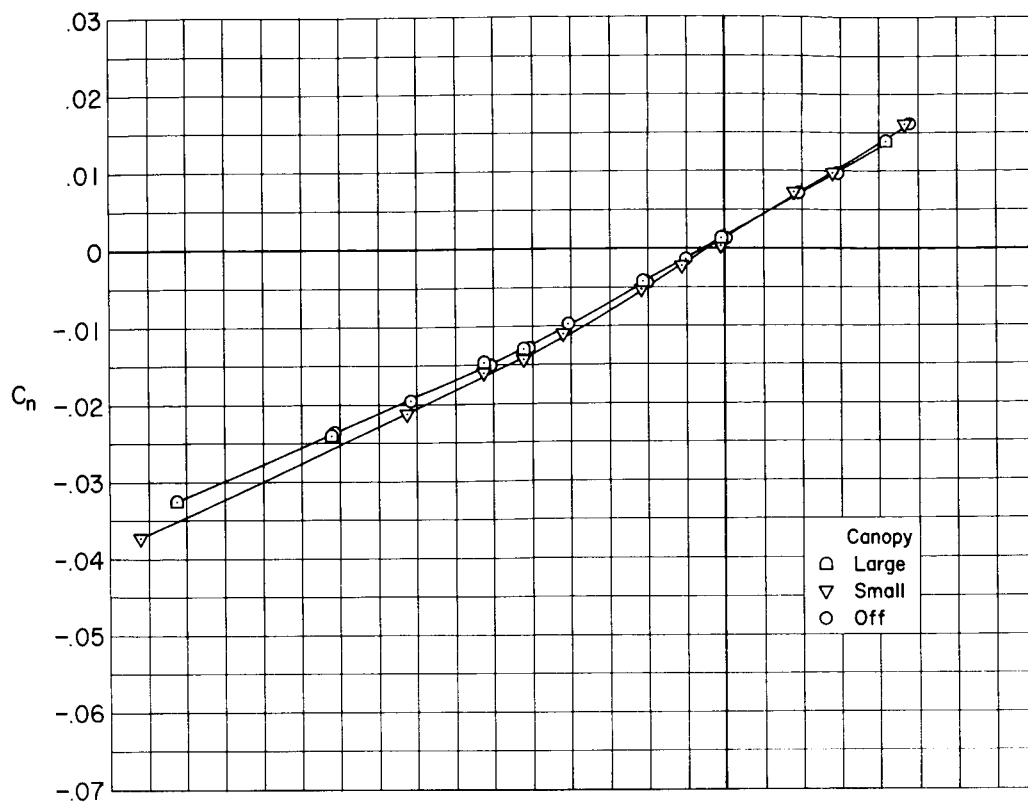


(a) Yawing-moment coefficient.

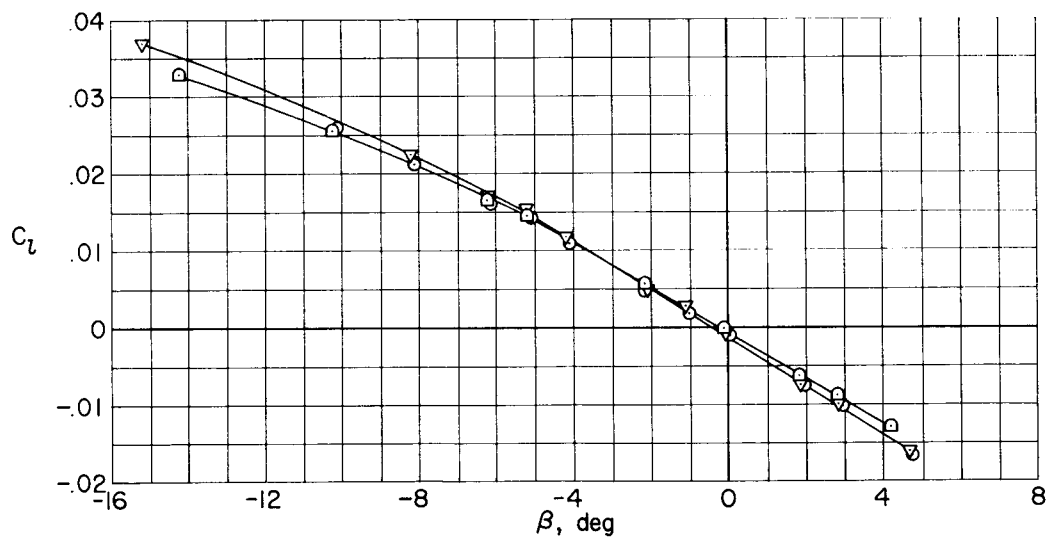


(b) Rolling-moment coefficient.

Figure 26.- Effects of rudder flare on the lateral-directional moment characteristics of the M2-F2 model in sideslip; $M = 10.4$, $\alpha = 30^\circ$, $\delta_f = 0^\circ$; stability axes.

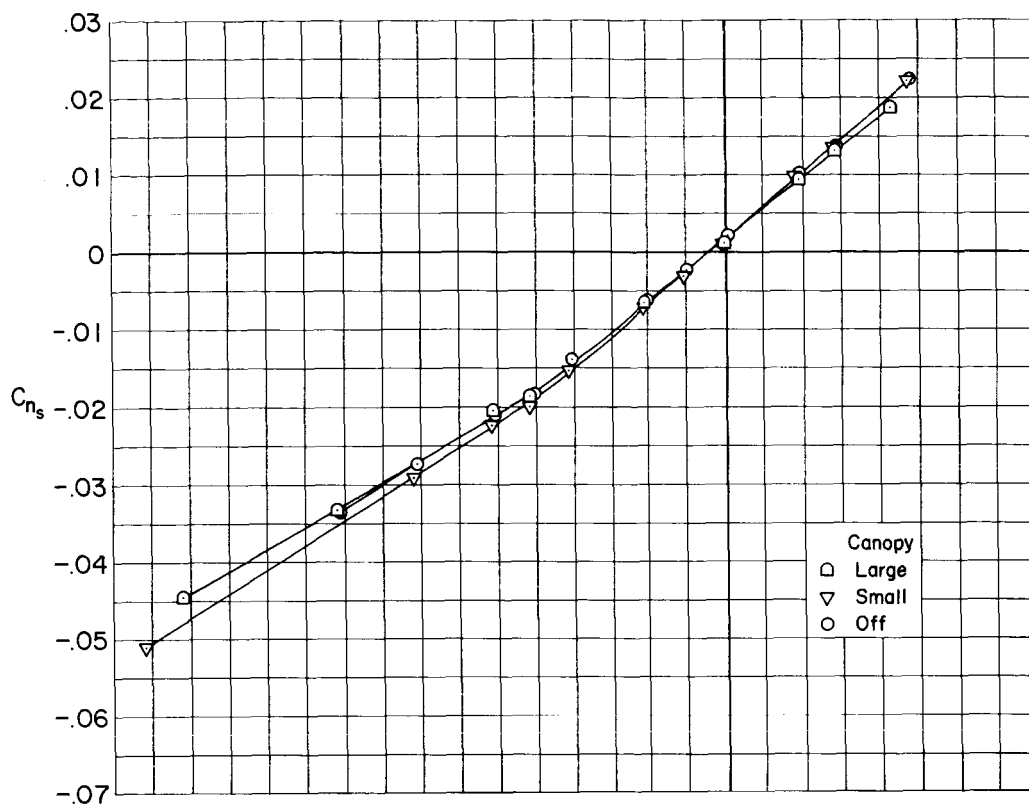


(a) Yawing-moment coefficient.

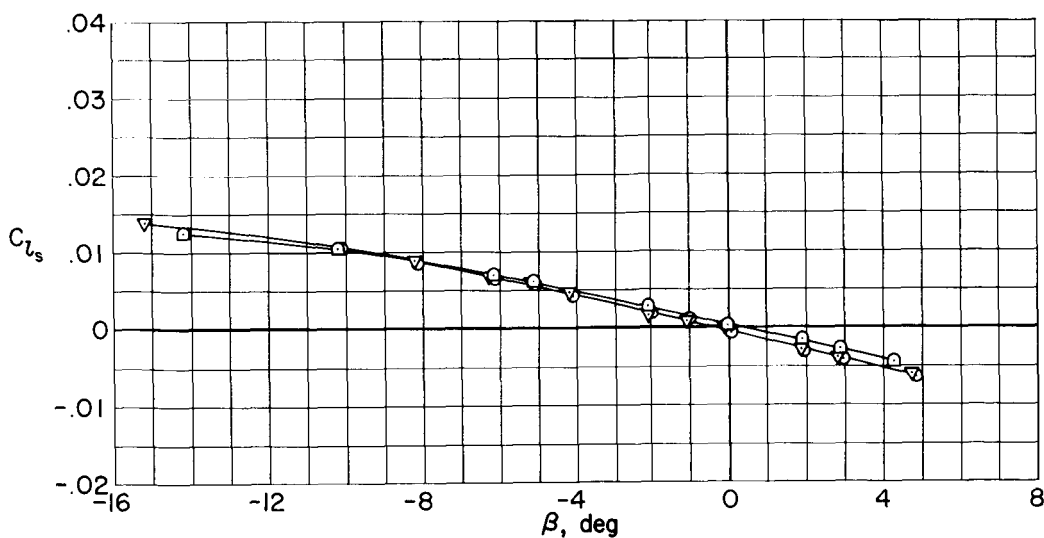


(b) Rolling-moment coefficient.

Figure 27.- Effects of canopy addition on the lateral-directional moment characteristics for the M2-F2 model; $M = 10.4$, $\alpha = 30^\circ$, $\delta_f = 35^\circ$, 25° rudder flare; body axes.

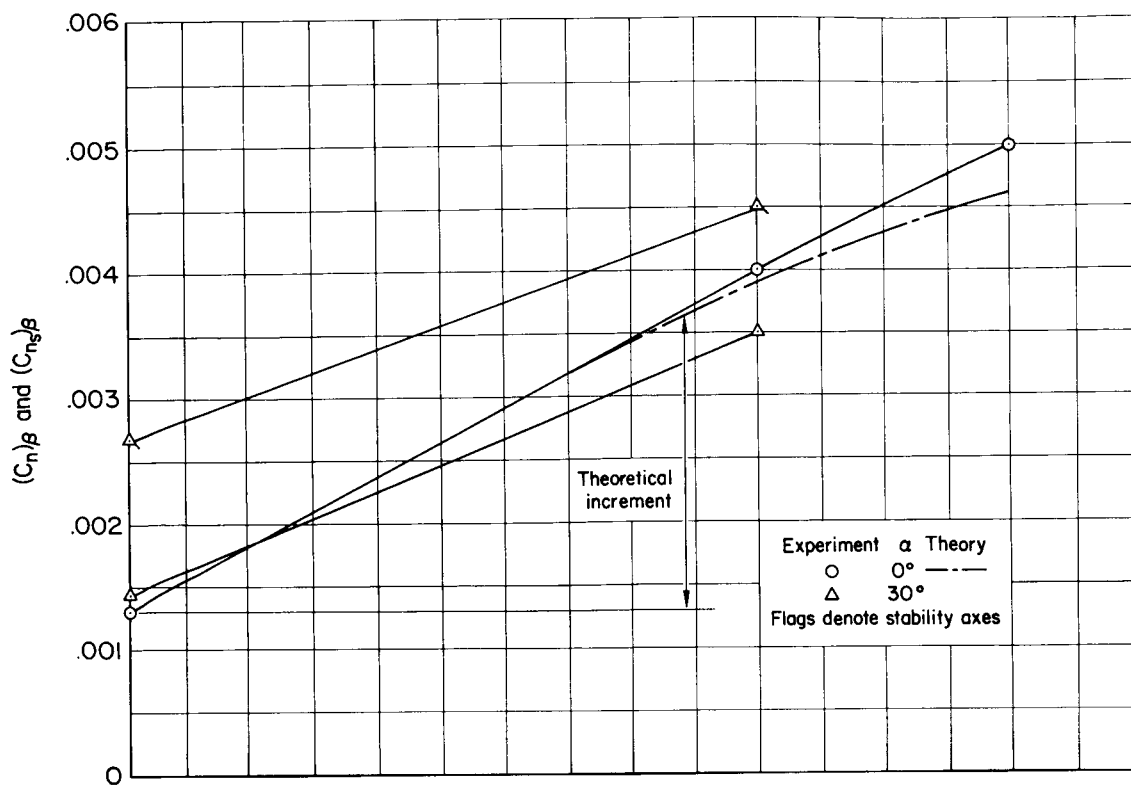


(a) Yawing-moment coefficient.

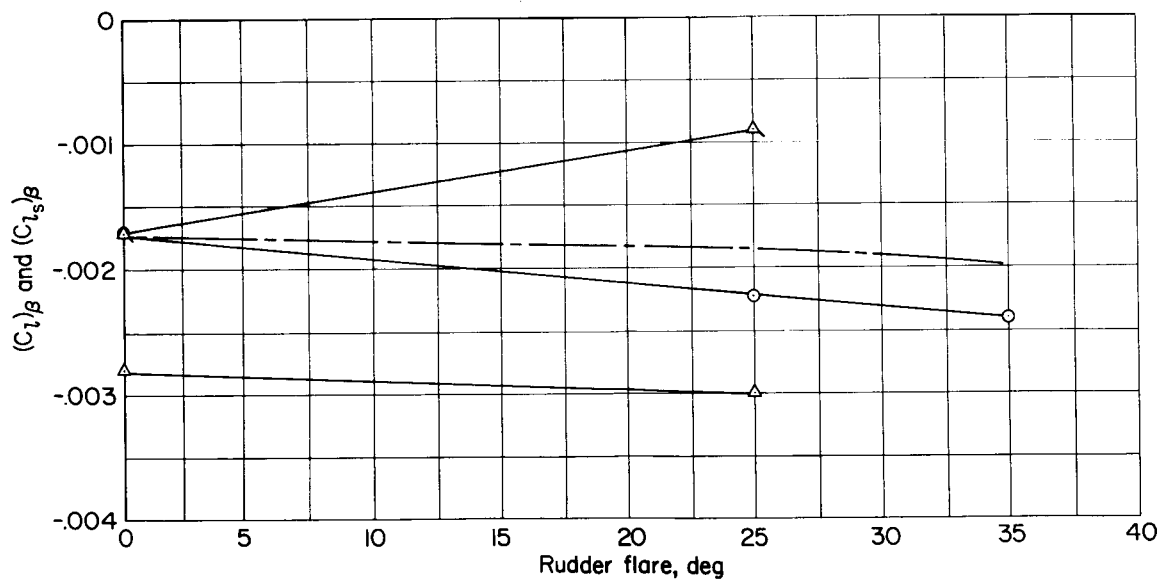


(b) Rolling-moment coefficient.

Figure 28.- Effects of canopy addition on the lateral-directional moment characteristics for the M2-F2 model; $M = 10.4$, $\alpha = 30^\circ$, $\delta_f = 35^\circ$, 25° rudder flare; stability axes.

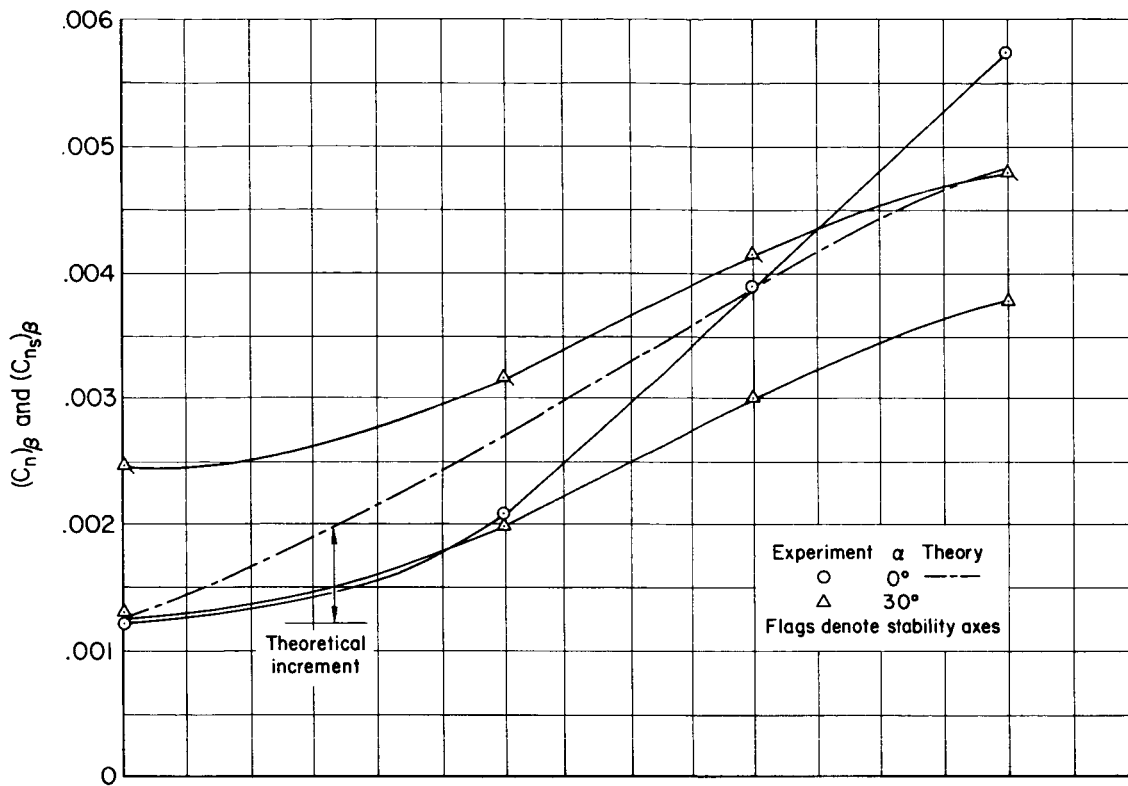


(a) Directional stability, $M = 5.2$.

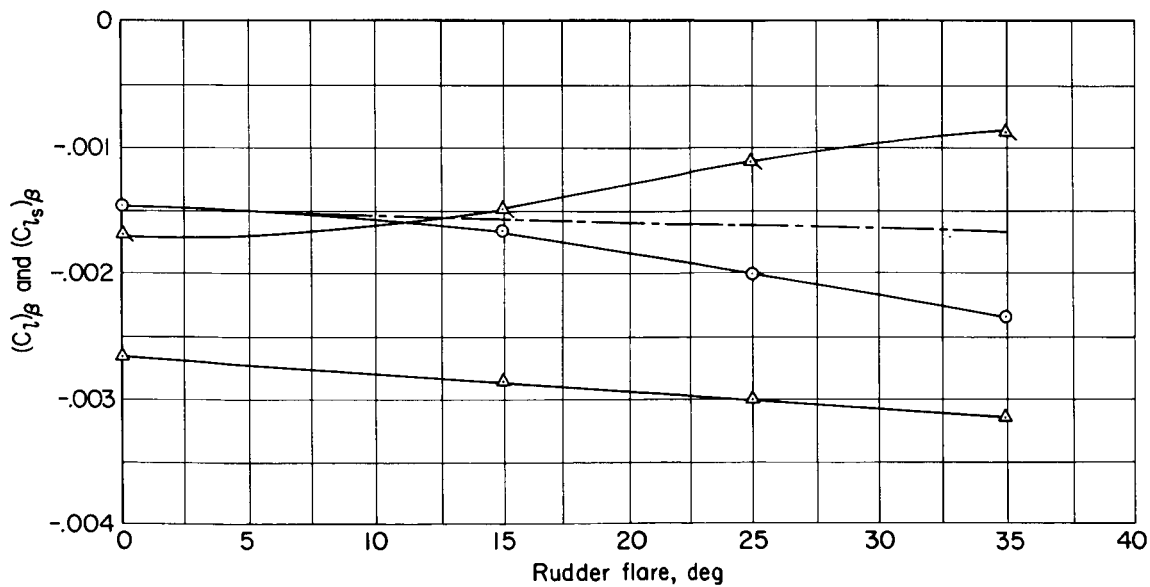


(b) Lateral stability, $M = 5.2$.

Figure 29.- Effects of rudder flare on directional and lateral stability.



(c) Directional stability, $M = 7.4$.



(d) Lateral stability, $M = 7.4$.

Figure 29.- Continued.

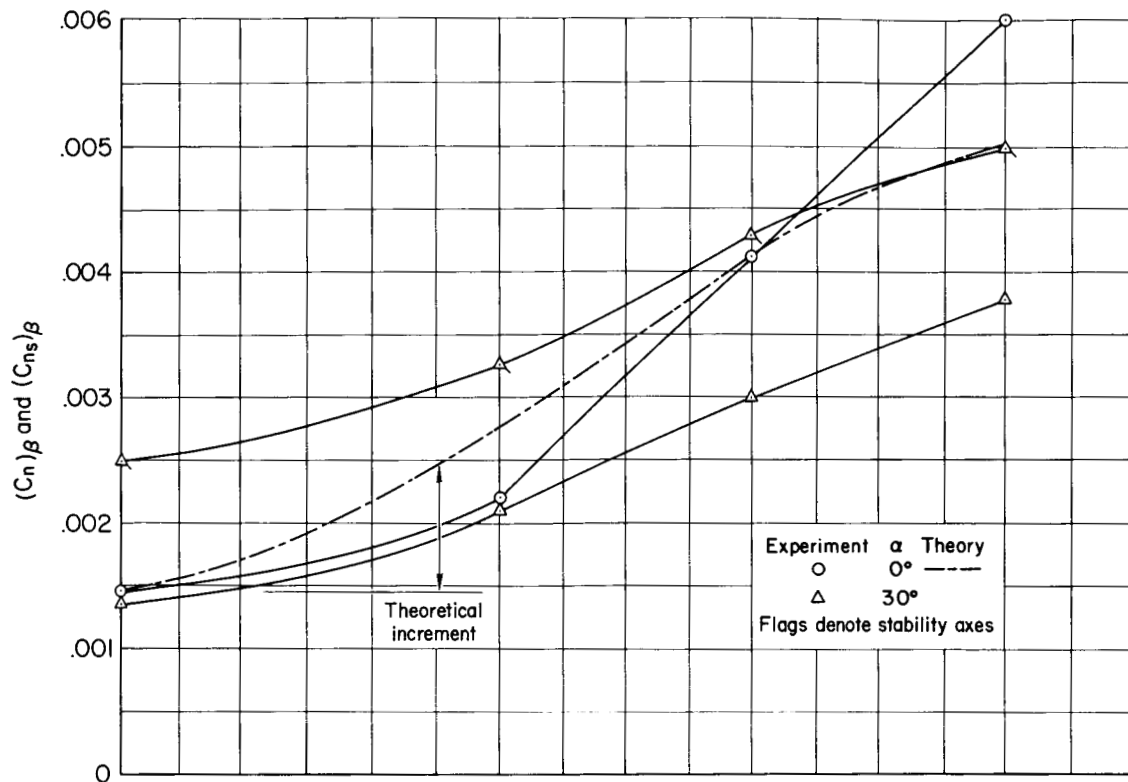
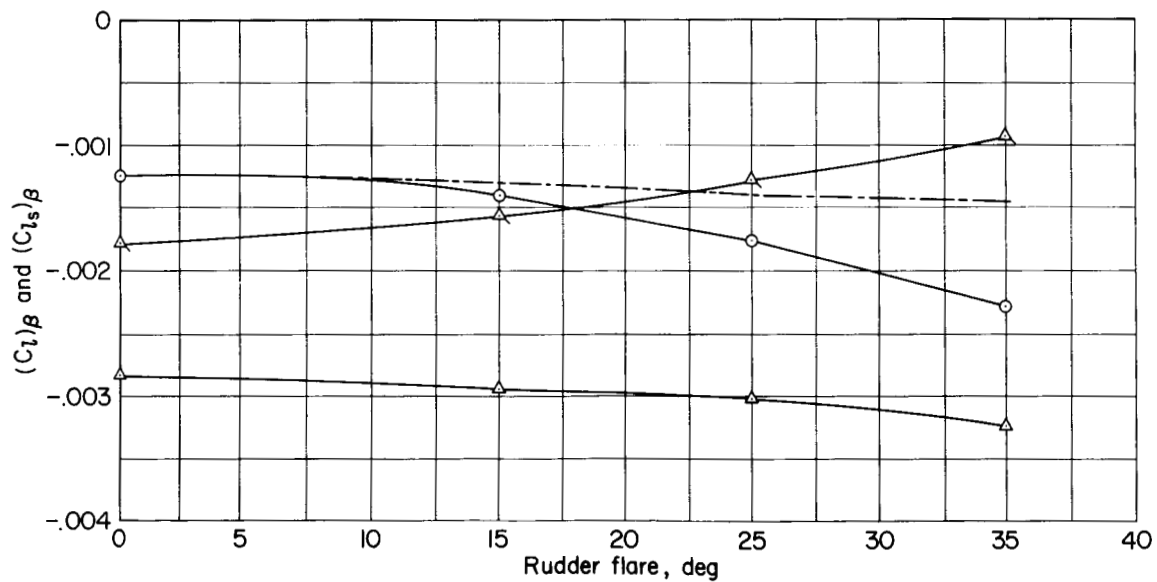
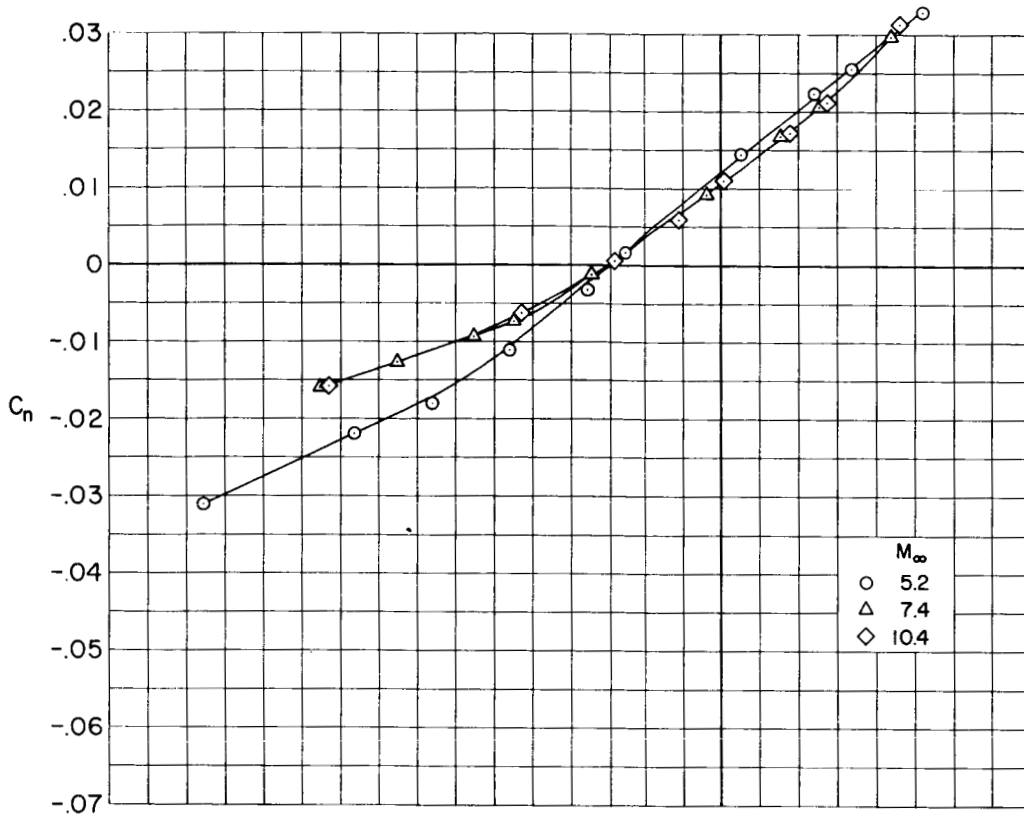
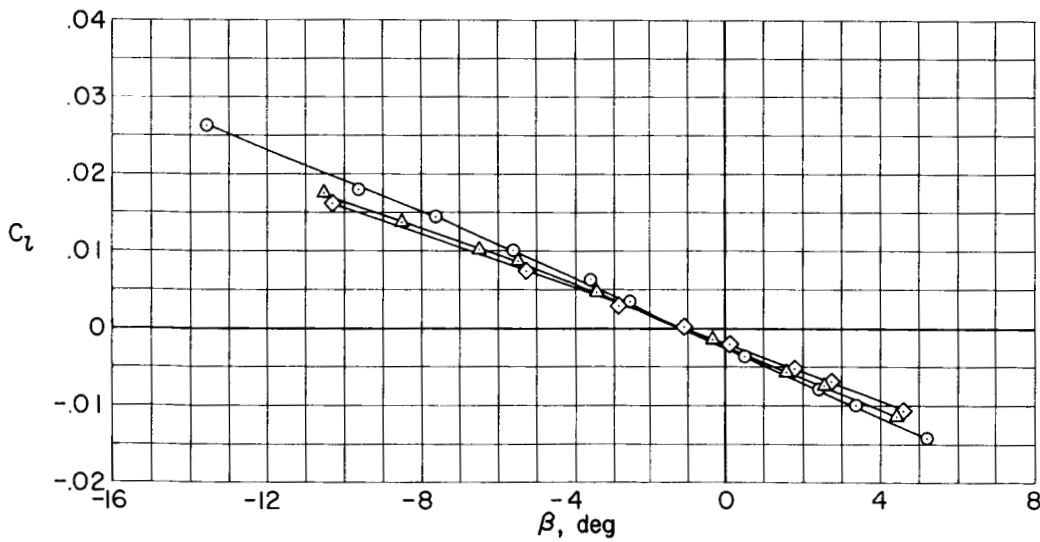
(e) Directional stability, $M = 10.4$.(f) Lateral stability, $M = 10.4$.

Figure 29.- Concluded.

CONFIDENTIAL



(a) Yawing-moment coefficient.



(b) Rolling-moment coefficient.

Figure 30.- Yawing-moment and rolling-moment coefficients for the M2-F2 model with 20° differential rudder deflection; $\delta_{r\text{left}} = 15^\circ$, $\delta_{r\text{right}} = 35^\circ$, $\alpha = 0^\circ$, $\delta_F = 60^\circ$.

CONFIDENTIAL

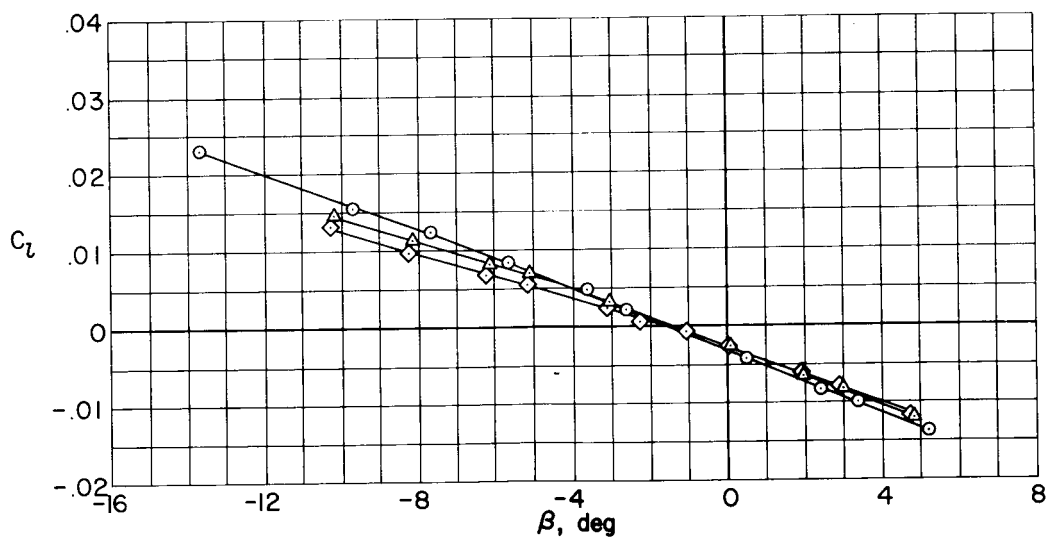
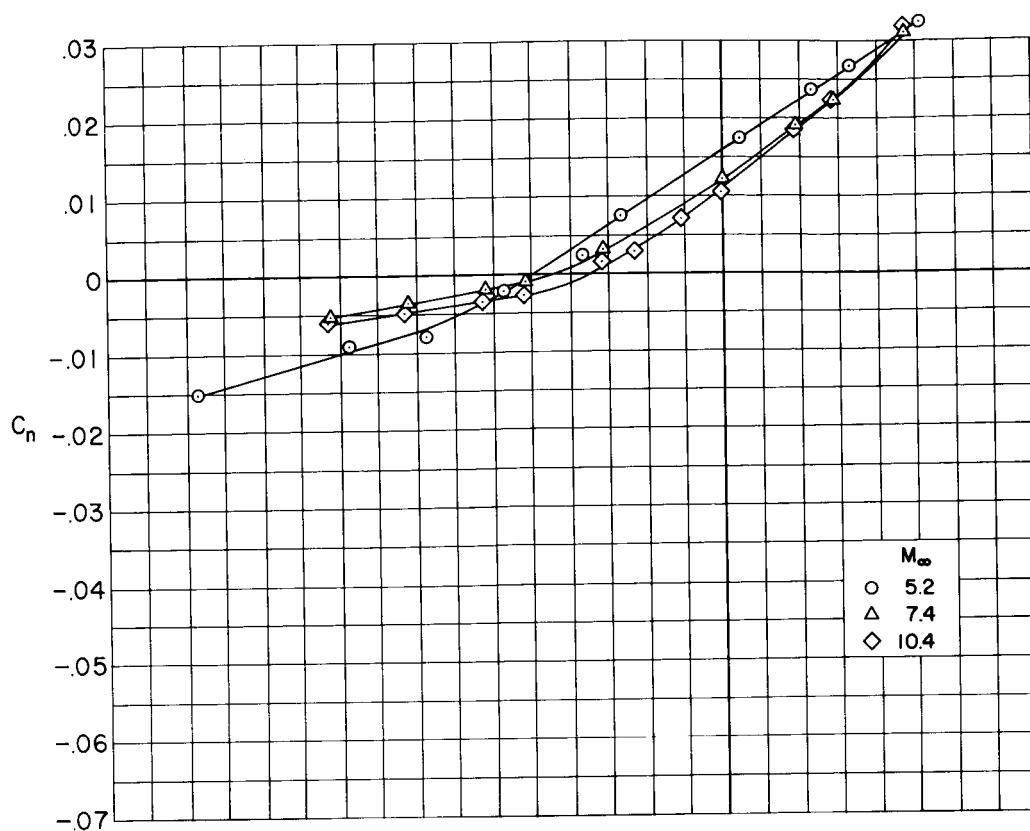
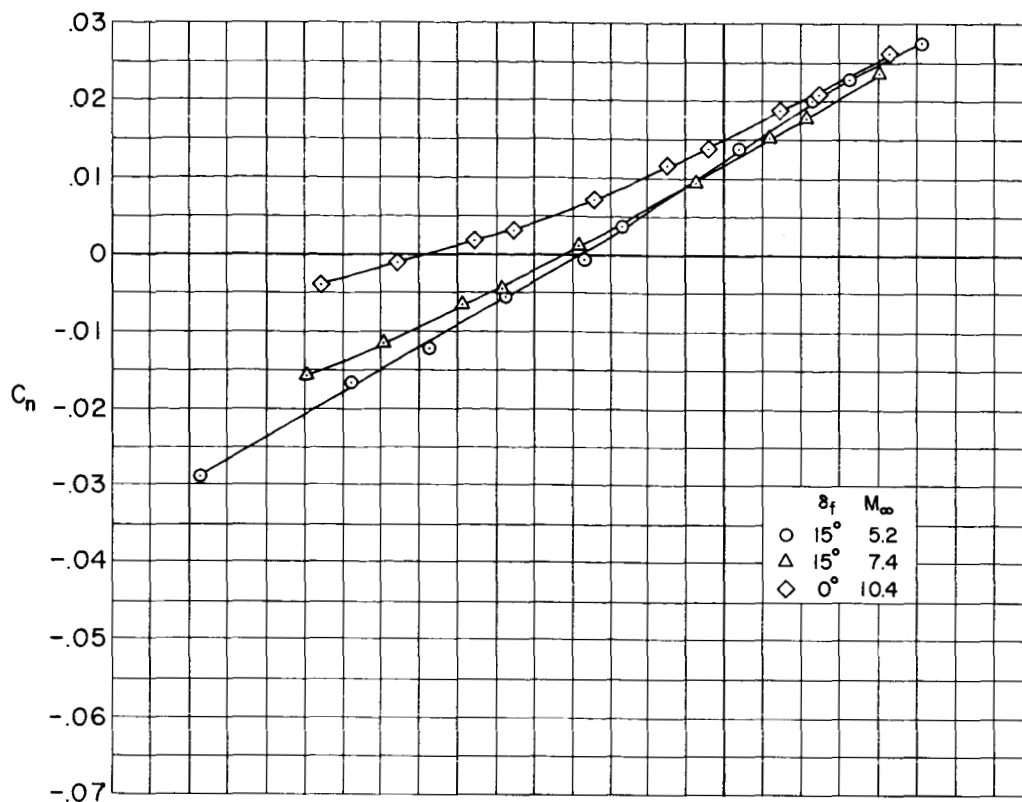
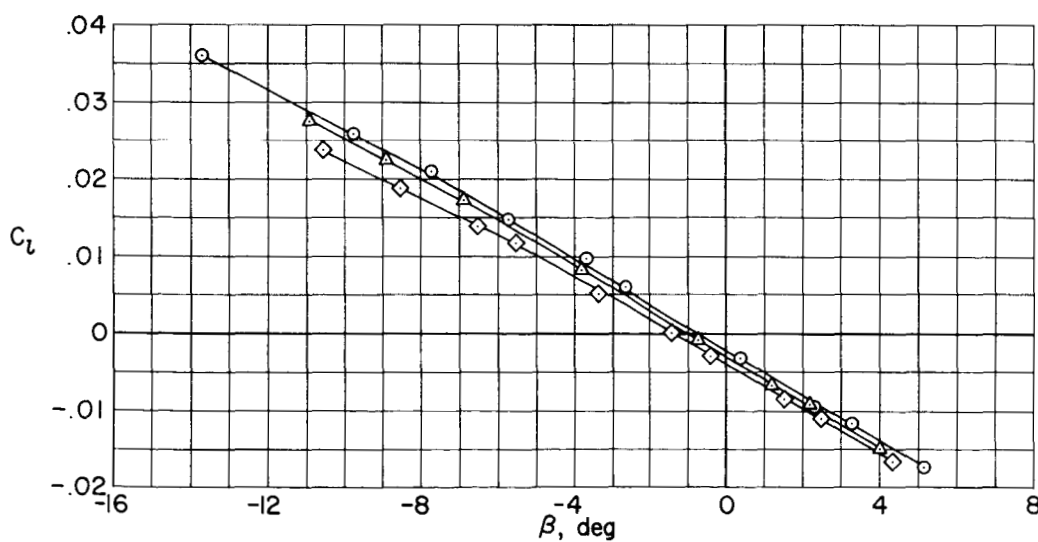


Figure 31.- Yawing-moment and rolling-moment coefficients for the M2-F2 model with 35° differential rudder deflection; $\delta_{r_{\text{left}}} = 0^\circ$, $\delta_{r_{\text{right}}} = 35^\circ$, $\alpha = 0^\circ$, $\delta_f = 60^\circ$.

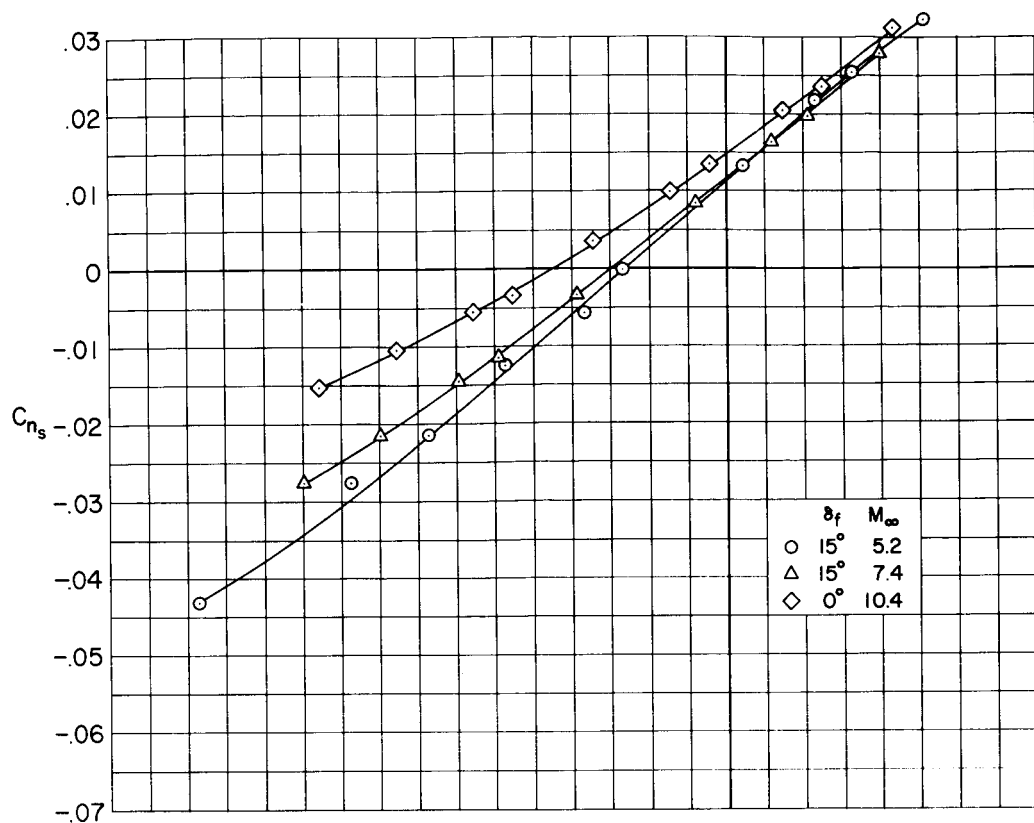


(a) Yawing-moment coefficient.

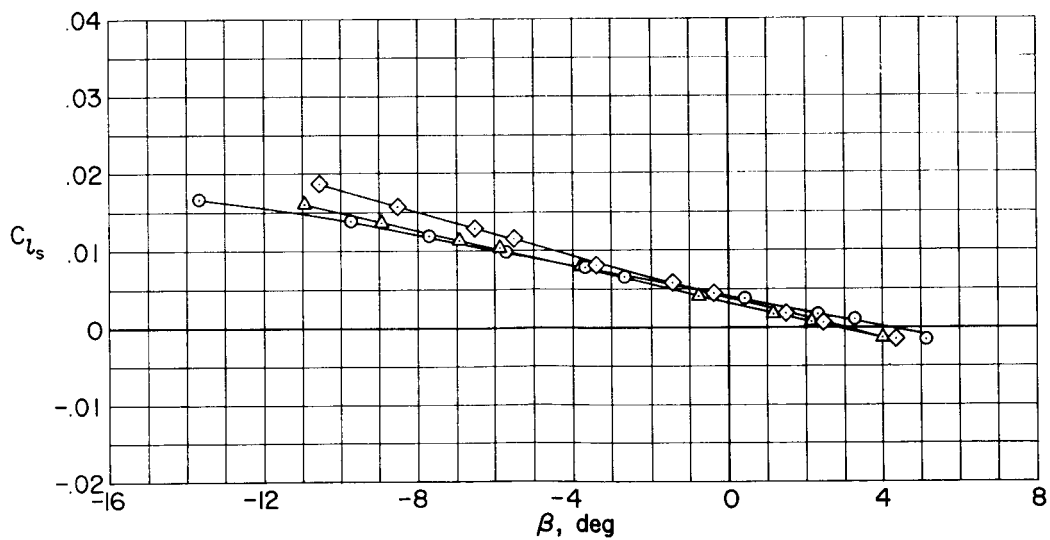


(b) Rolling-moment coefficient.

Figure 32.- Yawing-moment and rolling-moment coefficients for the M2-F2 model with 20° differential rudder deflection; $\delta_{r\text{left}} = 15^\circ$, $\delta_{r\text{right}} = 35^\circ$, $\alpha = 30^\circ$; body axes.

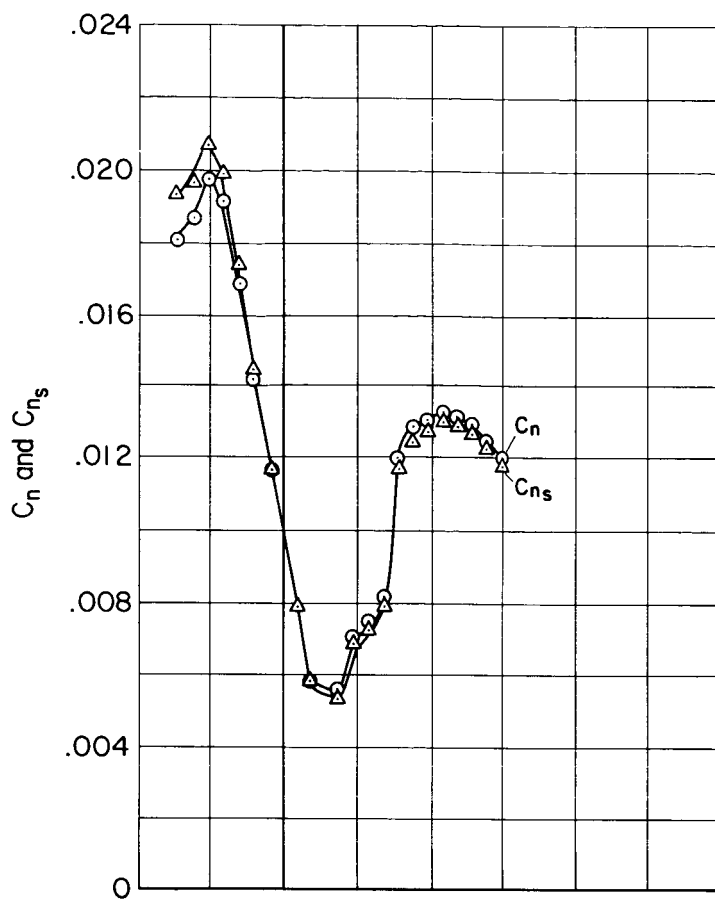


(a) Yawing-moment coefficient.

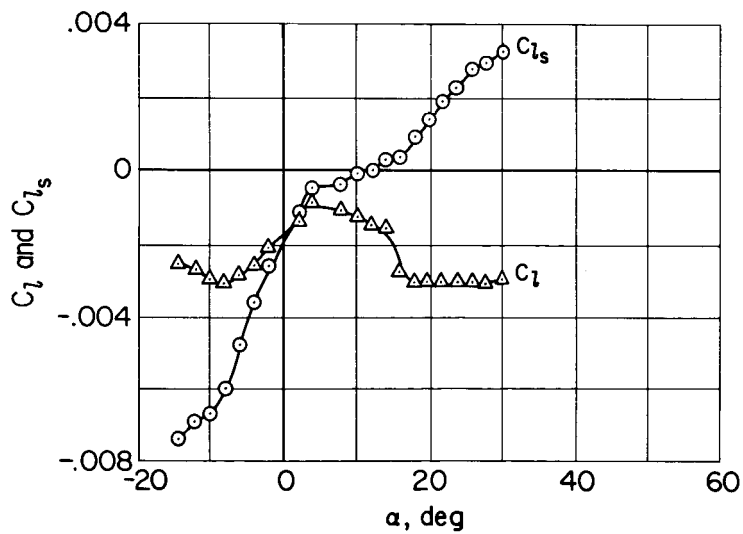


(b) Rolling-moment coefficient.

Figure 33.- Yawing-moment and rolling-moment coefficients for the M2-F2 model with 20° differential rudder deflection; $\delta_{r\text{left}} = 15^\circ$, $\delta_{r\text{right}} = 35^\circ$, $\alpha = 30^\circ$; stability axes.

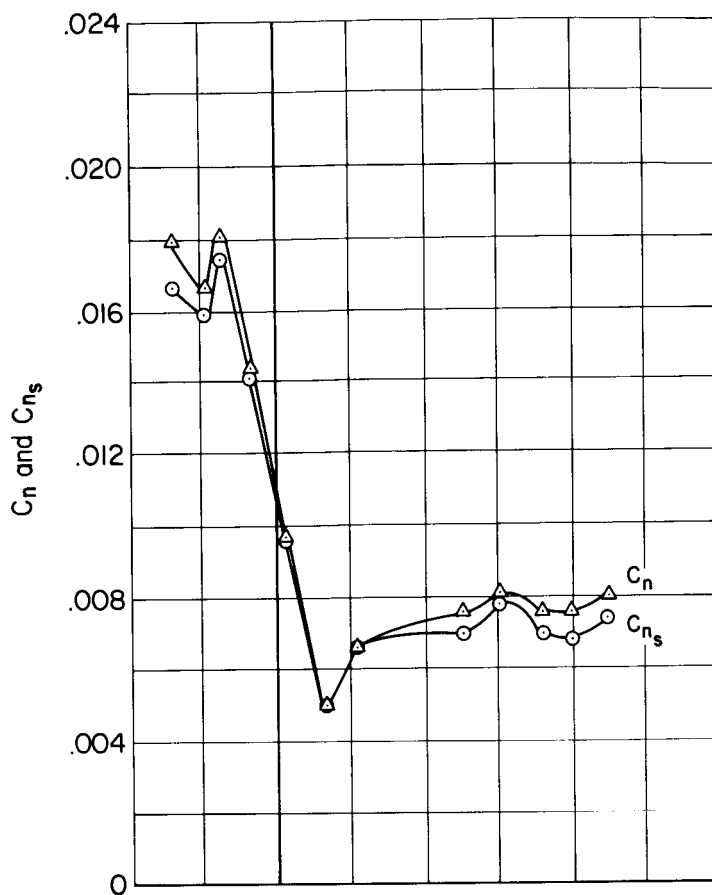


(a) Yawing-moment coefficient.

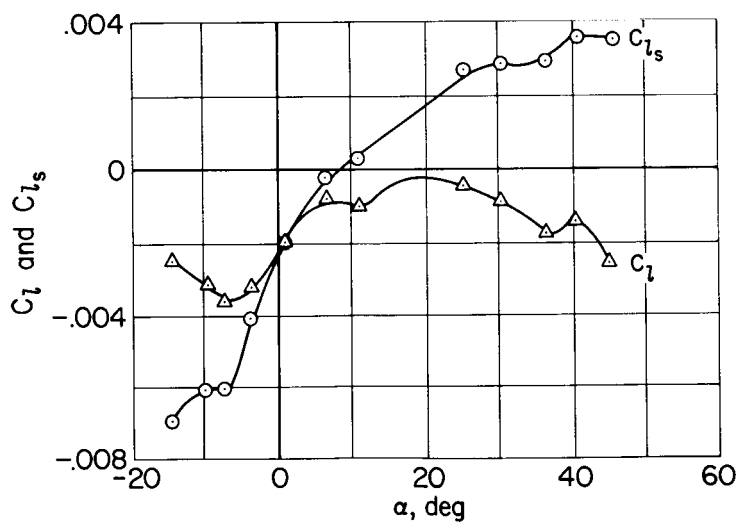


(b) Rolling-moment coefficient.

Figure 34.- Differential rudder characteristics for the M2-F2 model in pitch;
 $\beta = 0^\circ$, $\delta_{r\text{left}} = 15^\circ$, $\delta_{r\text{right}} = 35^\circ$, $M = 7.4$.

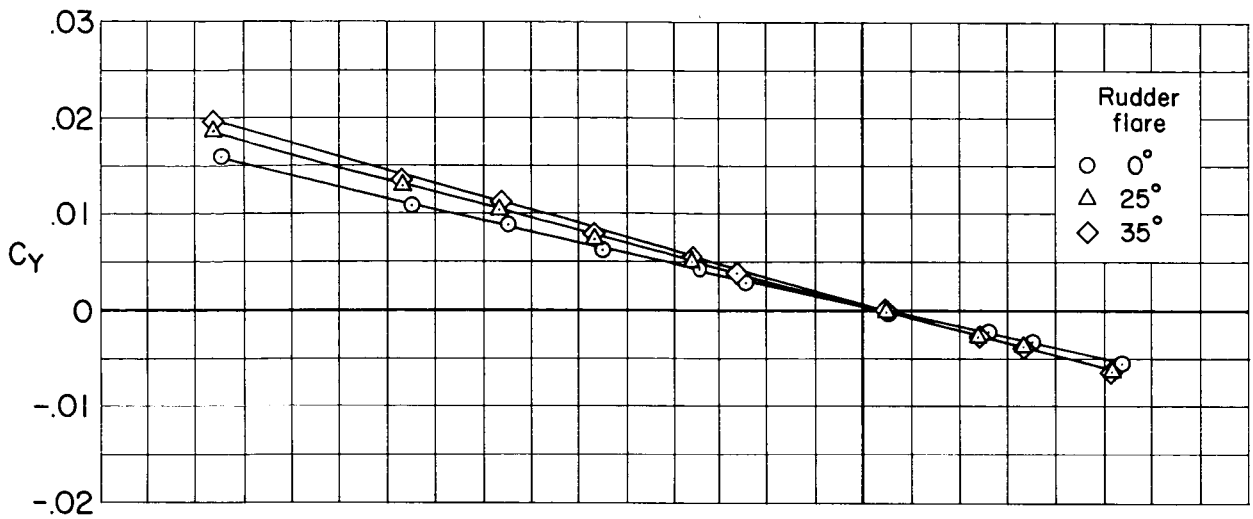


(a) Yawing-moment coefficient.

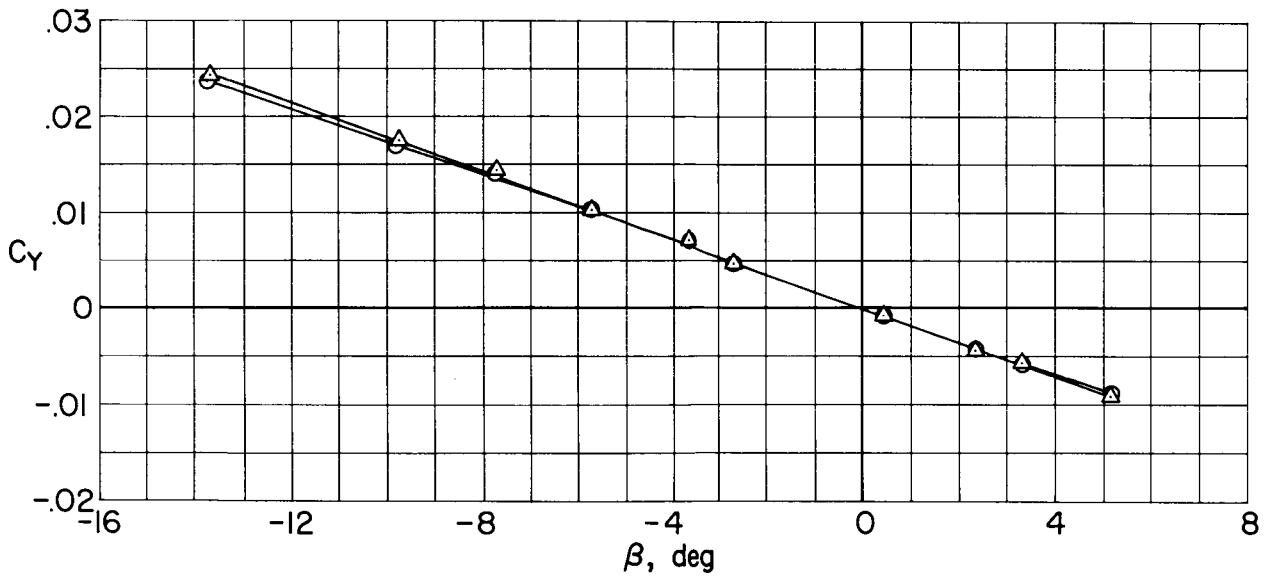


(b) Rolling-moment coefficient.

Figure 35.- Differential rudder characteristics for the M2-F2 model in pitch;
 $\beta = 0^\circ$, $\delta_{r_{left}} = 15^\circ$, $\delta_{r_{right}} = 35^\circ$, $M = 10.4$.

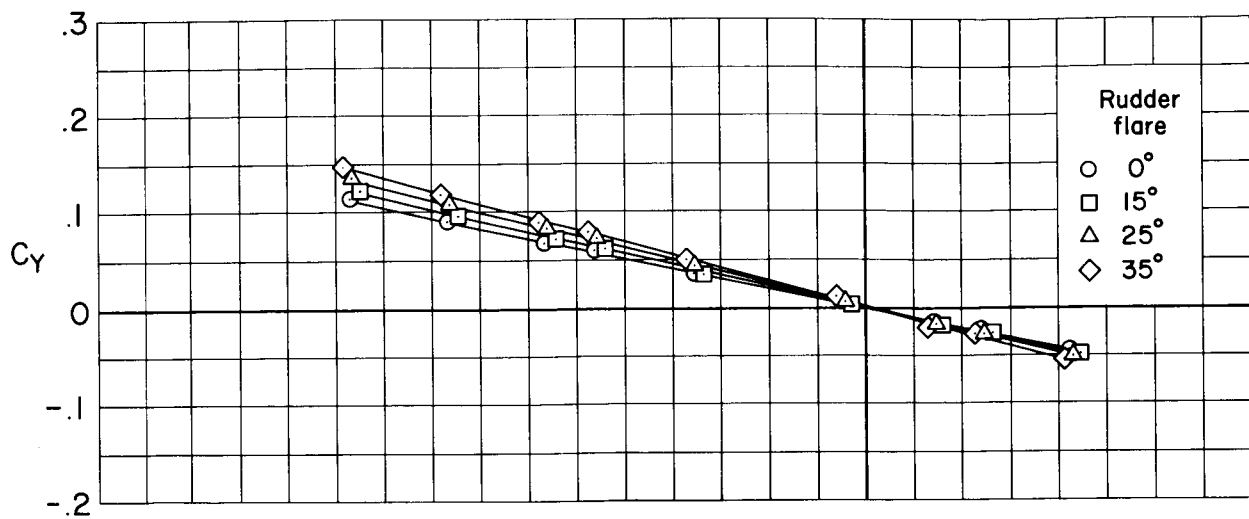


(a) $M = 5.2$, $\alpha = 0^\circ$, $\delta_f = 60^\circ$

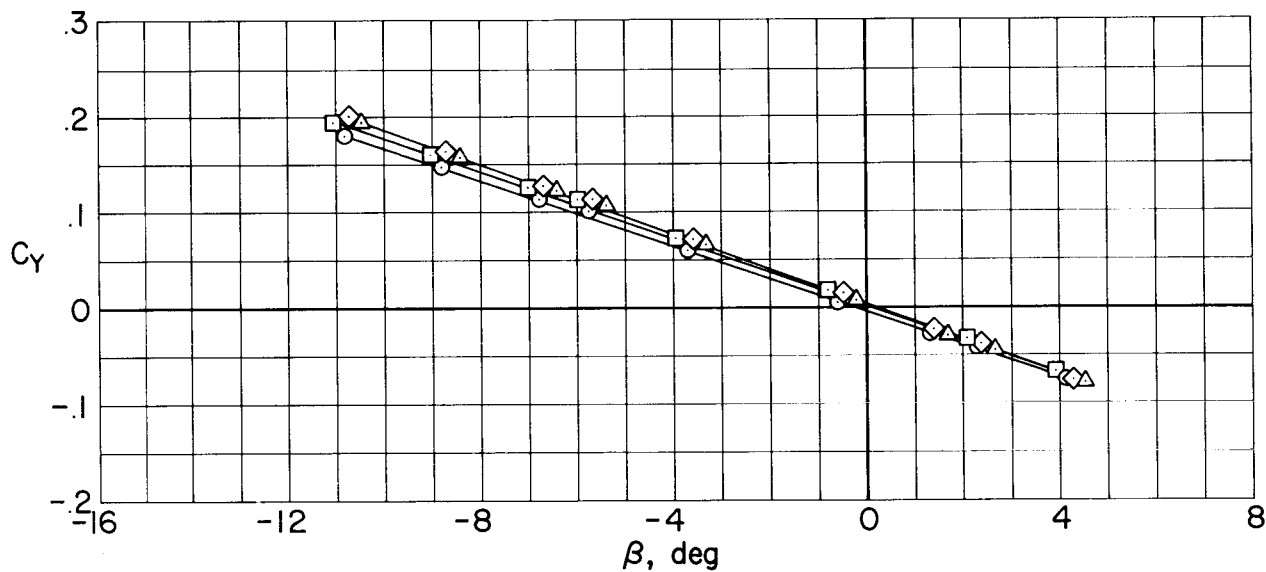


(b) $M = 5.2$, $\alpha = 30^\circ$, $\delta_f = 15^\circ$

Figure 36.- Variations of side-force coefficient with sideslip angle for the M2-F2 model with several different rudder-flare angles at angles of attack of 0° and 30° .



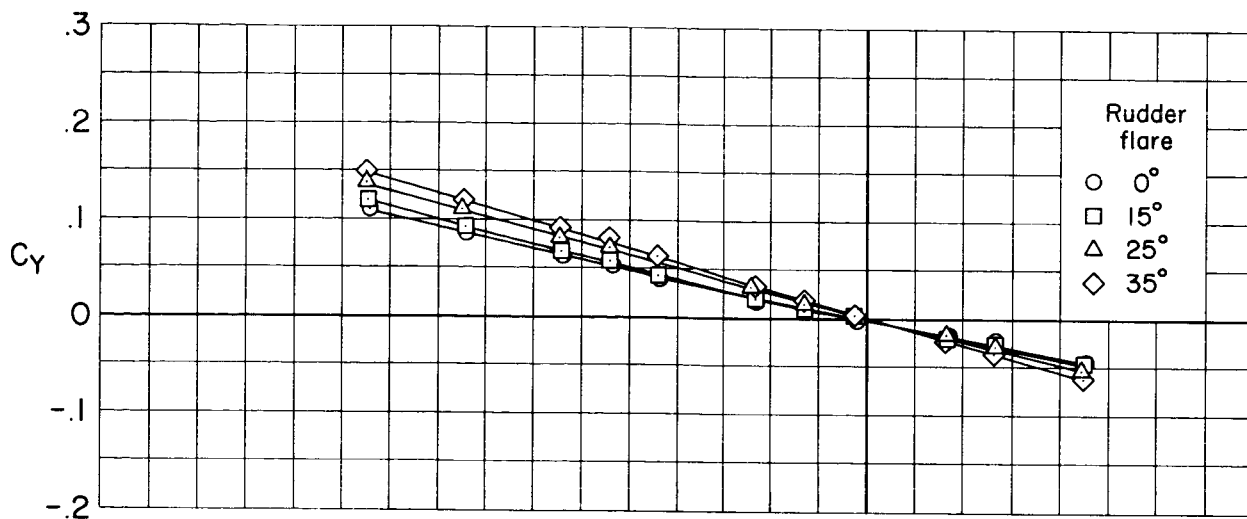
(c) $M = 7.4$, $\alpha = 0^\circ$, $\delta_f = 60^\circ$



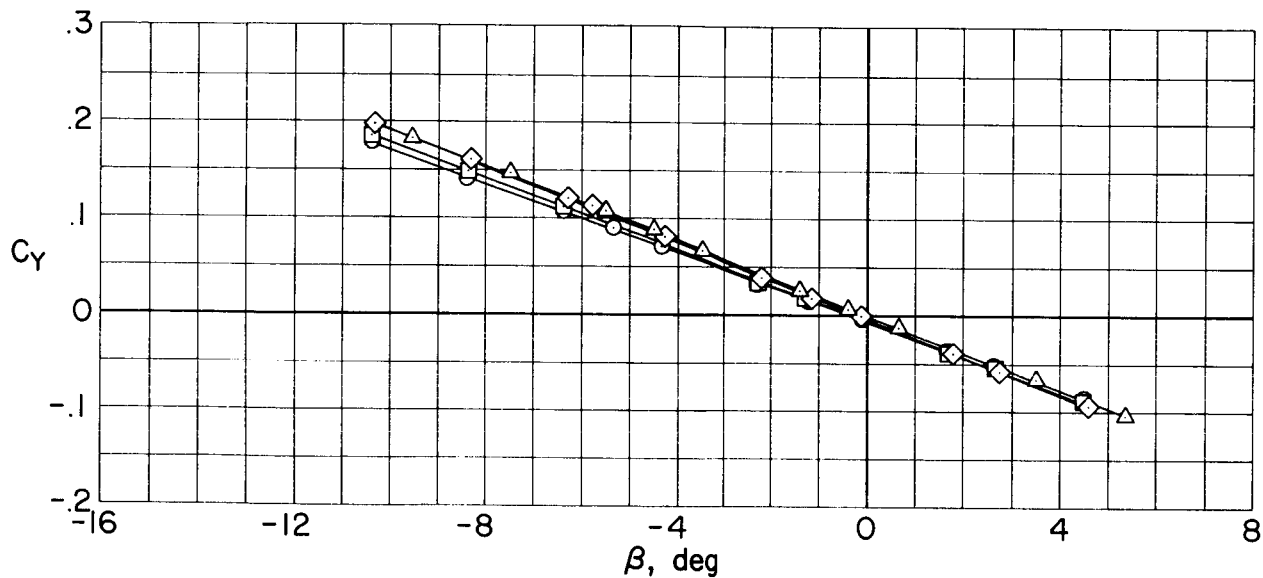
(d) $M = 7.4$, $\alpha = 30^\circ$, $\delta_f = 15^\circ$

Figure 36.- Continued.

CONFIDENTIAL



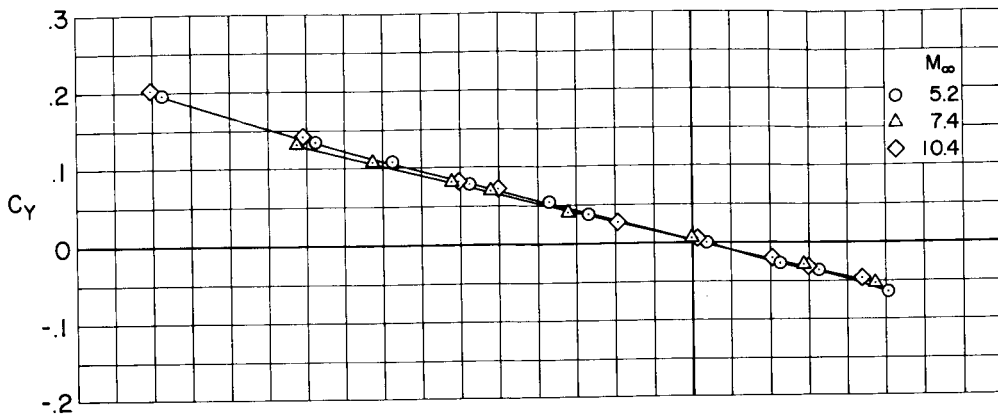
(e) $M = 10.4$, $\alpha = 0^\circ$, $\delta_f = 60^\circ$



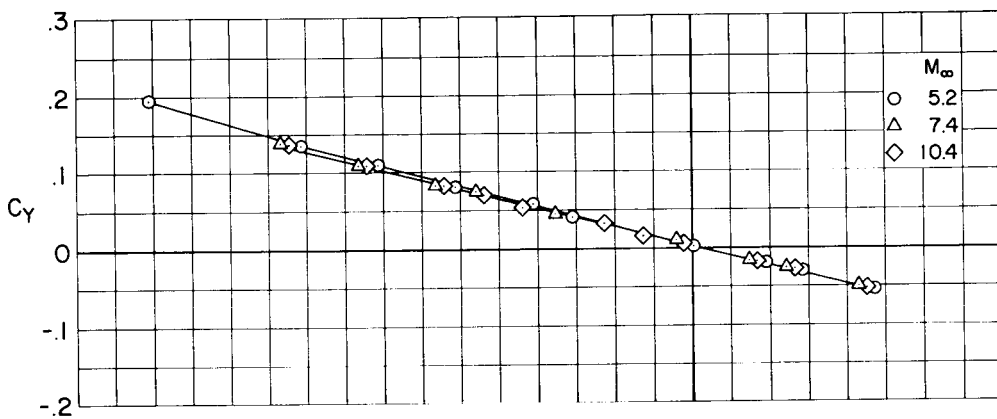
(f) $M = 10.4$, $\alpha = 30^\circ$, $\delta_f = 0^\circ$

Figure 36.- Concluded.

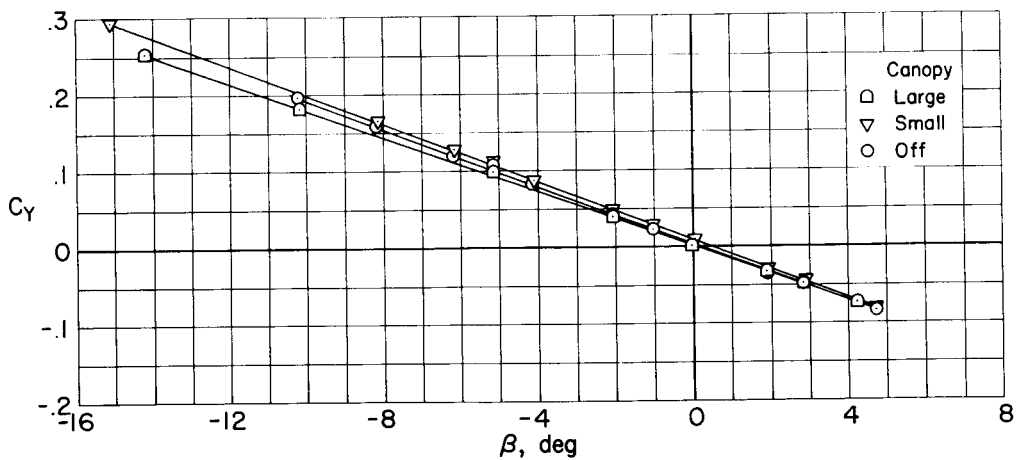
CONFIDENTIAL



(a) Large canopy, $\alpha = 0^\circ$, $\delta_f = 60^\circ$.

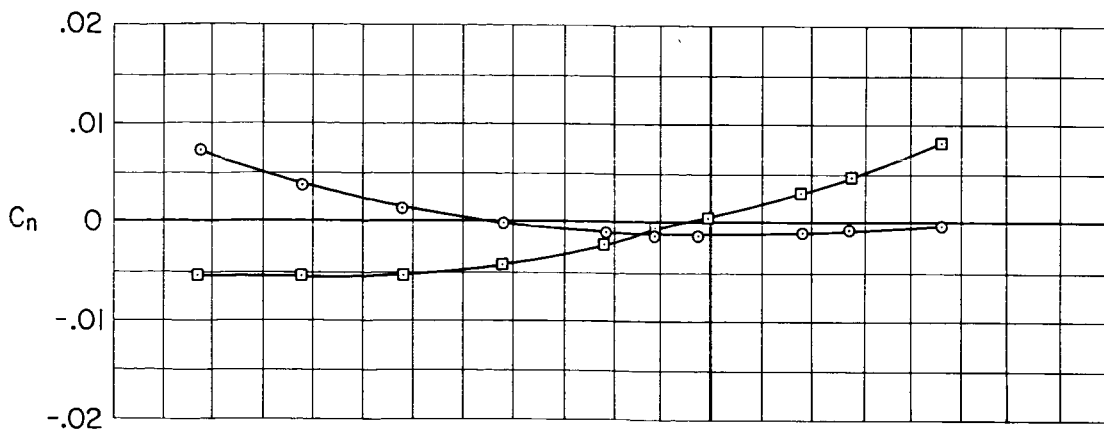


(b) Small canopy, $\alpha = 0^\circ$, $\delta_f = 60^\circ$.

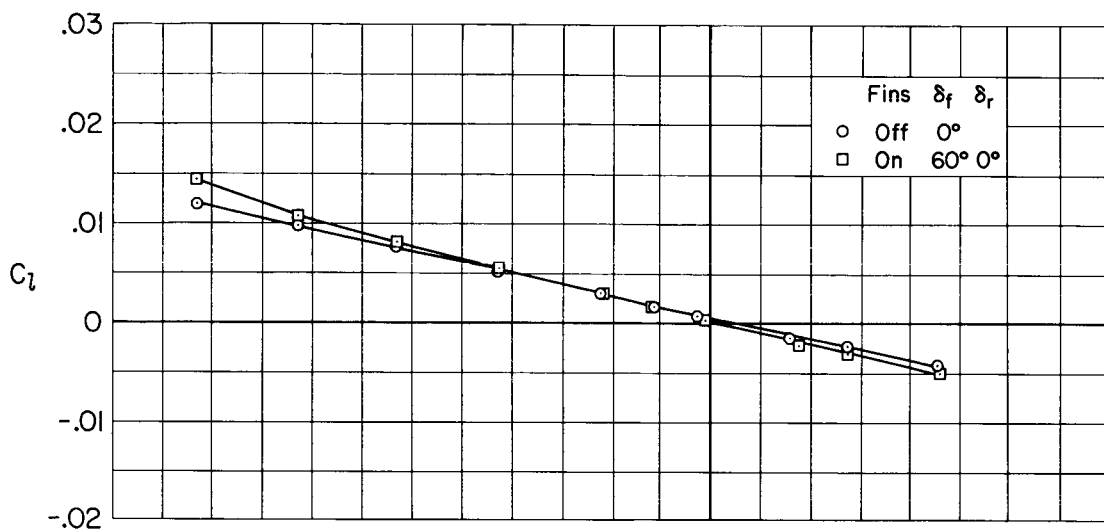


(c) $M = 10.4$, $\alpha = 30^\circ$, $\delta_f = 35^\circ$

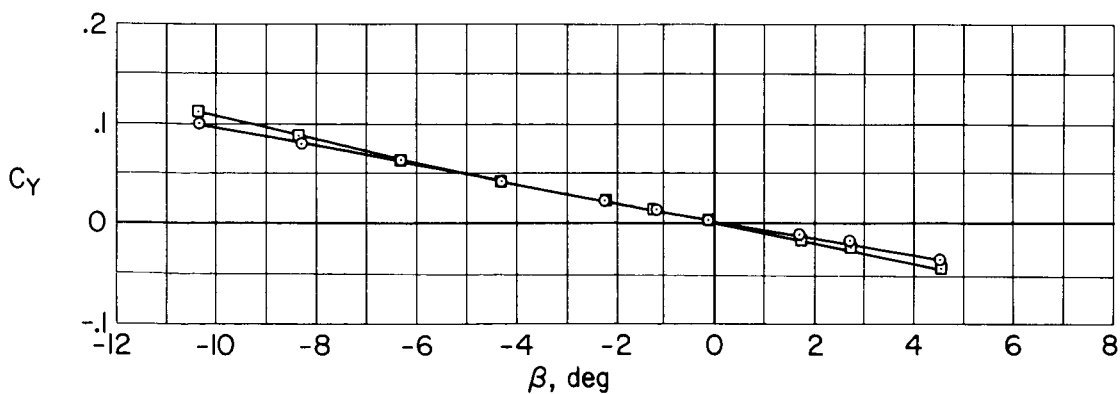
Figure 37.- Side-force coefficients for the M2-F2 model with and without the canopy.



(a) Yawing-moment coefficient.

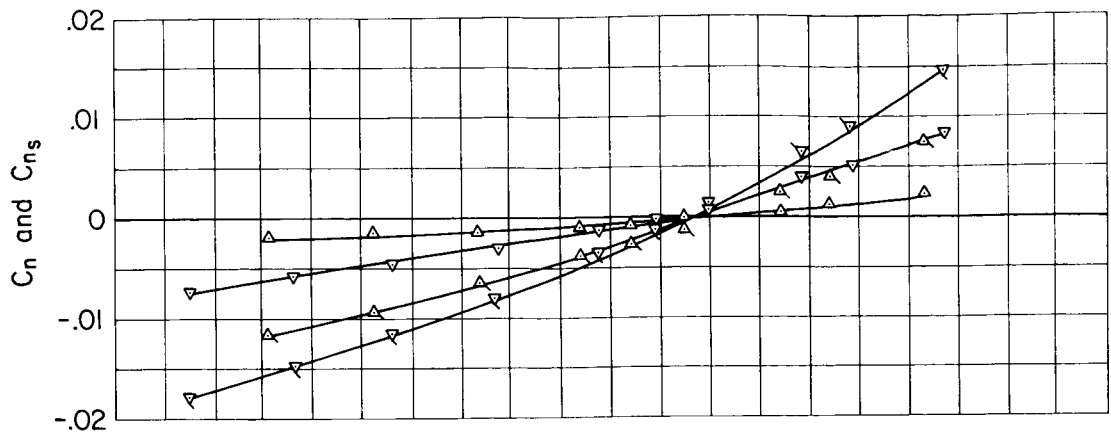


(b) Rolling-moment coefficient.

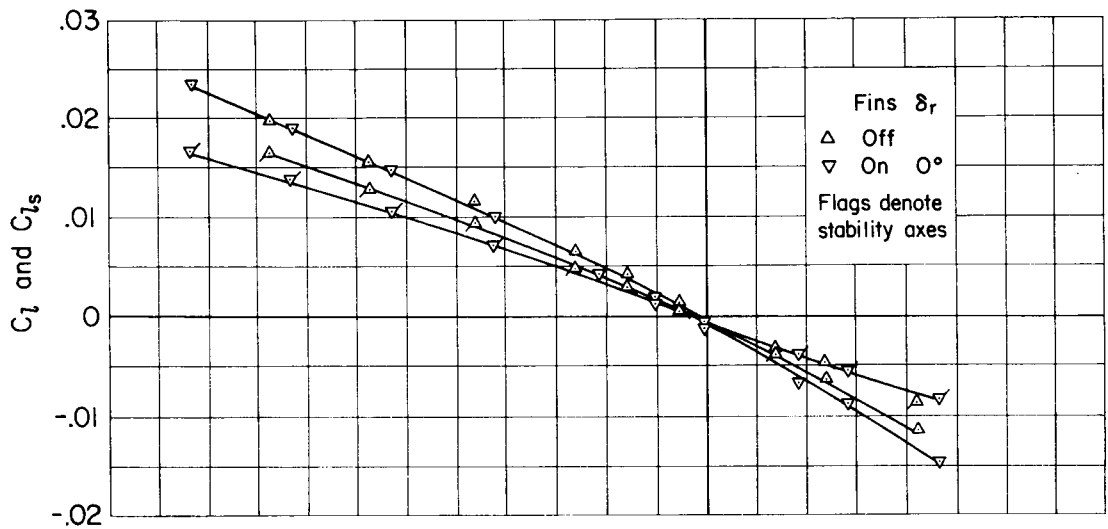


(c) Side-force coefficient.

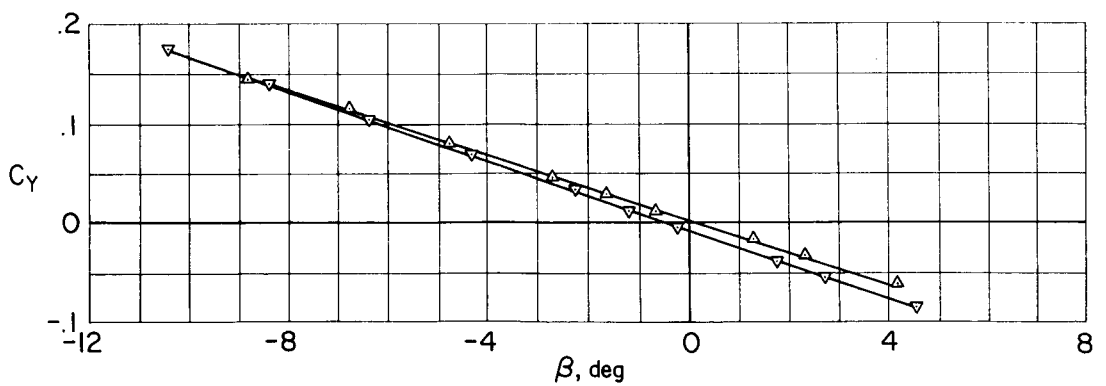
Figure 38.- Characteristics in sideslip of the M2-F2 body with and without fins;
 $M = 10.4$, $\alpha = 0^\circ$.



(a) Yawing-moment coefficient.



(b) Rolling-moment coefficient.



(c) Side-force coefficient.

Figure 39.- Characteristics in sideslip of the M2-F2 body with and without fins;
 $M = 10.4$, $\alpha = 30^\circ$, $\delta_f = 0^\circ$.

~~CONFIDENTIAL~~

UNCLASSIFIED

"The aeronautical and space activities of the United States shall be conducted so as to contribute . . . to the expansion of human knowledge of phenomena in the atmosphere and space. The Administration shall provide for the widest practicable and appropriate dissemination of information concerning its activities and the results thereof."

—NATIONAL AERONAUTICS AND SPACE ACT OF 1958

NASA SCIENTIFIC AND TECHNICAL PUBLICATIONS

TECHNICAL REPORTS: Scientific and technical information considered important, complete, and a lasting contribution to existing knowledge.

TECHNICAL NOTES: Information less broad in scope but nevertheless of importance as a contribution to existing knowledge.

TECHNICAL MEMORANDUMS: Information receiving limited distribution because of preliminary data, security classification, or other reasons.

CONTRACTOR REPORTS: Scientific and technical information generated under a NASA contract or grant and considered an important contribution to existing knowledge.

TECHNICAL TRANSLATIONS: Information published in a foreign language considered to merit NASA distribution in English.

SPECIAL PUBLICATIONS: Information derived from or of value to NASA activities. Publications include conference proceedings, monographs, data compilations, handbooks, sourcebooks, and special bibliographies.

TECHNOLOGY UTILIZATION PUBLICATIONS: Information on technology used by NASA that may be of particular interest in commercial and other non-aerospace applications. Publications include Tech Briefs, Technology Utilization Reports and Notes, and Technology Surveys.

Details on the availability of these publications may be obtained from:

SCIENTIFIC AND TECHNICAL INFORMATION DIVISION
NATIONAL AERONAUTICS AND SPACE ADMINISTRATION

Washington, D.C. 20546

~~CONFIDENTIAL~~